



BRNO UNIVERSITY OF TECHNOLOGY

VYSOKÉ UČENÍ TECHNICKÉ V BRNĚ

FACULTY OF ELECTRICAL ENGINEERING AND COMMUNICATION

FAKULTA ELEKTROTECHNIKY
A KOMUNIKAČNÍCH TECHNOLOGIÍ

DEPARTMENT OF MICROELECTRONICS

ÚSTAV MIKROELEKTRONIKY

DESIGN OF THE SYSTEM FOR THE CARBON COMPOSITE CONDUCTIVE LAYERS OF THE L-39NG AIRCRAFT TESTING AND THE OPTIMIZATION OF THE CONDUCTIVE

MATERIAL

MASTER'S THESIS

NÁVRH, MĚŘENÍ A OPTIMALIZACE VODIVÝCH VRSTEV HRBETNÍHO KRYTU LETOUNU L-39NG Z
DIPLOMOVÁ PRÁCE
UHLÍKOVÉHO KOMPOZITU

AUTHOR

AUTOR PRÁCE

Bc. Ngoc Nam Pham

SUPERVISOR

VEDOUCÍ PRÁCE

doc. Ing. Jiří Háze, Ph.D.

BRNO 2023

Master's Thesis

Master's study program **Microelectronics**

Department of Microelectronics

Student: Bc. Ngoc Nam Pham

ID: 243756

**Year of
study:** 2

Academic year: 2022/23

TITLE OF THESIS:

Design of the system for the carbon composite conductive layers of the L-39NG aircraft testing and the optimization of the conductive material

INSTRUCTION:

The goal of the work is the design and the realization of a measuring station for testing of the L-39NG aircraft dorsal cover conductive layers. It is made of the carbon composite. The cover of the L-39NG aircraft serves as a base for the installation of the DME/TRANSPONDER antenna and the flash beacon. Therefore it must meet the requirements for the overall resistance of the cover and electromagnetic compatibility, including connection to the surrounding structure. The measuring workplace will be used for the subsequent optimization and the selection of a suitable conductive material for the L-39NG aircraft dorsal cover. The goal is also experimental verification of the properties of the carbon composite conductive layers depending on the requirements for maintaining the functionality of the antennas on material samples (produced at the AERO Vodochody company).

RECOMMENDED LITERATURE:

Dle doporučení vedoucího práce.

**Date of project
specification:** 6.2.2023

**Deadline for
submission:** 23.5.2023

Supervisor: doc. Ing. Jiří Háze, Ph.D.

doc. Ing. Lukáš Fucik, Ph.D.
Chair of study program board

WARNING:

The author of the Master's Thesis claims that by creating this thesis he/she did not infringe the rights of third persons and the personal and/or property rights of third persons were not subjected to derogatory treatment. The author is fully aware of the legal consequences of an infringement of provisions as per Section 11 and following of Act No 121/2000 Coll. on copyright and rights related to copyright and on amendments to some other laws (the Copyright Act) in the wording of subsequent directives including the possible criminal consequences as resulting from provisions of Part 2, Chapter VI, Article 4 of Criminal Code 40/2009 Coll.



Diplomová práce

magisterský navazující studijní program **Mikroelektronika**

Ústav mikroelektroniky

Student: Bc. Ngoc Nam Pham

ID: 243756

Ročník: 2

Akademický rok: 2022/23

NÁZEV TÉMATU:

Návrh měření a optimalizace vodivých vrstev hřbetního krytu letounu L-39NG z uhlíkového kompozitu

POKYNY PRO VYPRACOVÁNÍ:

Cílem práce je návrh měřicího pracoviště pro testování vodivých vrstev hřbetního krytu letounu L-39NG vyrobeného z uhlíkového kompozitu. Kryt letounu L-39NG slouží jako základna pro instalaci antény DME/TRANSPONDER a zábleskového majáku a musí tedy splnit požadavky na celkový odpor krytu a elektromagnetickou slučitelnost včetně propojení s okolní konstrukcí. Měřicí pracoviště bude sloužit pro následné optimalizace výběru vhodného vodivého materiálu hřbetního krytu letounu L-39NG. Cílem jsou rovněž experimentální ověření vlastností vodivých vrstev uhlíkového kompozitu v závislosti na požadavcích zachování funkčnosti antén na materiálových vzorcích (vyrobených v podniku AERO Vodochody).

DOPORUČENÁ LITERATURA:

Dle doporučení vedoucího práce.

Termín zadání: 6.2.2023

Termín odevzdání: 23.5.2023

Vedoucí práce: doc. Ing. Jiří Háze, Ph.D.

doc. Ing. Lukáš Fucík, Ph.D.
předseda rady studijního programu

UPOZORNĚNÍ:

Autor diplomové práce nesmí při vytváření diplomové práce porušit autorská práva třetích osob, zejména nesmí zasahovat nedovoleným způsobem do cizích autorských práv osobnostních a musí si být plně vědom následků porušení ustanovení § 11 a následujících autorského zákona č. 121/2000 Sb., včetně možných trestněprávních důsledků vyplývajících z ustanovení části druhé, hlavy VI. díl 4 Trestního zákoníku č.40/2009 Sb.

Abstract

In recent decades, the use of composites has been dramatically preferred in the aerospace industry. The latest projects of the Czech aviation industry also focus on increasing the use of composites in new aircraft. This thesis focusses on the research of the electrical properties of the composite in order to optimize the choice of material. The thesis presents the design of an automatic measuring station used for measuring and testing the electrical properties of composite specimens produced by the company AERO Vodochody AEROSPACE a.s. For this purpose, the device LCR bridge R&S HM8118 is used, and the control program is designed in the MATLAB environment by using the SCPI language. The proposed system is then used for experimental verification of the electrical conductivity of composite samples. The measurement results will be the basis for the development of aviation conductivity composites in new aircraft. This thesis also presents the results of the lightning strike test on the selected composite specimens. Results of the lightning strike test provide deeper knowledge about the lightning strike protection ability of specimens. The development of a Non-destructive testing system based on the method of Electrical Impedance/Resistance Tomography is also presented in this thesis. The development is in the first stages, but the system is expected to be used as a structural health monitoring system.

Keywords

Composite materials, AERO Vodochody AEROSPACE a.s., SCPI, MATLAB, L-39NG, Lightning strike test, FPGA, Non-destructive testing, Electrical impedance tomography

Abstrakt

V posledních desetiletích je v leteckém průmyslu výrazně preferováno použití kompozitů. Nejnovější projekty českého leteckého průmyslu se zaměřují také na zvýšení využití kompozitů v nových letadlech. Tato práce se zaměřuje na výzkum elektrických vlastností kompozitu za účelem optimalizace výběru materiálu. Diplomová práce představuje návrh automatické měřicí stanice sloužící k měření a testování elektrických vlastností kompozitních vzorků vyráběných společností AERO Vodochody AEROSPACE as. K tomuto účelu je použito zařízení LCR bridge R&S HM8118 a řídicí program je navržen v prostředí MATLAB s použitím jazyka SCPI. Navržený systém je následně použit pro experimentální ověření elektrické vodivosti kompozitních vzorků. Výsledky měření budou základem pro vývoj kompozitů pro leteckou vodivost v nových letadlech. Tato práce také prezentuje výsledky testu úderu blesku na vybraných kompozitních vzorcích. Výsledky testu na úder blesku poskytují hlubší znalosti o schopnosti vzorků chránit před úderem blesku. V této práci je také představen vývoj nedestruktivního testovacího systému založeného na metodě elektrické impedance/odporové tomografie. Vývoj je v prvních fázích, ale očekává se, že systém bude využíván jako systém monitorování zdraví struktur.

Klíčová slova

Kompozitní materiály, AERO Vodochody AEROSPACE a.s, SCPI, MATLAB, L-39NG, Test úderu bleskem, FPGA, Nedestruktivní testování, Elektrická impedanční tomografie

Rozšířený abstrakt

V současné době se kompozitní materiály široce využívají v letecké technice jako náhrada konvenčních kovových konstrukčních materiálů za účelem snížení hmotnosti draku letadel. Společnost AERO Vodochody AEROSPACE a.s. se zaměřila na optimalizaci draku letounu L-39NG s cílem zvýšení využití kompozitního materiálu v konstrukci draku letounu. Jejich snahy se mimo optimalizace mechanických vlastností materiálu soustřeďují také do oblasti vývoje nových struktur s cílem zlepšení jejich elektrických vlastností a případně na odolnosti s ohledem na prevenci při zásahu blesku.

S ohledem na současné snahy společnosti AERO Vodochody AEROSPACE a.s. vznikl požadavek na testování kompozitních materiálů k posouzení jejich elektrických vlastností a požadavek na návrh automatizovaného měřicího pracoviště pro testování kompozitního materiálu pro potřeby vývoje.

Předmětem této diplomové práce je návrh automatizované pracoviště sloužícího k testování elektrických vlastností kompozitních materiálů vyrobených společností AERO Vodochody AEROSPACE a.s. Byl navržen program umožňující automatizovaný proces měření elektrické vodivosti kompozitního materiálu tak, aby bylo možné analyzovat chování testovaného vzorku kompozitního materiálu s možností porovnání s jinými vzorky při optimalizaci řešení materiálu a technologického procesu zpracování materiálu. Navržené pracoviště využívá rozhraní GPIB, jazyka SCPI v prostředí MATLAB. Navržené a realizované automatizované měřicí pracoviště bylo využito pro měření impedančních vlastností kompozitního materiálu.

Výsledky diplomové práce mohou být využity pro optimalizace kompozitního materiálu k dosažení požadovaných funkcí a vývoji nových vodivých vrstev kompozitních materiálů ve společnosti AERO Vodochody AEROSPACE a.s.

Dále v rámci řešení diplomové práce byla řešena otázka sestavení pracoviště a metodiky měření chování kompozitního materiálu s ohledem na prevenci zásahu bleskem. Cílem je sestavit pracoviště a metodiku měření, která by umožnila posouzení odolnosti materiálů vůči vysokonapěťovým elektrickým výbojům v souladu s RTCA/DO-160.

V rámci diplomové práce byly připravené vzorky kompozitního materiálu testovány vysokonapěťovými elektrickými výboji až napěťové úrovně 400 kV. Provedené experimenty ukazují na správnost sestaveného pracoviště pro testování kompozitních materiálů k posouzení jejich vlastností při případném zasažení elektrickým výbojem.

Dále za účelem posouzení elektrických vlastností kompozitních materiálů v rámci řešení diplomové práce bylo modelování elektrického magnetického pole využitím

programu Ansys. Na základě modelování jsme dospěli k požadavkům na velikosti testovaných vzorků kompozitních materiálů a tím zvýšit přesnost srovnávání vzorků kompozitního materiálu nejen z pohledu elektrické vodivosti, ale i z pohledu odolnosti vůči zásahu blesku. Navíc byl připraveno pracoviště využívající programovatelné hradlové pole (FPGA) k analyzování možností poruch využitím měření na kompozitních materiálech.

Bibliographic citation

PHAM, Ngoc Nam. Návrh měření a optimalizace vodivých vrstev hřbetního krytu letounu L-39NG z uhlíkového kompozitu [online]. Brno, 2023 [cit. 2023-05-23]. Dostupné z: <https://www.vut.cz/studenti/zav-prace/detail/152473>. Diplomová práce. Vysoké učení technické v Brně, Fakulta elektrotechniky a komunikačních technologií, Ústav mikroelektroniky. Vedoucí práce Jiří Háze.

Author's Declaration

Author: *Ngoc Nam PHAM*

Author's ID: *243756*

Paper type: *Master's Thesis*

Academic year: *2022/23*

Topic: *Design of the system for the carbon composite conductive layers of the L-39NG aircraft testing and the optimization of the conductive material*

I declare that I have written this paper independently, under the guidance of the advisor and using exclusively the technical references and other sources of information cited in the project and listed in the comprehensive bibliography at the end of the project.

As the author, I furthermore declare that, with respect to the creation of this paper, I have not infringed any copyright or violated anyone's personal and/or ownership rights. In this context, I am fully aware of the consequences of breaking Regulation S 11 of the Copyright Act No. 121/2000 Coll. of the Czech Republic, as amended, and of any breach of rights related to intellectual property or introduced within amendments to relevant Acts such as the Intellectual Property Act or the Criminal Code, Act No. 40/2009 Coll., Section 2, Head VI, Part 4.

Brno, May 22, 2023

author's signature

Acknowledgement

First of all, I am grateful to AERO Vodochody AEROSPACE a.s. for allowing me to work on the project L-39NG, and for preparing specimens for practical measurement, special thanks to Mr. Martin Honig, and Mr. Jan Vaclavik.

Especially, I am extremely grateful and indebted to my supervisors, Assoc. Prof. Jiri Haze and Prof. Jan Leuchter for their encouragement, support, and guidance.

I would also like to thank Ph.D. Alexander Otahal for helping to prepare the specimens and electrodes for measurement, and Ph.D. Michal Krbal for helping to conduct the Lightning strike test in the High voltage laboratory

Finally, I am grateful to Le Quy Don Technical Academy in Hanoi for financially supporting me during my studies in Brno.

Brno, May 22, 2023

Author's signature

Contents

1. THE AIM OF THE THESIS	16
2. COMPOSITE MATERIALS	17
2.1 COMPOSITE MATERIALS AND THEIR CLASSIFICATION	17
2.2 GENERAL ADVANTAGES OF COMPOSITE MATERIALS	19
2.3 GENERAL DISADVANTAGES OF COMPOSITE MATERIALS	20
2.4 COMPOSITE MATERIALS FOR AIRCRAFT STRUCTURES.....	21
2.4.1 Civil aircraft	22
2.4.2 Military aircraft	23
2.4.1 Czech aircraft.....	24
2.5 CHAPTER CONCLUSION.....	25
3. THE NEED OF CONDUCTIVE COMPOSITE	26
3.1 ELECTRIC POWER DISTRIBUTION	26
3.1.1 Challenges of composite aircraft	26
3.1.2 Solution – conductive composite as ground plane	27
3.2 LIGHTNING STRIKE PROTECTION	28
3.2.1 Test standard and specification	28
3.2.2 Mechanism of aircraft lightning strike.....	31
3.2.3 Aircraft lightning strike impacts	32
3.2.4 Solution – conductive composite.....	35
3.3 CHAPTER CONCLUSION.....	37
4. ELECTRICAL IMPEDANCE MEASUREMENT	38
4.1 IMPEDANCE MEASUREMENT METHODS	38
4.1.1 Wheaton bridge method	38
4.1.2 Resonant method.....	39
4.1.3 I-V method.....	39
4.1.4 RF I-V method.....	40
4.1.5 Network analysis method	40
4.1.6 Auto-Balancing Bridge method.....	41
4.2 CHAPTER CONCLUSION.....	42
5. PRACTICAL IMPEDANCE MEASUREMENT.....	43
5.1 SELECTION OF MEASURING INSTRUMENT AND ENVIRONMENT.....	43
5.1.1 Measuring instruments – R&S HM8118	44
5.1.2 SCPI standard and MATLAB environment	45
5.2 DESCRIPTION OF CONTROL PROGRAM.....	46
5.2.1 First part of MATLAB program	47
5.2.2 Second part of MATLAB program	51
5.3 EXPERIMENTAL MEASUREMENT	52
5.3.1 Description of specimens	52
5.3.2 Measured results – glassfiber composite	54
5.3.3 Measured result – carbon composite	58
5.4 CHAPTER CONCLUSION.....	59
5.4.1 Optimize selection of conductive layer.....	59

5.4.2	<i>Suggestion of specimen for future measurements</i>	61
6.	PRACTICAL LIGHTNING STRIKE TESTING	64
6.1	TEST STANDARD AND TEST SYSTEM	64
6.2	LIGHTNING STRIKE TO PROTECTED SURFACE.....	67
6.2.1	<i>Contact discharge test</i>	67
6.2.2	<i>Air discharge test</i>	68
6.3	LIGHTNING STRIKE TO UNPROTECTED SURFACE	69
6.4	CHAPTER CONCLUSION.....	70
7.	DEVELOPMENT OF EIT/ERT METHOD	71
7.1	STATE OF ART – NDT AND EIT/ERT METHOD	71
7.2	PROPOSED LCR METER BASED EIT SYSTEM.....	73
7.2.1	<i>Prepare of specimens</i>	73
7.2.2	<i>Measurement setup</i>	74
7.2.3	<i>Functional verification and measurement result</i>	76
7.3	DEVELOPMENT OF FPGA-BASED EIT/ERT SYSTEM	78
7.3.1	<i>Basic concept</i>	78
7.3.2	<i>VHDL design</i>	80
7.3.3	<i>Functional verification</i>	83
7.4	CHAPTER CONCLUSION.....	85
8.	CONCLUSION	87

FIGURES

Fig. 2.1	Classification of composite material and basic comparisons.....	18
Fig. 2.2	Composite materials in aircraft [10]	21
Fig. 2.3	Boeing 787 Dreamliner [11]	22
Fig. 2.4	The trend of using composite on Airbus fixed wing aircraft [12].....	23
Fig. 2.5	Composite materials in F35 fighter [15], [16]	24
Fig. 2.6	Jet trainer L-39NG – the white structure is made from composite [18].....	25
Fig. 3.1	Aircraft single-wire power distribution system [25].....	26
Fig. 3.2	Direct (left) and indirect(right) electrical ground bonding [23].....	27
Fig. 3.3	Aircraft lightning zone according to ES-91/ARP 5414 [38], [39]	29
Fig. 3.4	Lightning wave form according to ED-84/ARP 5412 [28].....	30
Fig. 3.5	Indicative 2D electrostatic model of an aircraft in ambient field [29], [30]	31
Fig. 3.6	Typical lightning current waveform during lightning swept stroke [29]	32
Fig. 3.7	Lightning direct impacts on bare metallic structure [28], [42]	33
Fig. 3.8	Lightning direct impacts on composite material [43]	34
Fig. 3.9	Lightning damage analysis [28].....	34
Fig. 3.10	Damage on bared and painted composite structures [28]	35
Fig. 3.11	Changes to lightning protection in Boeing B787.....	36
Fig. 3.12	Damages caused by lightning strike in fiberglass composite.....	37
Fig. 4.1	Wheatstone bridge method [46].....	38
Fig. 4.2	Resonant method [46].....	39
Fig. 4.3	Principle of I-V method [46]	39
Fig. 4.4	Principle of RF I-V method [46].....	40
Fig. 4.5	VNA configurations for impedance measurement [46]	41
Fig. 4.6	Auto-Balancing Bridge [46]	42
Fig. 5.1	Schematic of designed measuring station.....	43
Fig. 5.2	Simplify flowchart of MATLAB programs.....	47
Fig. 5.3	The user interface of the program - the first part	47
Fig. 5.4	The user interface of the program - the second part.....	51
Fig. 5.5	Setup of realized automatically measuring station.....	52
Fig. 5.6	Drawing of specimens prepared by AVA.....	53
Fig. 5.7	Specimen preparation for measurement.....	53
Fig. 5.8	Measured resistance and impedance of specimens of type M1556860.....	54
Fig. 5.9	Measured impedance and resistance of specimen SOP-057-3.....	55
Fig. 5.10	Differences between measured resistance along symmetrical paths.....	56
Fig. 5.11	Comparison of resistance measured between points B and C.....	57
Fig. 5.12	Dependence of phase shift on frequency	58
Fig. 5.13	Resistance of carbon composite specimen (linear representation).....	58
Fig. 5.14	Resistance of carbon composite specimen (logarithmic representation)	59
Fig. 5.15	Aluminum glass fiber M3903452 configuration.....	60
Fig. 5.16	Aluminum mesh – structure and example [52].....	60
Fig. 5.17	Boundary effect – distribution of current density	62
Fig. 5.18	Suggested shape of specimen and simulation setup.....	62
Fig. 5.19	Dependence of measured resistance on dimension of specimen.....	63
Fig. 5.20	Boundary effect in different specimen’s dimensions.....	63
Fig. 6.1	Flowchart for High Voltage and High Current Tests [53].....	65
Fig. 6.2	Principle of SGDA high voltage impulse test system [54]	66

Fig. 6.3	Lightning strike test setup.....	66
Fig. 6.4	Test impulse voltage wave form and damages – contact discharge test	67
Fig. 6.5	Test impulse voltage wave form and damage – air discharge, +80 kV.....	68
Fig. 6.6	Test impulse voltage wave form and damages – air discharge , -80 kV	69
Fig. 6.7	Test impulse voltage wave form – air discharge test, $U_{set} = 400$ kV	70
Fig. 6.8	Damage caused by lightning strike to unprotected surface.....	70
Fig. 7.1	Basic principle of EIT/ERT method [66], [67]	72
Fig. 7.2	Structural damage visualization using ERT/EIT method (simulation data).....	72
Fig. 7.3	LCR meter-based EIT system.....	74
Fig. 7.4	Flowchart of EIDORS basic operation [70].....	75
Fig. 7.5	Functional verification of modified FEM model	75
Fig. 7.6	Specimen with defect cause by lightning strike.....	76
Fig. 7.7	Damage localization using EIT/ERT method	76
Fig. 7.8	L-39NG dorsal cover (above) with 22 (below, left) and 16 (below, right) electrodes tomography	77
Fig. 7.9	Block diagram of developed EIT/ERT system	79
Fig. 7.10	HX711 ADC circuit diagram	80
Fig. 7.11	State diagram of HX711 driver.....	81
Fig. 7.12	State diagram of I2C driver	82
Fig. 7.13	State diagram of UART driver.....	83
Fig. 7.14	Measurement setup of FPGA-based EIT/ERT sytem	83
Fig. 7.15	Specimen for functional verification of FPGA-based developed system	84
Fig. 7.16	Tomography of specimen - measured by FPGA.....	84
Fig. 7.17	Tomography of specimen with lightning strike damage - measured by FPGA	85

TABLES

Table 3-1	Standards and specifications covering aircraft LSP [36]	28
Table 3-2	Lightning zone definition and corresponding current waveform [28], [39].....	30
Table 5-1	Technical data of the R&S HM8118 LCR Mater [48].....	44
Table 5-2	R&S HM8118 accuracy [48]	45
Table 5-3	Description of measured specimens.....	52
Table 5-4	Main parameters of compared meshes.....	61

INTRODUCTION

This master's thesis focuses on the testing and optimization of conductive composite materials used for producing dorsal cover of the L-39NG aircraft in company AERO Vodochody AEROSPACE a.s. (AVA). The composite materials must meet the requirement for electrical conductivity concerning electrical energy distribution, lightning strike protection (LSP), and electromagnetic interference (EMI) shielding. This thesis is a part of projects to develop composite materials used in the structure of new-generation aircraft, mainly L-39NG aircraft. The main results of these recent projects focus on the mechanical behaviors of composites. However, for aircraft structures, the electrical behaviors of composites are also important factors affecting the selection of suitable materials.

Impedance measurement and lightning strike testing of several composite material specimens prepared by AVA are presented in this thesis. The testing and measuring results provide a large amount of knowledge about the electrical behaviors and LSP ability of these specimens, forming the basis for optimizing composite materials and the corresponding conductive layer for use in the manufacturing of aircraft structures. The development of systems for Non-destructive testing (NDT) of these specimens using the Electrical Impedance/Resistance Tomography (EIT/ERT) method is also presented. These systems are developed to detect the hidden damage in the aircraft structures caused by lightning strikes and/or any other reason.

The master's thesis is divided into eight basic parts. Chapter 1 briefly presents the aim of the thesis. Analyses of the composites, their properties, and their use in the aviation industry are presented in Chapter 2. Chapter 3 focuses on the need to use conductive composites in aircraft structures. The basic definition and equation used in impedance measurement and the most common methods of measuring impedance are introduced in Chapter 4. Chapter 5 represents the first practical part of the thesis, combining the introduction of the used measuring instrument, environment, toolbox, and description of the proposed program and measurement results. The optimization of material selection based on the measured results is also shown in Chapter 5. The lightning strike test, including test standards, test system, and results, is given in chapter 6. Chapter 7 provides a study about the state of the art of NDT methods, as well as method EIT/ERT, and introduces the development of systems for EIT/ERT measurement, mainly in the beginning stages. The last chapter is the conclusion of the thesis.

1. THE AIM OF THE THESIS

The main task of the thesis is measuring and testing specimens of conductive composites which are prepared by AVA for manufacturing the dorsal cover of the L-39NG aircraft. From the results of measuring and testing, the optimization of the conductive layer will be offered.

The first interest of this thesis is the design and realization of a measuring system for the impedance measurement of prepared specimens. Due to the large number of required measurements, it is important to design an automatic measuring system that enables remote control measuring instruments to conduct measurements automatically.

The second task is to experimentally verify the electrical properties of composite specimens' conductive layer. The specimens are made from composite structures, which are used for manufacturing L-39NG dorsal covers. The cover of the L-39NG aircraft serves as a base for the installation of the DME/TRANSPONDER antenna and the flash beacon. Therefore, it must meet the requirements for the overall resistance of the cover and electromagnetic compatibility, including connection to the surrounding structure. The suitable methodology, method, and instrument for measurement must be selected from the analysis and comparing of existing options.

On the basis of analyzing measured values, the optimization of material selection must be offered. The measured values are analyzed regarding not only the requirements for overall resistance but also the requirements for maintaining the functionality of the antennas. The requirements are defined by AERO Vodochody AEROSPACE a.s.

-

2. COMPOSITE MATERIALS

This chapter presents research on composite materials regarding their classification, as well as general advantages and disadvantages in comparison with traditional metals. The remarkable applications of composite materials in the aviation industry and technologies are also explained in this chapter.

2.1 Composite materials and their classification

A composite material (or composite) is defined as a combination of at least two materials or phases with differences in the molecular level, physical and chemical properties to give a unique combination of properties. The constituent materials of the composite are mechanically separated from each other. Each of these materials remains in its original form and retains its chemical, physical and mechanical properties although they create together properties of the composite. The resulting properties of the composite are generally better than the properties of its individual constituents because they can gain the desirable properties of each constituent [1]–[5].

The two constituents of the composite are identified as the reinforcement and the matrix. The matrix is primarily a continuous phase that fulfills function of the reinforcement binder to form shape of the component. In addition, the matrix is also in charge of other critical functions, such as maintaining the proper orientation and distribution of the reinforcements, maintaining the dimensional stability of the product, the transmission of forces to reinforcements under loading and transfer of forces between reinforcements, and protecting the reinforcements from abrasion and the surrounding environment. The matrix can be either Ceramic, Metal, or Polymer. In terms of strength and stiffness, Ceramics are the best, followed by Metal, while Polymer materials are the worst. On the other hand, Ceramic is brittle, and Metal has better ductility [1]–[5].

The properties of the matrix can affect a number of properties of composite materials. These properties are called matrix-dominated properties, which include temperature resistance, environmental resistance, damage resistance, longitudinal compression strength, transverse tensile strength, and shear strength [3].

The second constituent of the composite is the reinforcement or discontinuous phase. The reinforcement ensures strength and stiffness of the composite; therefore, it is usually much stronger, stiffer and has better mechanical properties compared with the matrix. The reinforcements can be made from various materials, such as Carbon, Graphite, Glass, Boron, Aramid, or any their combination. To select suitable materials, main considered properties of reinforcement are electrical conductivity, electrical permeability, stiffness, static strength, impact strength, fatigue performance, and thermal properties [1]–[5].

Reinforcements are divided into fiber and particle. Particulate reinforcements are characterized by equiaxed shapes, the dimensions in all directions are approximately the same, e.g. spherical, or plate shapes. Fiber reinforcements have one dimension significantly larger than the others. Due to the greatest strength along their axis of fiber, fiber reinforcements are stronger and stiffer than particulate ones, while the particulate is superior in terms of cost. Reinforcing fiber can be continuous (with high length-to-diameter ratio) or discontinuous (with small length-to-diameter ratio). The fiber form is mainly selected based on the type of applications (structural or nonstructural). For structural applications, continuous fibers are recommended to obtain better strength and stiffness, whilst discontinuous fibers are suggested for nonstructural applications because of their lower cost, greater flexibility, and being more amenable to fabrication processes (for example: weaving or forming over radii) [1]–[5].

Fig. 2.1 shows a simplified composite classification and some basic comparisons of their properties.

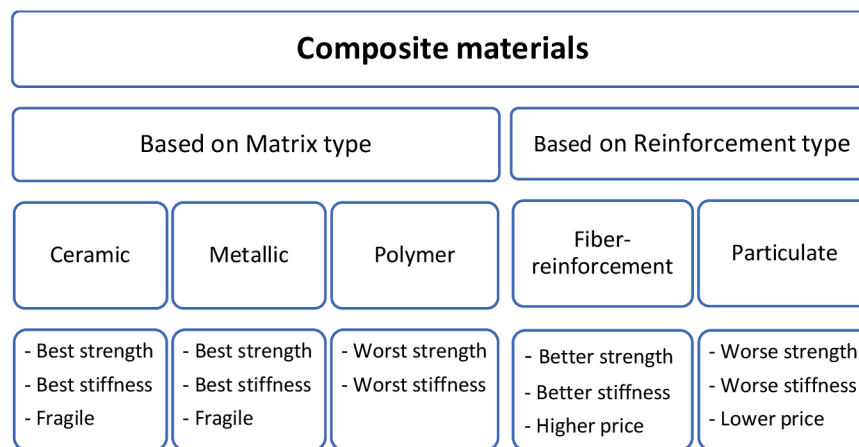


Fig. 2.1 Classification of composite material and basic comparisons

For decades, metals have been the most widely used materials in most applications. That is the main reason for the comparison of properties of composites and metals to decide if composites can be a desirably important alternative to traditional metals. The next section of the chapter will present general advantages and disadvantages of composite materials, compared with traditional metals

2.2 General advantages of composite materials

Basic advantages of composite materials over conventional engineering materials include [1]–[5]:

- **Parts integration capability:** the use of composite materials allows the replacement of several metal components with a single composite component.
- **Capability of in-service monitoring:** using sensors embedded in composite structure allows in-service monitor fatigue damages in structures, these sensor-embedded materials are called smart materials.
- **Higher specific stiffness and strength (stiffness-to-density ratio, strength-to-density ratio):** compared with traditional metals such as steel and aluminum, with the same stiffness and strength, composite materials allow weight to be reduced by 3 to 5 times.
- **Lower coefficient of thermal expansion (CTE):** by choosing proper materials and structures, it is possible to reduce the CTE to a very small value, improving the dimensional stability of the composite structure.
- **Better corrosion resistance:** traditional metals corrode in the presence of water and air, so they require special coatings or alloys. The use of suitable matrices gives the composites very good corrosion resistance.
- **Better electrical permeability:** metals are not electrically permeable, thus not allowing radio frequencies to pass through. In contrast, glass fiber, epoxy, and other materials are electrically permeable. These composites made from these materials are advantageous to use as radar cover.
- **Better stealth:** many composites are capable of significantly reducing the radar signature of aircraft. Because of this advantage, a new trend in aviation technology and industry is to use external structures made of new composite materials in fighters and other military aircraft.
- **The possibility of producing complex shapes:** complex parts in some cases cannot (or can be very difficult to) be produced from metals. However, composites make it possible to produce parts of complex shapes as a whole, thus reducing the requirements for welding and connections between individual parts. This also increases the reliability of the product.
- **Lower manufacturing costs:** the composite manufacturing process requires lower pressure and temperature than metal manufacturing or processing. Therefore, tooling costs for the production and processing of composite materials are usually much lower.

These outstanding advantages make composites become the most important and the most widely used materials in different industries and technologies. This thesis; however, will focus mainly on composite materials used in aerospace and military applications.

2.3 General disadvantages of composite materials

Beside discussed advantages composite materials suffer from a number of downsides, the most prominent of which are [1]–[5]:

- **Higher material costs:** compared with steel and aluminum at the same weight, raw material costs for composites can be 5 to 20 times higher. Besides, due to the risk of galvanic corrosion between aluminum and carbon composite, fasteners that are compatible with carbon composite (typically titanium and high-strength steel fastener) are much more expensive.
- **Sensitivity to Moisture and Temperature:** some properties of composites, mainly matrix-dominated properties, are sensitive to temperature and moisture environments, because of the degraded properties of polymer matrix. In addition, moisture can be absorbed by composites and affects their properties and dimensional stability.
- **Impact resistance, residual strength, and damage detection:** laminated composites, compared with metals, typically have lower resistance to impact damage. The individual plies may separate due to the impact, causing the reduction of the residual strength. The medium and small sized delamination caused by a minor impact can be difficult to detect with the naked eye since there may not be a visual indication of the delamination.
- **Thermal and electrical conductivity** of composite materials depends on their constituent. Thermal and electrical conductivity requirements depend on the application and must meet a compromise with other requirements. That is the reason why sometimes there are problems. For example, the composite material of glass fiber and epoxy matrix is used for the production of L-39NG aircraft covers because it meets the requirement of mechanical properties. However, it is an electrical insulator, so it does not meet the requirements for protection against lightning strike and EMI. As a result, it is necessary to modify the structure of the composite with a suitable method in order to meet the requirements of electrical conductivity.

In addition, the use of composite materials currently has another significant obstacle. The properties of the composite depend on its constituent and structure to a large extent. A small change in constituent or structure can significantly change the properties of the composite. Therefore, there is currently a great lack of technological and technical databases of the composite. In contrast, the properties of traditional metals have already been clearly defined when there are a number of databases, handbooks, and recommendations for designing parts and products with metals.

Some of these above limitations will be solved in this thesis, which focuses on automatically measuring the properties of new composite to optimize the material selection, and on Non-Destructive Testing (NDT) to monitor the health or detect the defect of structures made from composite.

2.4 Composite materials for aircraft structures

For decades, metals and their alloys have played an important role in the aerospace industry. Aluminum was a prominent material during the First World War. Steel was also used, but to a lesser extent. Titanium and nickel have been used since the 1970s. The use of metals in place of former aviation materials such as wood, cloth and twine began when aircraft speed began to increase significantly, and the strength and wind resistance of aircraft had to be improved [2], [3], [6]–[9].

However, aerospace technology and industry still need better materials that allow eliminating a number of disadvantages of metals and their alloys, and aerospace is one of the first to realize the benefits of using composites. Disadvantages of metals and their alloys include high weight, susceptibility to corrosion and maintenance requirements. In aerospace applications, the weight of structures is an important determinant of their performance. From the early 1960’s, the U.S. Air Force’s studies promised that using boron composite and aerospace structural application provided a weight savings of 25 to 50 percent. From these results, composite materials began to be used in the aerospace industry from the second half of the 1970s. Due to the advantage of low-weight, composites helped missiles, airplane, and rockets to fly faster, higher, and farther, and to use fuel more efficiently. Fig. 2.2 presents the use of composite materials in the aerospace industry in both military and civilian aircraft [2], [3], [6]–[9].

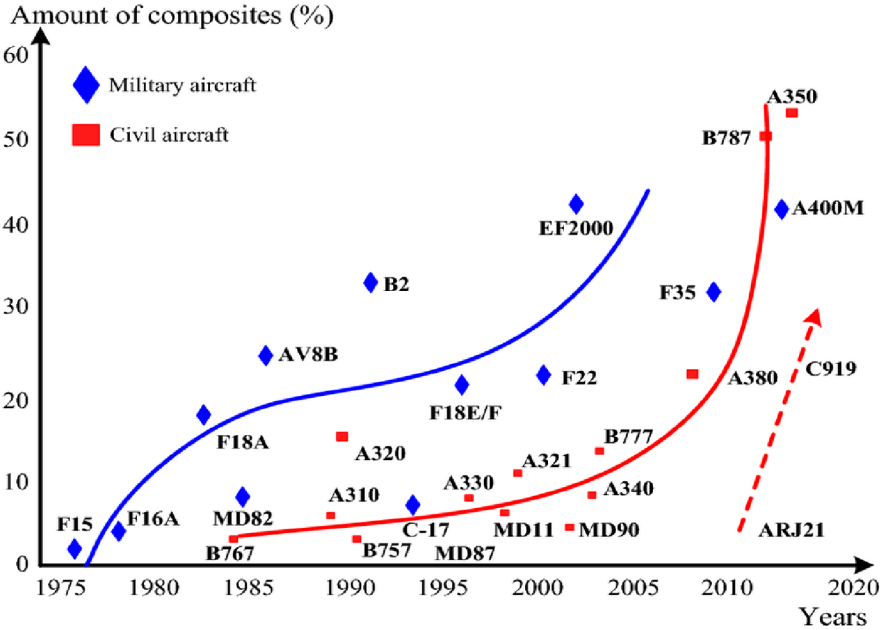


Fig. 2.2 Composite materials in aircraft [10]

2.4.1 Civil aircraft

In the 20th century, as shown in Fig. 2.2, composite materials were used in civil fixed wing aircraft in a very limited proportion, mostly around 10% of total weight, while in military aircraft this proportion already reached value around 30%. Since the beginning of the 21st century, civil aircraft have increased the use of composite dramatically. The weight proportion of used composites in civil fixed wing aircraft increased to a similar, and ultimately greater than it in military. The reason can be the reduction in the manufacturing cost of composite materials, the improvement of carbon fiber and epoxies’ properties, and the requirements to reduce aircraft emissions. [4].

The first example is Boeing 787 Dreamliner aircraft – see Fig. 2.3 – in which more than 50% total weight is produced from composites. Compared to the former Boeing 777 aircraft, the proportion of aluminum and its alloys was significantly reduced, from more than 60% to 20%. On the contrary, the weight proportion of the composite increased considerably, from 10-15% to 50%. According to data from Boeing, using composite on the Boeing 787 not only reduces weight by 20% compared to using aluminum, but also saves up to 50,000 rivets on each aircraft. Any location with rivets would require maintenance and inspections as a potential failure site. The use of composite; therefore, significantly reduces maintenance requirements.

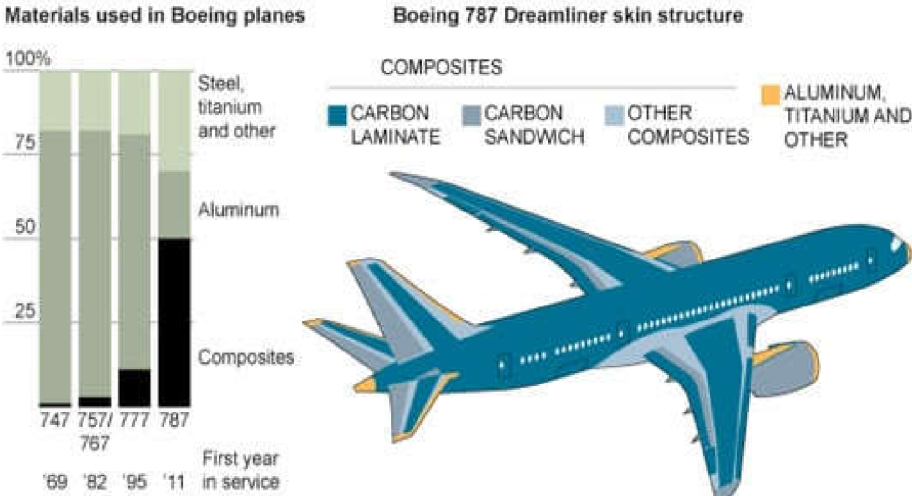


Fig. 2.3 Boeing 787 Dreamliner [11]

Fig. 2.4 presents trends in the use of composites on Airbus fixed wing aircraft. The composite weight ratio has increased steadily, from around 5% in the 1970s to more than 50% in 2013 (for the A350 XWB). It can also be seen that almost the entire wings, the belly fairing, and the empennage of the A350 XWB are made of composite. According to data from Airbus, the use of composite reduces the maintenance costs of the aircraft structure by up to 50%. The wing inspection is required once in 12 years compared to 8 years for the A380.

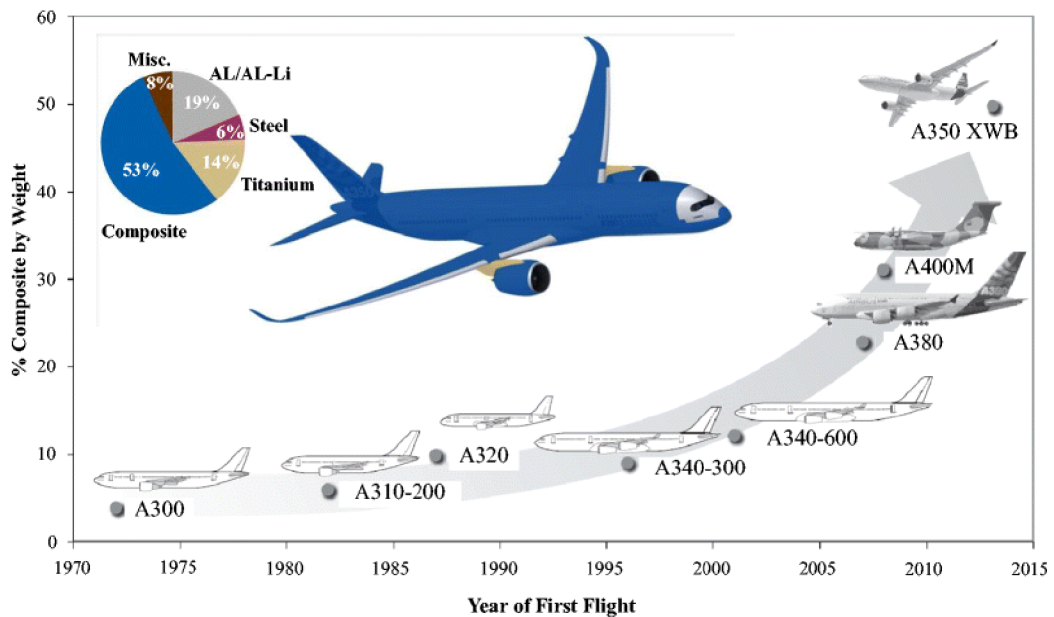


Fig. 2.4 The trend of using composite on Airbus fixed wing aircraft [12]

2.4.2 Military aircraft

Military aircraft used composite materials earlier than civilian aircraft; the application of composites in military aircraft can be considered to start in the 1970s – Fig. 2.2. At this time, the historically famous military aircraft manufacturer McDonnell Douglas used composite materials on combat aircraft. F15 with a very small percentage, only a few percent. In the 1980s, the weight ratio of F18 fighters increased to about 20%. Lockheed Martin started using composites on their aircraft around the same time as McDonnell Douglas, on the F16 fighter jets. In their state-of-the-art F35 aircraft, the weight ratio of the composite already reaches 35%. Fig. 2.5 shows the use of composite on the Lockheed Martin F-35, in which covers, wings, underbody hangers, fuel tanks and other critical aircraft parts are made of composite materials [4], [9], [13], [14].

The main advantage, which is also the reason why composite is preferred in military aircraft over conventional materials, is light weight and better stealth (better radar signature). The newly developed composite material for military aircraft was reported to be able to absorb up to 95% of the incident electromagnetic radiation of radars. In addition, existing stealth coatings for military aircraft require periodical maintenance and repainting. The use of structural radar-absorbing material will significantly reduce maintenance requirements and costs [4], [9], [13], [14].

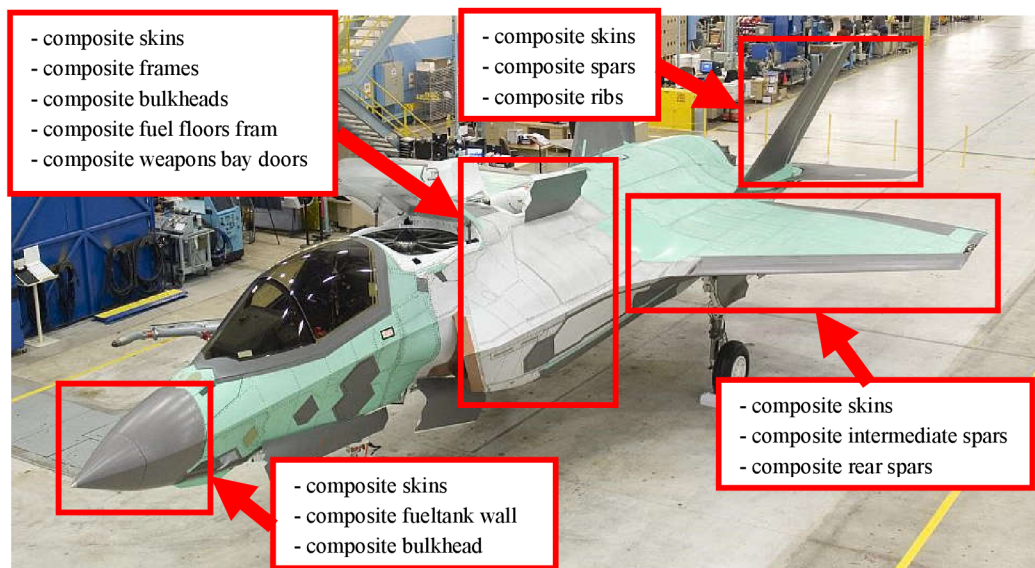


Fig. 2.5 Composite materials in F35 fighter [15], [16]

2.4.1 Czech aircraft

The Czech aviation industry does not lag behind current trends. One of the latest projects of Aero Vodochody Aerospace a.s. (AVA) is developing a new generation of the L-39NG jet trainer – see Fig. 2.6. The design of the aircraft is based on the legendary L-39 airframe, which was produced for almost 40 years and delivered to the air forces of 36 countries around the world, including the air forces of the Czech Republic and the Socialist Republic of Vietnam. Besides the change in avionics and engine systems, AVA also focused on optimizing the L-39NG airframe using composite materials.

The use of composite material in L-39NG provides new-generation aircraft with lighter weight and higher resistance to corrosion, which increases the lifespan of the airframe. To compare, the empty weight of L-39NG is 3100 kg, while the empty weight of L-39C is about 3500 kg. Despite having lighter empty weight, L-39NG has a higher maximum take-off weight (5800 – 6300 kg) than L-39C (4700 kg). The lifespan of the airframe is also increased from 3000-4500 flight hours (in L-39C) to more than 15000 flight hours. Structures made from composite in the aircraft L-39NG can be seen in Fig. 2.6. The development of new composite materials is effortfully focused on, which will orient towards optimization of the material's electrical properties [17]–[22].

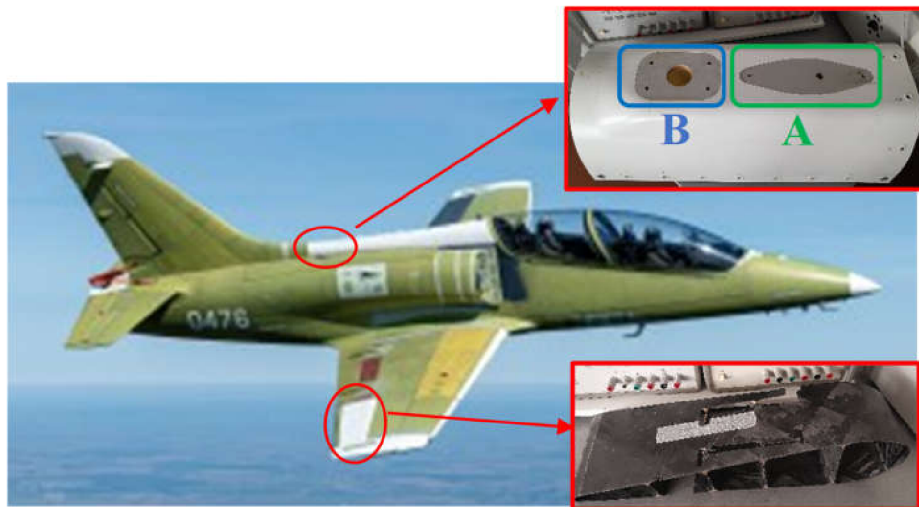


Fig. 2.6 Jet trainer L-39NG – the white structure is made from composite [18]

As shown in Fig. 2.6, the dorsal cover and the wings of L-39NG aircraft are made from composite. In the dorsal cover, aluminum plate A serves as the base for the installation of the flash beacon, while aluminum plate B is the base for the installation of the DME/TRANSPONDER antenna. The used composite must meet the requirements for the overall resistance of the cover, while not affecting the antenna functions. The conductive composite structure will be discussed in the next chapter; however, it is based on using additional metallic mesh. The window size of metallic mesh depends on the operating frequency of the antenna. The DME/TRANSPONDER antenna operates in the 960-1215 MHz ARNS (Aeronautical Radio Navigation Service) frequency band. To not affect the operation of the antenna, the size of the metallic window now cannot be smaller than the wavelength of the antenna signal, in this case, is about 246 – 312 mm.

2.5 Chapter conclusion

This chapter provides a study of composite materials, including their basic definition, general advantages and disadvantages. The use of composite materials for aircraft structures is also presented, showing the rapidly increasing of interest in using composite as primary aircraft structures. The Czech aircraft industry's interest in using composite materials is also presented by the L-39NG showcase. However, the conventional composite structure with fiberglass has the limitation of low electrical conductivity, causing a number of issues when used as primary aircraft structures. The next chapter will describe these issues in detail and show the importance of conductive composite materials in the aircraft industry.

3. THE NEED OF CONDUCTIVE COMPOSITE

This chapter presents the study of conductive composites in aircraft structure, their importance, and technologies and techniques to achieve small, but enough electrical conductivity used in aircraft industry.

3.1 Electric power distribution

Composite materials, as discussed above, have the disadvantage of having small electrical conductivity. Therefore, composite aircraft suffer from a number of challenges regarding their poor electrical conductivity, the main ones of which are electric power distribution, control of static electricity, and lightning strike. This subchapter will focus on problem of electric power distribution in composite aircraft [23].

3.1.1 Challenges of composite aircraft

Almost all power distribution systems of aircraft consist of a single wire that is connected to the positive output of the battery and/or generators. The distribution of negative output is taken in charge by the airframe which is usually called the ground – see Fig. 3.1. This energy distribution topology is called a negative-ground power distribution system, or single-wire system. The other topology is called a two-wire system which uses two wires (one positive and one negative) to distribute the electric power for electric equipment of the entire aircraft [23]–[25].

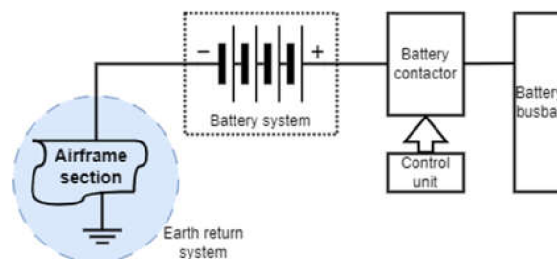


Fig. 3.1 Aircraft single-wire power distribution system [25]

Traditional aircraft were made of metal, mainly aluminum. The small electrical resistance of aluminum allows the aircraft fuselage to carry the current easily to distribute negative voltage throughout the entire aircraft. One of the main reasons that composite materials are preferred in manufacturing aircraft structures is to reduce the aircraft's total weight. However, the low electrical conductivity of composite materials leads to the need of more cables and conductive structures to maintain the distribution of electrical energy, which can cause a significant increase in the aircraft's total weight. In addition, the current trend of fly-by-wire in aerospace applications also increases the stress on electrical energy distribution. For example, the Airbus A380 airliner has up to

100000 wires with more than 40000 connectors. These huge numbers of cables have a total length of nearly 500 km with a weight of 5700 kg. In addition, the harness-to-structure mounting materials such as hooks and cable ties have also weighed up to nearly 2000 kg. The Boeing B787 also has approximately 500 km of wires with a total weight, including their harness materials nearly 7400 kg, which is about 3% of total aircraft weight. It is obvious that the composite used for aircraft structure must have good electrical conductivity to reduce the total weight of aircraft effectively [24], [26], [27].

3.1.2 Solution – conductive composite as ground plane

As discussed above, due to the low electrical conductivity of composite materials, composite aircraft must face challenges of negative voltage distribution over the airframe. One of solutions is using two wires topology. However, due to the fly-by-wire trend, modern aircraft use more electric and electrical devices, two-wire topology significantly increases the total weight and complexity of power distribution systems [23]–[27].

Another notable solution is to modify the structure of the composite to achieve a conductive composite material. The most common modification is to integrate one or more layers of metal window screens (usually aluminum window screens) into an existing composite structure during manufacturing. These layers form the path for negative voltage distribution; hence, they are called ground. To maintain power distribution to all equipment and the entire airframe including the control panel and electrical equipment racks, structural flooring and bulkheads must be covered by the ground [23]–[27].

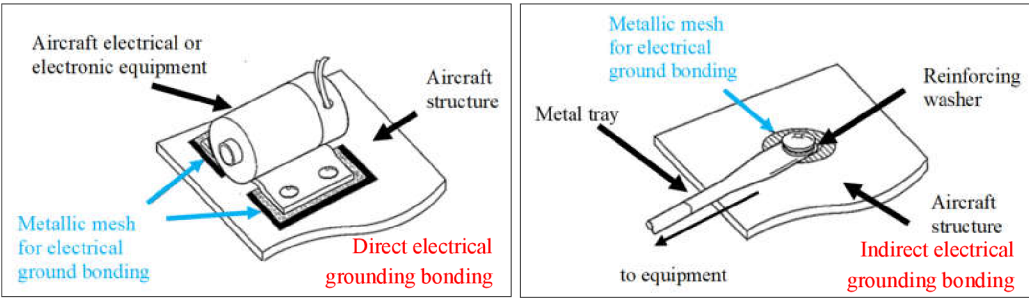


Fig. 3.2 Direct (left) and indirect(right) electrical ground bonding [23]

To bond electric equipment easily, the ground plane must be located toward the inside of the aircraft. Fig. 3.2 shows two methods to connect the electrical equipment to the ground plane. The first one, the direct electrical bonding method, mounts the equipment adjacent to the ground plane, and the equipment is mounted directly to the ground plane. The second method, indirect bonding, is used to connect equipment that is not adjacent to the ground plane by using a flexible metal tray (bonding jumper) [23].

3.2 Lightning strike protection

The other critical challenge of composite aircraft is lightning strike protection (LSP). Lightning strike on airplanes is not a rare phenomenon. On average, an aircraft can be struck once to twice a year, depending on its operability and location. A lightning strike on an aircraft can be remarkably endangered if it is not properly managed, so it is a dangerous risk that needs carefully considering [7], [28]–[33].

3.2.1 Test standard and specification

Lightning strike protection (LSP) in aerospace applications has already been paid attention to since the 1950s. In the mid-1950s, the first airplane LSP test standards and specifications were published by the United States (US) Federal Aviation Administration (FAA) and the US Department of Defense (DoD). One of these is MIL-B-5087B specification, which deals with bonding, electrical, and LSP for aerospace systems. Bonding is used not only for the electrical interconnection and installation of aircraft electrical and electronic equipment but also used as the solution for LSP [34]–[37].

However, in the 1960s, a number of aviation disasters caused by lightning strikes were reported. For example, in December 1963, all 81 passengers and crews on a Boeing 707 commercial airliner were killed after a lightning strike ignited fuel in the reserve tank on the left wings of the aircraft. In May 1965, an air force C-130 was struck to radome by lightning. The strike punctured an eight-inch hole in the radome, set a pylon on fire, and damaged the radar equipment. Fortunately, there was not any human damage. These reported accidents particularly urge to improve the existing LSP design and test standards. The Society of Automotive Engineers (SAE) Committee on Electromagnetic Compatibility (SAE AE4) was requested to formulate improved standards. In 1976, the first report named Lightning Test Waveforms and Techniques for Aerospace Vehicles and Hardware (or SAE AE4L-76) was published. Its revised version SAE AE4L-78 was also published two years later. These reports were immediately used as a standard for both civil and military aircraft by the US. A number of certification agencies in other countries and regions also adopted these reports.

Table 3-1 Standards and specifications covering aircraft LSP [36]

Category	General	Military aircraft	Commercial aircraft
Lightning environment	STANAG 4236 MIL-STD-464	MIL-STD-1795A	ED-84/ARP 5412
Requirements on equipment	STANAG 4327		RTCA/DO-160 ED-84/ARP 5412
Design requirements		STANAG 3659 MIL-STD-1795A	ED-84/ARP 5414

A list of existing standards and specifications according to their categories and covering area is shown in Table 3-1. Since most standards and specifications have short, non-specific guidance, and even lack guidance, to achieve the requirements efficiently in these standards and specifications, it is important to create suitable guidance documents. The SAE Lightning committee (SAE AE2) and the European Organization for Civil Aviation Equipment (EUROCAE) Working Group 31 (EUROCAE WG31) were assigned to discuss and publish such guidance or recommendations. The most important recommendations can be referred to as ED-84/ARP 5412 (Aircraft Lightning Environment and Related Test Waveforms) and ED-91/ARP 5414 (Aircraft Lightning Zoning). These recommendations provide the interaction of lightning with aircraft, in terms of lightning zoning(ED-91/ARP 5414) – as shown in Fig. 3.3, and the waveform (ED-84/ARP 5412) – as shown in Fig. 3.3. The definition of each lightning zone including corresponding applied current waveform is shown in Table 3-2 [30], [34]–[37].

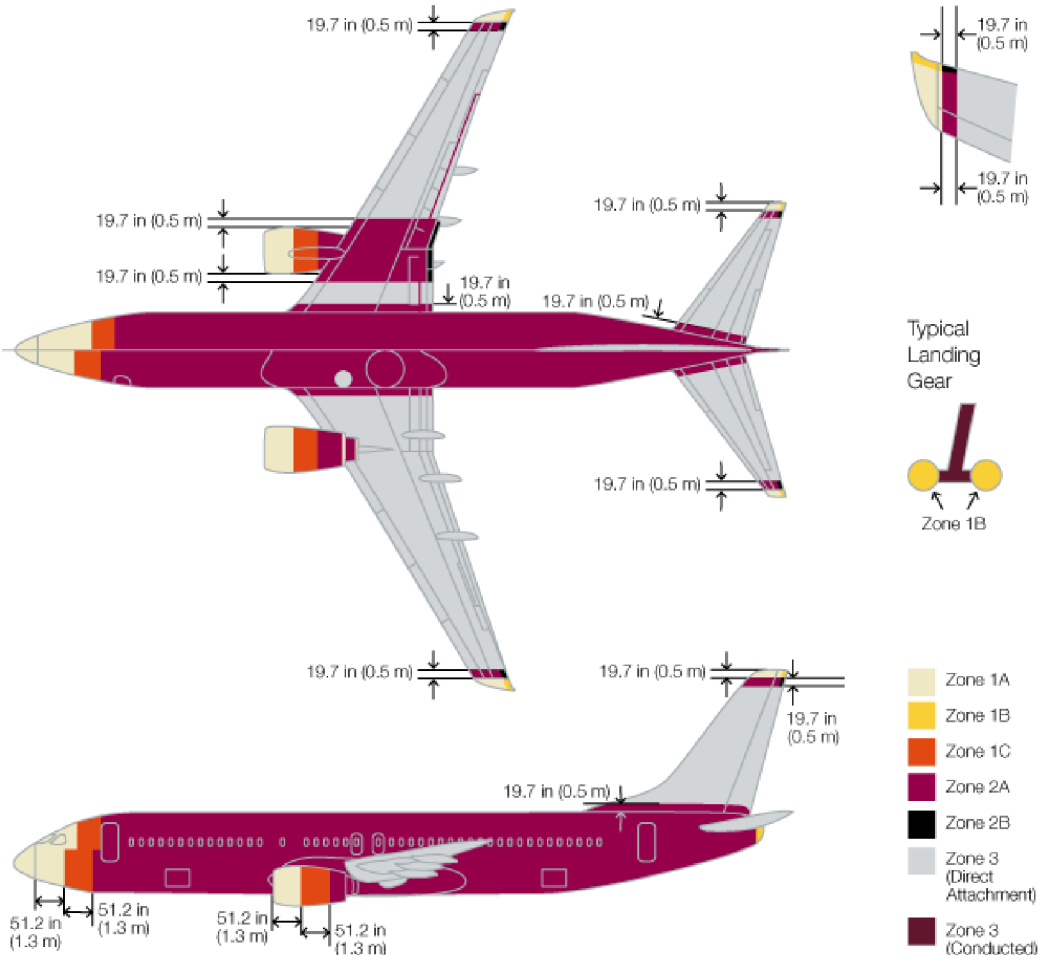


Fig. 3.3 Aircraft lightning zone according to ES-91/ARP 5414 [38], [39]

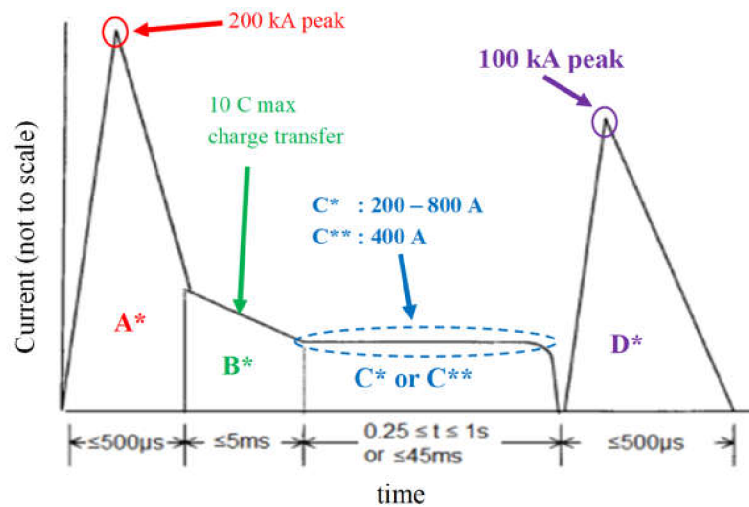


Fig. 3.4 Lighting wave form according to ED-84/ARP 5412 [28]

Table 3-2 Lightning zone definition and corresponding current waveform [28], [39]

Aircraft zone	Description	Definition	Current components
1A	First return stroke zone	All areas of the airplane surfaces where a first return is likely during lightning channel attachment with a low expectation of flash hang on.	$A^*+B^*+C^{**}$
1B	First return stroke zone with a long hang on		$A^*+B^*+C^*$
1C	Transition zone for first return stroke zone	All areas of the airplane surfaces where a first return stroke of reduced amplitude is likely during lightning channel attachment with a low expectation of flash hang on.	
2A	Swept stroke zone	All areas of the airplane surfaces where a first return of reduced amplitude is likely during lightning channel attachment with a low expectation of flash hang on.	$D^*+B^*+C^{**}$
2B	Swept zone with a long hang on		$D^*+B^*+C^*$
3	Strike locations other than Zone 1 and Zone 2	Those surfaces not in Zone 1A, 1B, 1C, 2A, or 2B, where any attachment of the lightning channel is unlikely, and those portions of the airplane that lie beneath or between the other zones and/or conduct a substantial amount of electrical current between direct or swept stroke attachment points.	$A^*/5+B^*+C^*$

3.2.2 Mechanism of aircraft lighting strike

There are two mechanisms of lightning strikes on aircraft. The first one that is more frequent (up to 90% of aircraft lightning strikes) is lightning triggered by the presence of aircraft in a region with an intense electrostatic field. In general, the electrostatic field in thunderclouds is much less than this breakdown value which is about 3 MV/m. However, this electrostatic field will polarize any object inside its region; in our case, it will polarize the aircraft. Due to the fact that the electrostatic field is enhanced locally at the sharp points of the object, the electric field near aircraft surfaces with high enough curvature, such as wing tips, pitot tubes, and nose tips, may reach values higher up to 10 times the ambient field. Fig. 3.5 indicates the 2D electrostatic model of an aircraft in an ambient field calculated by Morgan et al. in [30]. It is obvious that the aerodynamic shape of aircraft can amplify the electrostatic field significantly, even to the break-down limit of air, and cause a lightning strike. The second mechanism is rarer, accounting for only about 10% of all events. It occurs when one or more branches of natural lightning are intercepted by an aircraft [28]–[33].

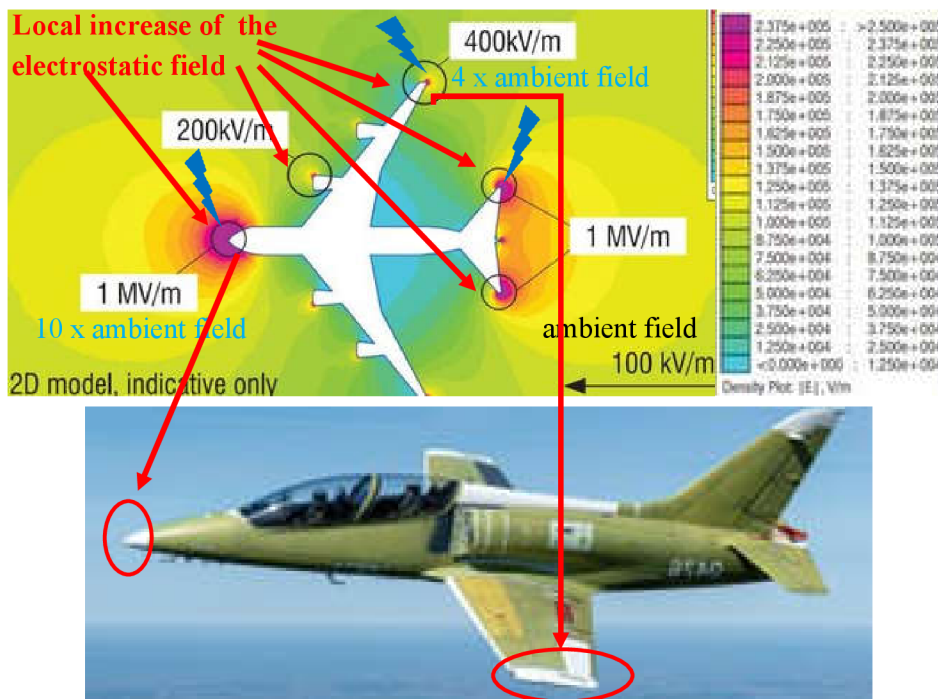


Fig. 3.5 Indicative 2D electrostatic model of an aircraft in ambient field [29], [30]

The bi-directional leader theory is often used to explain the mechanism of lightning strikes. Because of the floating characteristic of an in-flight aircraft, the aircraft will become a part of the lightning current path (between two clouds, or between a cloud and the ground). Hence, during the lightning strike, there are two

attachment points in the aircraft surface: one entry point and one exit point for the lightning current.

It is important to consider that during the strike, the aircraft moves relatively to the lightning current path. As a result, attachment points are stretched along the aircraft fuselage. If the gap between the lightning current path and the aircraft surface is broken down, a new attachment point is formed. Therefore, during a lightning strike, the aircraft will be struck, not once but several times, until the aircraft escape from the region of thundercloud. This phenomenon is called lightning swept stroke. The typical lightning current waveform during lightning swept stroke is shown in Fig. 3.6. [28]–[33].

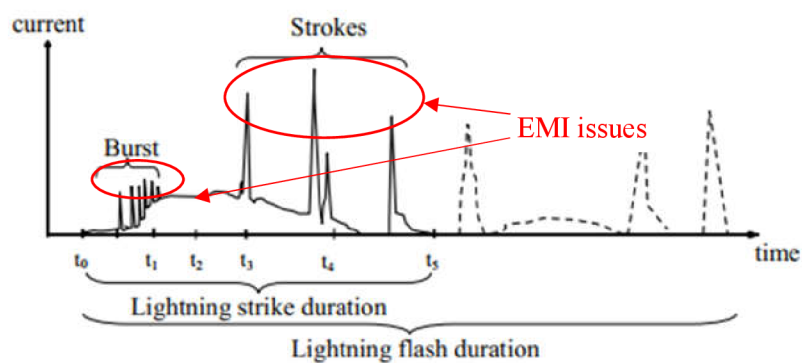


Fig. 3.6 Typical lightning current waveform during lightning swept stroke [29]

3.2.3 Aircraft lightning strike impacts

Aircraft lightning strikes might cause various serious impacts on the aircraft, which can be categorized into direct effects and indirect ones. While direct impacts concern physical damage happening at attachment points of lightning current, indirect effects are related to the interference due to electromagnetic coupling (EM coupling) with electrical/electronic systems and cabling. As shown in Fig. 3.6, the lightning current waveform can be composed of a large number of high current peaks. The electric current injects at the entry points and then flows through all electrically conducting parts to reach exit points. The high current peak; therefore, might cause through EM coupling remarkable electromagnetic interference (EMI) to the aircraft's electrical and electronic equipment [28]–[33].

The main focus of the thesis; however, is on the direct effect of lightning strikes on aircraft structures, which causes physical damages to structures and external devices, at the attachment points. Direct impacts have complex origins including different constraints. The main constraints can be categorized into thermal constraints and mechanical constraints. Furthermore, direct effects of a lightning strike also include other constraints such as sparking at the fastener or junction, or break of the dielectric at the attachment points of lightning [28]–[31].

Thermal constraints have three main mechanisms. The first one is related to Joule heating, so the heat is generated in the volume of the material and amount of generated heat is proportional to material resistance. The second mechanism is direct heat flow from the lightning arc, occurring at the attachment points. This constraint is a combination of heat flux by conduction and heat flux by electron or ion recombination. The last mechanism is radiated flux of the heat emitted by the lightning path. Thermal constraints are applied not only at the attachment points but also in any aircraft part through which a high lightning current flows. The consequence can be erosion, deformation, or puncture of the fuselage at the attachment points. The heat generated can also cause the explosion of the conductor [28], [29], [40], [41].

Mechanical constraints are also applied in both lightning attachment points and any other part through which a high lightning current flows. Mechanical constraints also have three main mechanisms. The first component is overpressure resulting from the explosion of the lightning channel. The explosion comes from a rapid increase in temperature (within a few microseconds) and generates the propagation of a strong shock wave (in the radial direction of the arc). The second one is called magnetic force which is caused by current circulation. Magnetic force contributes a significant part to the mechanical constraint on both materials and in the arc column. The current flowing in the volume of materials also causes a mechanical constraint on the skin, which is called the magnetic pressure effect. The last mechanism is the expansion of structure caused by a very fast increase in material temperature, which gives also other contributions to the mechanical stress of aircraft structure [28], [29], [40], [41].

The lightning direct impact on bare metallic structures is usually very low thanks to their low resistance. In almost all cases, the damage is insignificant with small burning marks and pitting. The painted metallic structures; however, have more significant damages due to the concentration of the arc in the attachment location. The consequence can be melting of the structure, even puncture (if the material is thin enough). Although the puncture size, in any case, is small ($\phi \leq 10$ mm), it can cause a catastrophe accident if the puncture is in the fuel tank area. Therefore, for civil aircraft, the minimum required thickness of aluminum skin is 2 mm [28], [29], [41], [42]. The lightning direct impact on the bare metallic structure is shown in Fig. 3.7

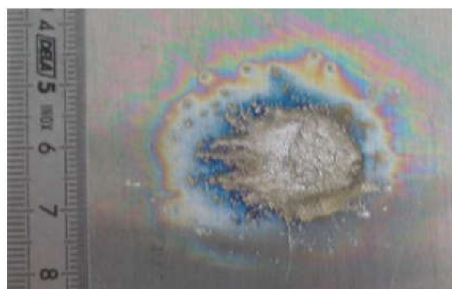


Fig. 3.7 Lightning direct impacts on bare metallic structure [28], [42]

Damages caused by lightning direct impacts on composite structures are usually more serious than on metallic structures. The main reasons are limitations on the electrical and thermal conductivity of existing composite materials. The damage to the composite structure can be divided into three major states:

- fiber breakage, damage, and sublimation
- resin deterioration,
- delamination of the composite [28], [29], [41].

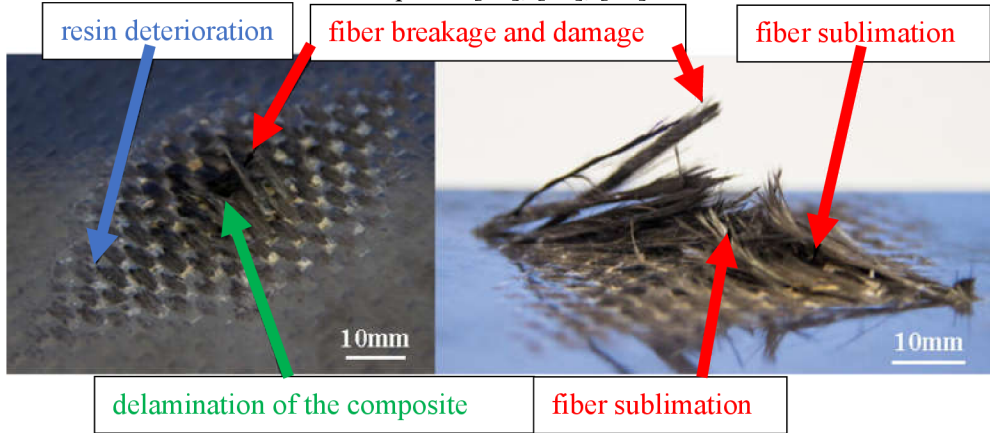


Fig. 3.8 Lightning direct impacts on composite material [43]

Fig. 3.8 shows an example of lightning direct impacts on composite material. It is clear that the first two states, fiber brake(or damage) and resin deterioration, are surface damages caused mainly by the effect of very high temperatures (up to 30000 K). The last one, delamination of the composite, is structural (or core) damage and related to the overpressure given by the explosion in the surface and the propagation of strong shockwave. It is important to consider that the surface damage or visible damages often have small area; however, the core damages, or hidden damages, due to the delamination of the composite, can be much wider (up to thousands of times) and more serious. That is because it can cause significant degradation of structural properties and impact flight safety [28], [29], [41]–[43]. Fig. 3.9 shows the analysis of lightning damages in a composite structure, which clearly shows serious damages caused inside the composite by the delamination of the composite.

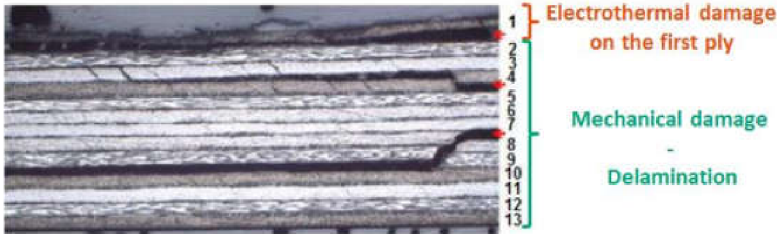


Fig. 3.9 Lightning damage analysis [28]

Another important thing, as in the case of metallic structures, is the paint or any other dielectric layers on the surface of the composite has remarkable effects on structural damage. Several researches and tests conducted by Airbus emphasized that the paint thickness affects the damage's seriousness. The reason is the same as in metallic structures since the dielectric layer prevents the free spreading of the lightning arc. The energy; therefore, is concentrated at attachment points and causes more significant damage, even puncture – as shown in Fig. 3.10 [28]

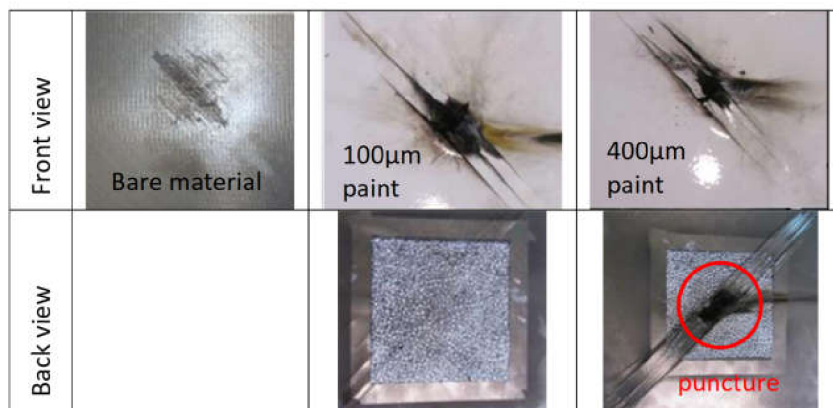


Fig. 3.10 Damage on bared and painted composite structures [28]

3.2.4 Solution – conductive composite

As discussed above, it is an emergency challenge to protect composite aircraft against lightning strike damage. There are a number of LSP technologies have been developed for this goal, which can be categorized into 3 main methods:

- wire banded shields,
- ground strap,
- composite structure modification [39].

The first two methods are easier and save research and development (R&D) costs and time. Therefore, they are suitable as temporary solutions in prototype. For example, in the first versions of L-39NG, the ground strap method is currently used. However, they increase the total weight, and more importantly, increase the complexity of the cable system in the aircraft. The complexity of the cable system in an aircraft can be a significant factor affecting the efficiency of aircraft maintenance, thereby reducing flight safety and the lifetime of the aircraft [39].

The most attractive and effective method; however, required longer and more expensive R&D is a modification of the composite structure. The first way to modify the non-conductive composite structure to a conductive one is using surface metallic protection. The basic principle of using surface metallic protection is to force the lightning current to flow through the protection layer instead of the structure. The metal layer has higher conductivity so that the lightning current can be more easily spread and

does not cause significant damage to the structure as well as protection layers. The additional function of metallic layers is that provide EMI shielding for the aircraft's electronic equipment [23], [28]–[30], [33], [35], [38], [39].

For LSP and EMI shielding purposes, it is obvious that continuous metallic foil is the best selection. However, the continuous metallic foil has issue of drapability, which cause wrinkles during manufacturing. Another and more important issue are adhesion to the original composite structure. To solve the wrinkles issues, metallic deposition technologies such as Physical Vapor Deposition (PVD) or Chemical Vapor Deposition (CVD), which are familiar technology in microelectronic, can be applied. Nevertheless, the cost and complexity of these technologies can be remarkable issues in production large structures. The most used technique to solve adhesion, as well as wrinkles issues, is to create areas that have no metal, so matrix can flow and bind the metallic layer with other reinforcement layers together. Examples are the use of expanded metal foil or metallic mesh. In comparison, expanded metal foil is made from a unique foil while metallic mesh is made of different wires that meshed. Therefore, the metallic mesh has worse conductivity due to contact resistance between different wires. In the same principle, it is possible to use metallic coated fiber for LSP and EMI shielding. However, this solution is shown that has less LSP effectiveness. Measured results in this thesis found in the next chapter also show the similar conclusion [28], [29], [38], [41], [42].

Another way to achieve a sufficiently conductive mixture which is the most discussed method in recent times is the addition of conductive fillers to the nonconductive matrix. The most attractive conductive fillers are Carbon nanotubes, Graphene, or metal particles. However, the LSP and EMI shielding effectiveness of these materials is still controversial. For example, in 2019, Boeing decided to change the LSP structure in the B787. The copper foil in LSP structures was removed and wing fuel tanks were protected only by carbon composite– as shown in Fig. 3.11. However, these changes were rejected by the Federal Aviation Administration (FAA). Although FAA changed its decision later, these changes have been discussed until now, especially after the two Boeing 737 MAX crashes. It was also reported that the addition of conductive filler to the matrix affects the mechanical properties of laminates thus causing detriment to the design [12], [28], [30]–[33], [38], [39], [43]–[45].

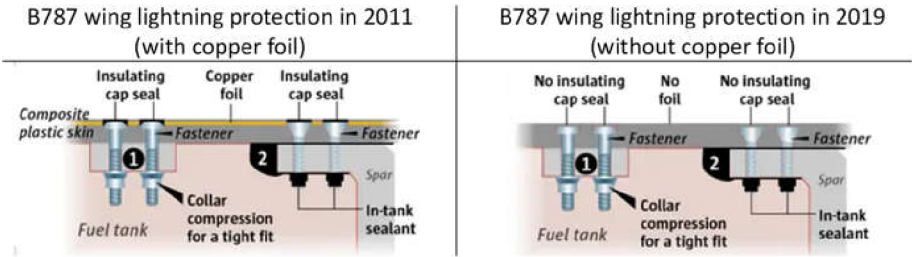


Fig. 3.11 Changes to lightning protection in Boeing B787

3.3 Chapter conclusion

This chapter presents emerging challenges in composite aircraft due to the electrical non-conductive property of conventional composite materials. The two most serious issues are electric power distribution and lightning strike protection. Electric power distribution systems in composite aircraft can increase the total weight and the complexity of cabling in the aircraft, then affect the maintenance. The more dangerous risk can be referred to as lightning damage. Therefore, test standards and specifications to achieve aircraft lightning protection are presented. Then, the lightning strike, including its mechanism and impact on aircraft is carefully discussed. Finally, methods to protect composite aircraft are described. The most interesting method is modifying the composite structure to achieve enough electric conductivity by adding expanded metal foil or metallic mesh to the composite structure. Carbon composites, which are the most regularly discussed composite recently, are also an attractive solution, but must be demonstrated more. The EMI shielding issue is also briefly mentioned as an issue related to lightning strike protection. This thesis is related to solving a similar issue. The main goals are to compare the conductivity of different composite specimens with metal expanded foil and metallic mesh to optimize their selection and test the lightning protection ability of these specimens. For these goals, the next chapter will discuss the electrical impedance measurement which will be used in the practical part of the thesis.

The lightning strike testing and results will be discussed in Chapter 6. However, Fig. 3.12 shows the damages caused by the 400 kV lightning strike test, which was realized in the practical part of the thesis. Can be seen clearly the effect of using metallic mesh as the additional layer for lightning strike protection of composite material. The damage on the surface without metallic mesh was seriously larger, while the damage on the protected surface is almost negligible. The testing results will be discussed more in Chapter 6, including the dependence of damages on the polarization and amplitude of lightning trike.

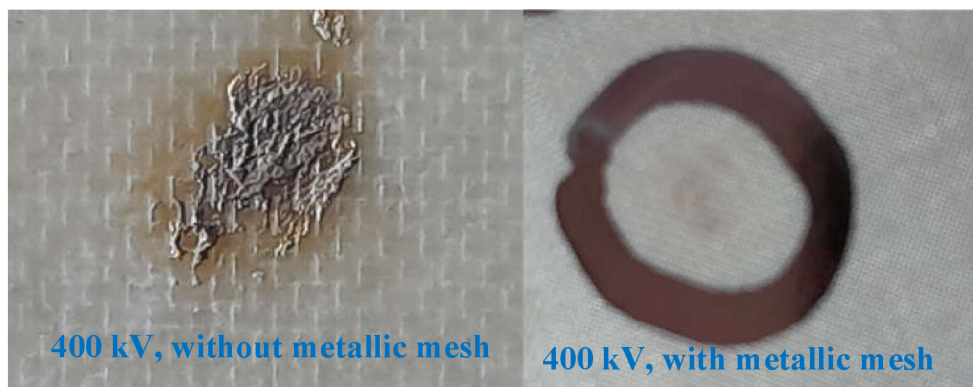


Fig. 3.12 Damages caused by lightning strike in fiberglass composite

4. ELECTRICAL IMPEDANCE MEASUREMENT

The first measurement is measuring electrical impedance of the material specimens prepared by AVA. This chapter introduces methods for impedance measurement.

4.1 Impedance measurement methods

There are a number of methods to measure impedance, each of which has advantages and disadvantages. This sub-chapter will present and compare the most used methods to select the most suitable method to measure characteristics of material specimen. These most used methods are [46]

- Wheaton Bridge method,
- resonant method,
- I-V method,
- RF I-V method,
- network analysis method,
- auto-Balancing Bridge method.

4.1.1 Wheaton bridge method

The principle of this method is very simple and presented by circuit in Fig. 4.1. When no current flows through detector D, the value of the unknown impedance Z_x can be determined by

$$Z_x = \frac{Z_1}{Z_2} Z_3, \quad (4.1)$$

where Z_1 , Z_2 and Z_3 are the impedances of other known elements which can be any combination of resistors, capacitors, and coils [46]. Because of this principle, the method is referred to as the null method in some literature.

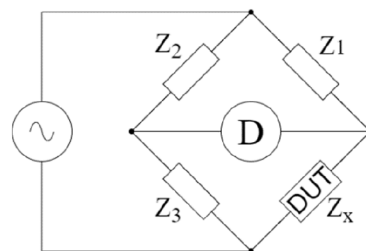


Fig. 4.1 Wheatstone bridge method [46]

The advantages of this method are the simple principle and high accuracy. However, it requires manual adjust of known elements so that the current flowing through the detector is zero; therefore, it is not suitable for a large number of measurements.

4.1.2 Resonant method

By adjusting the value of capacitor C in Fig. 4.2, it is possible to turn the circuit to resonant mode. In this state, the unknown values of L_x and R_x are determined using the value of the capacitor, the frequency of the test signal and the quality factor Q [46].

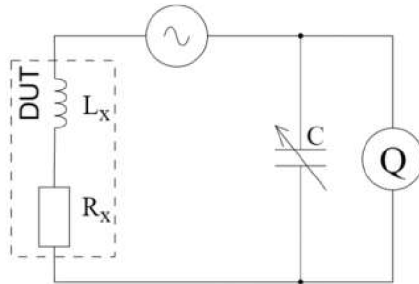


Fig. 4.2 Resonant method [46]

In terms of development, the resonant method is one of the oldest methods, and in terms of theoretical knowledge and experimental experience, it is one of the most demanding methods. Therefore, this method is no longer commonly used nowadays.

4.1.3 I-V method

The I-V method works on the basis of Ohm's law, and its principle is shown in Figure 3.4. The unknown impedance is then determined by the relation

$$Z_x = \frac{V_1}{I} = \frac{V_1}{V_2} Z_0, \quad (4.2)$$

where V_1 and V_2 are the voltage drops across the known impedance Z_0 and the unknown impedance Z_x , I is the current flowing through these impedances.

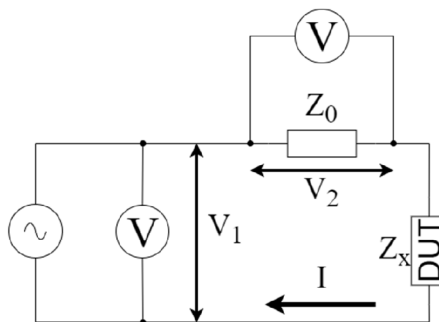


Fig. 4.3 Principle of I-V method [46]

In practice, the low loss transformer is preferred as a known impedance than resistor to prevent the effects of a low value resistor in the circuit. The main advantage of this method is the simple principle and connection. On the other hand, the measuring frequency is limited by the transformer used [46].

4.1.4 RF I-V method

This method is essentially an I-V method with modifies to measure in the higher frequency range, especially for measuring radio frequency (RF) components. Therefore, impedance-matched measurement circuits (typically 50 Ω) and precision coaxial test ports are used. Fig. 4.4 shows 2 different connections:

- the connection on the right is used for low-impedance measurements, the unknown impedance Z_x is determined by relation (4.3),
- the connection on the left is used for high-impedance measurements, the unknown impedance Z_x is determined by relation (4.4):

$$Z_x = \frac{V}{I} = \frac{2 \times Z_0}{\frac{V_2}{V_1} - 1}, \quad (4.3)$$

$$Z_x = \frac{V}{I} = \frac{R}{2} \left(\frac{V_2}{V_1} - 1 \right), \quad (4.4)$$

where V_1 and V_2 are the voltage drops across the known reference impedance Z_0 (typically 50 Ω), V is the voltage drop across the unknown impedance Z_x and I is the current through the impedance Z_x .

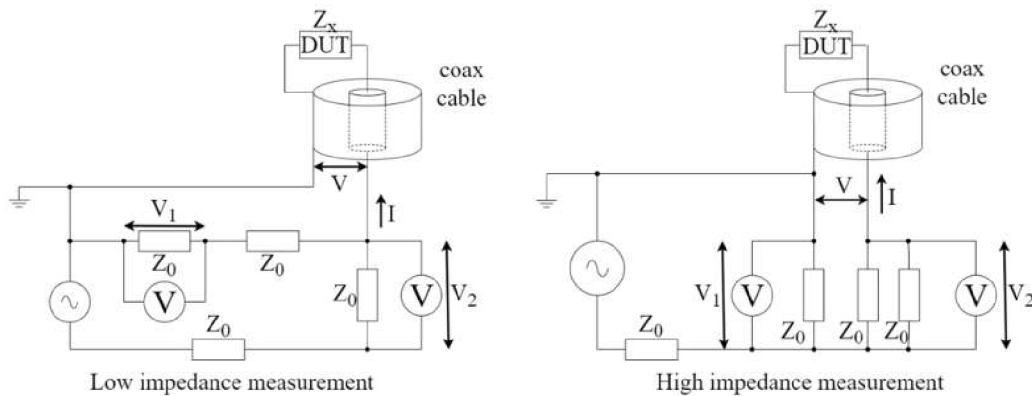


Fig. 4.4 Principle of RF I-V method [46]

4.1.5 Network analysis method

Network analyzer measurement is a special method intended mainly for measuring RF components. It enables measurements in the area of high frequency with high accuracy. The basis of its principle are the theory of the electric linear circuit in which the tested circuit can be designated as a gate (single-gate, double-gate or multi-gate), and the theory of Scattering parameters (S-parameters, scattering parameters).

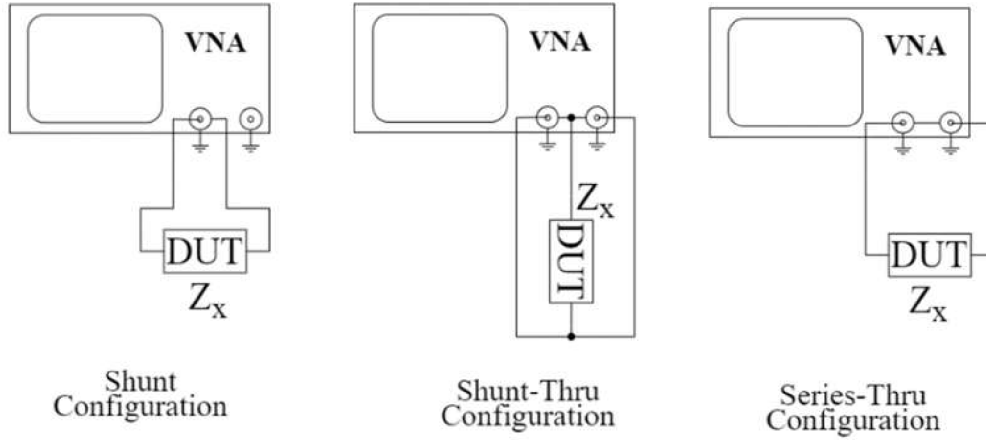


Fig. 4.5 VNA configurations for impedance measurement [46]

By using a vector network analyzer (Vector Network Analyzer - VNA), S-parameters are measured in the case of a double gate are 4 parameters – S_{11} , S_{12} , S_{21} , S_{22} . There are 3 configurations for measuring impedance, which are called shunt, shunt-thru and series-thru connections and shown in Fig. 4.5. Impedance in each connection is then calculated by relations (4.5), (4.6), (4.7), where Z_0 is the terminal impedance of devices and coaxial cables (typically 50Ω) [47].

$$Z_x = Z_0 \frac{1+S_{11}}{1-S_{11}}, \quad (4.5)$$

$$Z_x = Z_0 \frac{S_{21}}{2(1-S_{21})}, \quad (4.6)$$

$$Z_x = Z_0 \frac{2(1-S_{21})}{S_{21}}. \quad (4.7)$$

4.1.6 Auto-Balancing Bridge method

Measuring with an automatically balanced bridge is currently the most widely used method in modern measuring devices. Its most important advantages are high accuracy, a wide measuring frequency spectrum and a wide spectrum of measured impedances. A simplified principle of the method is shown in Fig. 4.6.

The comparator ensures that its inputs are at the same voltage level, the "Low" point; therefore, has zero voltage and is called the "virtual ground" point. The voltages V_x and V_r are the voltage drops on the DUT and the known resistance R_r . The input impedance of the comparator is assumed to be infinitely large, so its input current is zero and the currents I_x and I_r can be considered equal.

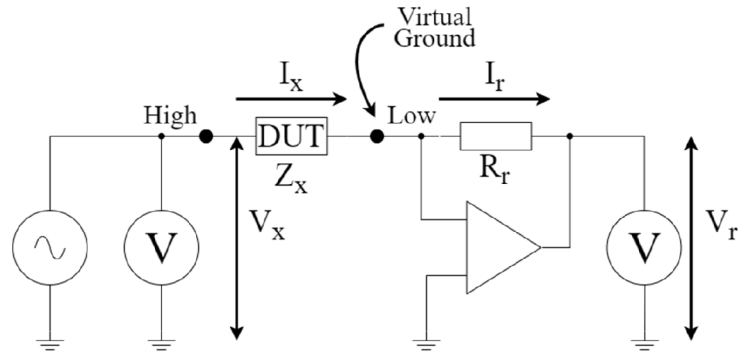


Fig. 4.6 Auto-Balancing Bridge [46]

The principle of the method is then expressed by using equations (4.8) and (4.9):

$$I_x = \frac{V_x}{Z_x} = I_r = \frac{V_r}{R_r}, \quad (4.8)$$

$$Z_x = \frac{V_x}{V_r} \times R_r \quad (4.9)$$

It is clear from the principle of the method that the frequency characteristic of the comparator is the most important factor affecting the accuracy of the method. For simple comparators, as the frequency increases, the accuracy decreases considerably, and then the accuracy of the method also decreases. However, most common auto-balanced bridges have high accuracy down to the kHz range.

The materials are designed and prepared to produce the cover and wings of the jet trainer; therefore, they must have very low electrical impedance (in the milliohm range). To measure such small impedance values, the auto-balancing method was selected due to its high accuracy and wide measuring bandwidth.

4.2 Chapter conclusion

This chapter provides the study of electrical impedance measurement. The basic terms and equations used in measuring and computing the electrical impedance of electronic components and materials are introduced. The most common impedance measurement methods, including the Wheaton bridge method, the resonant method, the I-V method, the RF I-V method, the network analysis method, and the auto-balancing method are also presented and compared. From the comparison, the auto-balancing bridge method is selected due to its high accuracy and wide measuring bandwidth. The next chapter will present the first practical part of the thesis, which is about measuring the impedance of composite specimens prepared by AVA to optimize the conductive layer.

5. PRACTICAL IMPEDANCE MEASUREMENT

This chapter focuses on the first practical work of the thesis. Basically, it is about the design of a program in the MATLAB environment for controlling the LCR bridge R&S HM8118 using SCPI standard. The schematic of the designed measuring station is shown in Fig. 5.1, including the equivalent circuit diagram of the LCR meter. The MATLAB-based program enables the computer to configure the LCR meter, control the LCR meter to automatically conduct measurements, and acquire measured data from the LCR meter. Acquired data are then processed and visualized for further analysis. This chapter will describe each part of the designed measuring station and the implementation of the station. The results of impedance measurements conducted by using the implemented station will also be presented and discussed.

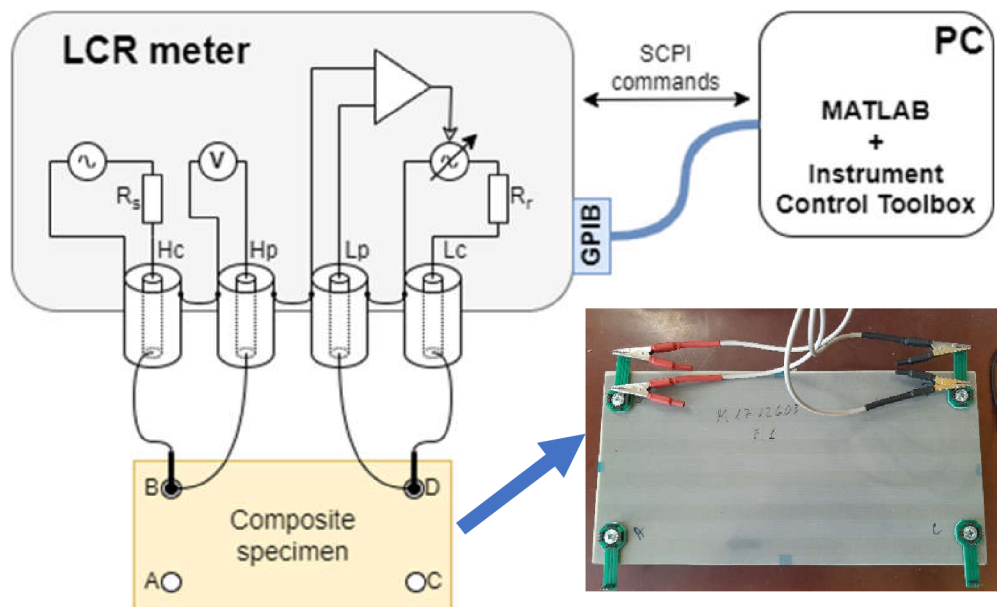


Fig. 5.1 Schematic of designed measuring station

5.1 Selection of measuring instrument and environment

This part presents the selection of the measuring instrument and the development environment for designing and realizing the measuring station. The measuring instrument and development environment are selected based on not only the selected measurement method, which is discussed above, but also on their availability, and their comparison to the other existing options.

5.1.1 Measuring instruments – R&S HM8118

As discussed in the previous chapter, the auto-balancing bridge method is selected for measuring the impedance of composite materials prepared by AVA. The main reasons are its high accuracy and wide measuring bandwidth. The used measuring instrument in this thesis is R&S HM8118, which is a measuring device designed for impedance measurement using the automatically balanced bridge (LCR bridge) method with alternating signals. The equivalent circuit of LCR meter can be seen in Fig. 5.1. The direct quantities that the LCR bridge measures are the impedance Z and the phase shift φ . Other quantities are derived from the measured values of impedance and phase shift.

The R&S HM8118 has four terminals Lc, Hc, Lp, and Hp. The first two, Lc and Hc, are used to apply the test current to the DUT, and the other two, Lp and Hp are measured terminals to measure the drop voltage on the DUT. The instrument then computes the impedance of DUT using equation (4.9). To increase the measurement's accuracy, R&S HM8118 has the option to average the measured results. The final result is computed as the average value of a number of measured values. Another factor affecting the accuracy of measurement is measurement speed. R&S HM8118 provides three optional measurements of speed, which are:

- 1.5 measurement per second (FAST mode),
- 8 measurement per second (MEDIUM mode),
- 14 measurement per second (SLOW mode).

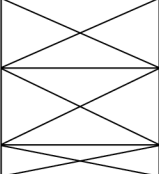

The other basic features and technical parameters of the R&S HM8118 are listed in Table 5-1.

Table 5-1 Technical data of the R&S HM8118 LCR Meter [48]

Parameters	Range	Notes
Test frequency	20 Hz – 200 kHz	± 100 ppm accuracy
AC test signal level	50 mV _{rms} – 1,5 V _{rms}	$\pm (5\% + 5\text{mV}_{\text{rms}})$ accuracy
Internal bias voltage	0 VDC – 5 VDC	10 mV resolution
External bias voltage	0 VDC – 40 VDC	Fused 0.5A
Internal bias current	0 mA – 200 mA	1 mA resolution

The accuracy of the LCR bridge measurement depends not only on the frequency of the test signal and the impedance of the DUT, but also on the amplitude of the test signal, measurement speed, bias voltage or bias current, and other device settings. Table 5-2 shows the measurement errors of the R&S HM8118 bridge as a function of the frequency of the test signal and the impedance of the tested object with the following factory settings: test signal amplitude: 1V, measurement speed: SLOW/MEDIUM (errors are doubled at FAST speed), bias voltage/ bias current: off, constant voltage: off.

Table 5-2 R&S HM8118 accuracy [48]

Frequency Impedance	20 Hz – 1kHz	1 kHz 10 kHz	10 Hz – 100 kHz	100 kHz – 2 MHz
4 MΩ – 100 MΩ	$0.2 \% + \frac{ Z }{1.5 \text{ G}\Omega}$		$0.5 \% + \frac{ Z }{100 \text{ M}\Omega}$	
1 MΩ – 4 MΩ	$0.1 \% + \frac{ Z }{1.5 \text{ G}\Omega}$			
25 kΩ – 1 MΩ	$0.05 \% + \frac{ Z }{2 \text{ G}\Omega}$	$0.1 \% + \frac{ Z }{1.5 \text{ G}\Omega}$	$0.2 \% + \frac{ Z }{100 \text{ M}\Omega}$	$0.5 \% + \frac{ Z }{10 \text{ M}\Omega} + \frac{5 \text{ m}\Omega}{ Z }$
100 Ω – 25 kΩ			$0.2 \% + \frac{ Z }{100 \text{ M}\Omega}$	
2.5 Ω – 100 Ω	$0.1 \% + \frac{1 \text{ m}\Omega}{ Z }$		$0.2 \% + \frac{2 \text{ m}\Omega}{ Z }$	
0.01 mΩ – 2.5 Ω	$0.3 \% + \frac{1 \text{ m}\Omega}{ Z }$		$0.5 \% + \frac{2 \text{ m}\Omega}{ Z }$	

For example, an ideal 10 pF capacitor has a measured impedance value of 15 MΩ at a frequency of 1 kHz. According to Table 5-2, the relative measurement error of the R&S HM8118 bridge will be calculated by:

$$\delta = 0,2 \% + \frac{|Z|}{15 \text{ G}\Omega} = 0,2 \% + \frac{15 \text{ M}\Omega}{15 \text{ G}\Omega} = 1.2 \%, \quad (5.1)$$

the absolute error of the impedance measurement is calculated by:

$$\Delta = \delta |Z| = 1.2 \% \times 15 \text{ M}\Omega = 180 \text{ k}\Omega, \quad (5.2)$$

and the absolute error of capacitance measurement is calculated by:

$$\Delta = \delta C = 1.2 \% \times 10 \text{ pF} = 0,12 \text{ pF}. \quad (5.3)$$

5.1.2 SCPI standard and MATLAB environment

The SCPI standard (Standard Commands for Programmable Instrument) is an ASCII-based instrument command language designed for test and measurement instruments. This standard contains a collection of commands, syntaxes, and rules for controlling programmable instruments in an automated measuring system, which is independent of the data transfer protocol. SCPI commands can be divided into 2 groups – Command commands and Subsystem commands [49]–[51]. Common commands are used to manage state registers, synchronize, and save data. They are defined by the IEEE 488.2 standard and are easily recognized by starting with an asterisk (*). Subsystem commands are distinguished by a colon (:) that appears at the beginning of the command and between keywords. Each command subsystem is essentially a set of commands that correspond to a function of the device.

A variety of environments, such as VEEPro, LabView, or MATLAB, can be used to issue SCPI commands to the device. Although VEEPro and LabView are environments designed for instrument control, their ability to solve scientific and technical problems is very limited compared with MATLAB. The usual solutions are that VEEPro or Labview control the instrument to carry out the measurements. The measurement results are then transferred to MATLAB for analysis and processing. Such solutions are bulky and inconvenient as they use multiple environments. Therefore, to conduct the thesis, MATLAB is chosen as the only environment to implement the control program for measuring devices.

In order to control programmable instruments with MATLAB, the Instrument Control Toolbox is available, which allows you to directly connect a computer (with MATLAB) to the instruments. Connections are physically implemented via a standard communication interface, for example, GPIB, RS-232, USBTMC interface.

GPIB (IEEE-488), RS-232 and USBTMC interfaces are available in R&S HM8118 LCR Meter. These devices are then controlled either by a predefined driver (driver), e.g., VXIplug&play, or by means of SCPI text commands. To write/read data to/from devices (or write/read data to/from interfaces) via GPIB (IEEE-488), RS-232 and USBTMC interfaces, the used MATLAB commands are:

- `write` – writing/sending data to the device,
- `writeline` – writing/sending lines of ASCII data to the device,
- `writebinblock` – write/send one binary block to the device,
- `read` – read data from the device,
- `readline` – read lines of ASCII data from the device,
- `readbinblock` – read one binary block from the device,
- `writeread` – sending a command to the device and reading the response.

5.2 Description of control program

The proposed measuring station is essentially a MATLAB program, allowing remote configuring and calibrating of the instruments, remotely controlling the instruments to automatically conduct measurements, and acquiring measurement data. To manipulate the measuring station, a graphical user interface (GUI) is also developed in the MATLAB environment. GUI also contains various tables and graphs visualizing the important measured results, allowing fast analysis of these results. The simplify flowchart for MATLAB program is shown in Fig. 5.2.

The program is divided into two parts. The first part of the program is designed to eliminate manual work when setting up and controlling the basic functions of the device. The second part of the program enables controlling the devices to operate automatic measurement and data acquisition, which will save time when measuring a large number of specimens. More detailed descriptions of each part are presented in the next part.

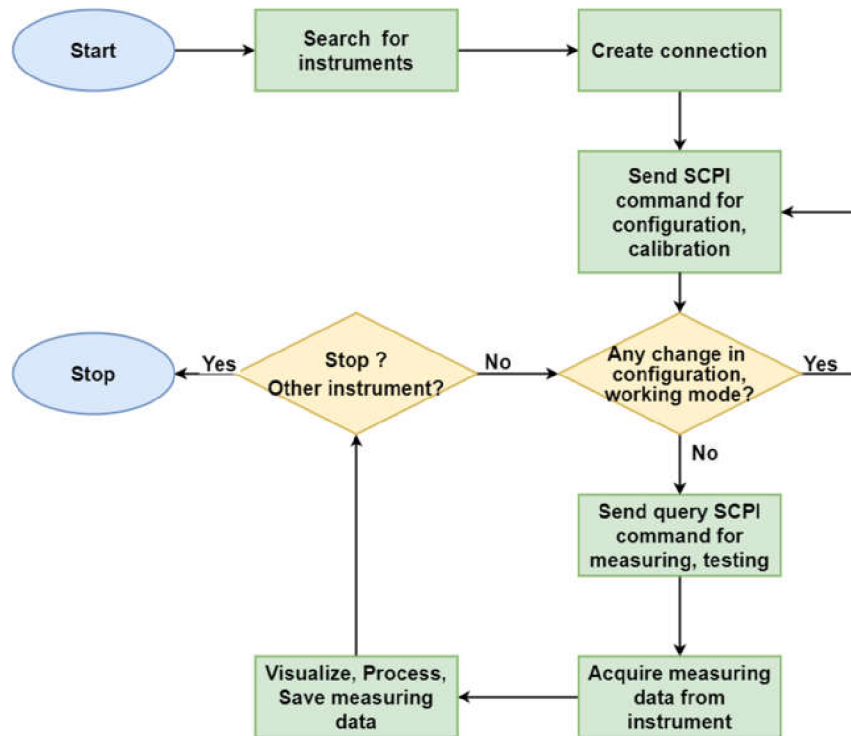


Fig. 5.2 Simplify flowchart of MATLAB programs

5.2.1 First part of MATLAB program

Fig. 5.3 shows the user interface of the first part of the program, which enables remotely setting up and controlling the basic functions of the device. For this purpose, the user interface contains several buttons, drop-down lists, checkboxes, tables and text edit fields, the function of which will be gradually.

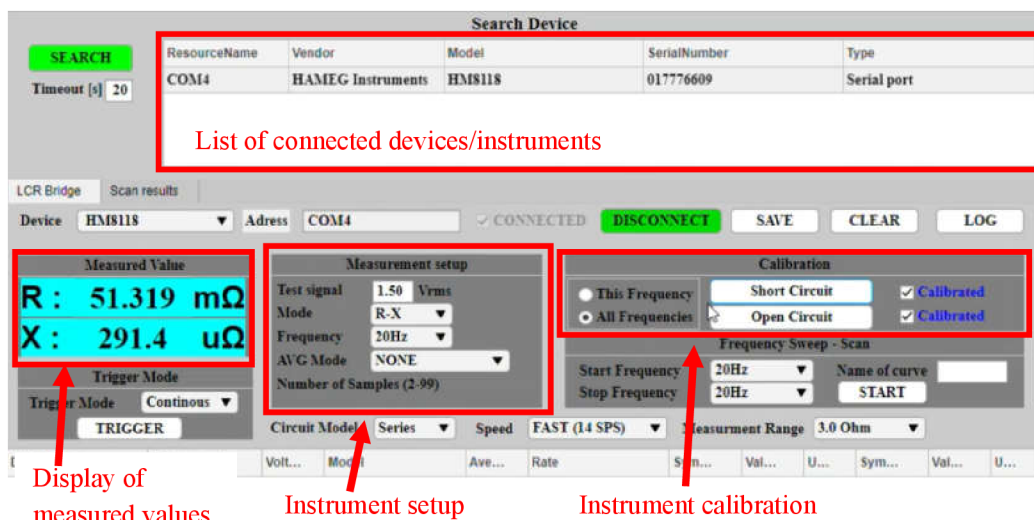


Fig. 5.3 The user interface of the program - the first part

Pushing the **SEARCH** button starts the search for connected devices. The program will scan all devices physically connected to the computer. The list of connected devices, including their identification data, will be displayed in the table to the right of the **SEARCH** button. MATLAB commands used to search for physical connected devices are:

- `serialportlist()` – for serial interfaces (RS-232),
- `displayevlist()` – for GPIB (IEEE-488) and VISA interfaces.

The **Device** drop-down list includes the names of all physically connected devices which are available for controlling and communicating. After selecting the device to connect, the identification address of the selected device will be displayed in the **Address** field.

The **CONNECT** button is used to create a communication channel between the computer and the device. The MATLAB commands used to create a communication channel are:

- `serialport ()` – for serial interfaces (RS-232),
- `visadev ()` – for GPIB (IEEE-488) and VISA interfaces.

The measurement results will be displayed in the **Measured Value** tab and in a table at the bottom of the interface (with option **LOG**). These results can be saved by using the **SAVE** button to text files (.txt files) or excel files (.xlsx files) for further processing.

The **Trigger Mode** tab is used to select the measurement trigger mode, either automatically, manually, or externally via the BNC connector on the rear panel of the device.

The **Measurement Setup** tab contains all the elements for setting the measurement parameters, which are:

- **Field Test signal** – setting the amplitude of the test signal,
- **Frequency** drop-down list – selection of the frequency of the test signal,
- **Mode** drop-down list – selection of measured quantities,
- **AVG Mode** drop-down list – selection of the mode of averaging the measured results,
- field **Samples (2-99)** – setting the number of measurements for calculating the average values of the measured results,
- **Speed** drop-down list – selection of measurement speed,
- checkbox with field **V_bias (0V-5V)** (or **I_bias (1mA-0.2A)**) – selection of the DC bias mode and setting of the bias signal amplitude, their display depends on the selection of the measured quantities,
- **Circuit Mode** drop-down list – selection of equivalent circuit type, typically series equivalent circuit is selected for low impedance measurement,
- **Measurement Range** drop-down list – selection of the impedance range of the tested object.

An example of MATLAB commands used to set up the device is:

```
%% =====
% Voltage -----
app.LCR_Volt = app.LCR_SelectedTestSignal_EditField.Value;
writeline(app.LCRBridge, "VOLT " + app.LCR_Volt);

% Circuit model -----
app.LCR_SM_Frequency = app.LCR_SelectedFrequency_DropDown.Value;
[~, Locb] = ismember(app.LCR_SelectedFrequency_DropDown.Value,...
                    app.LCR_SelectedFrequency_DropDown.Items );
writeline(app.LCRBridge, "FREQ " + app.LCR_Frequencies(Locb));

% Mode -----
[~,Locb] = ismember(app.LCR_SelectedMeasurementMode_DropDown.Value,...
                    app.LCR_SelectedMeasurementMode_DropDown.Items );
app.LCR_Mode = num2str(Locb-1);
writeline(app.LCRBridge, "PMOD " + app.LCR_Mode)

% Measurement Speed -----
[~, Locb] = ismember(app.LCR_SelectedSpeed_DropDown.Value,...
                    app.LCR_SelectedSpeed_DropDown.Items);
app.LCR_RateNumber = num2str(Locb-1);
writeline(app.LCRBridge, "RATE " + app.LCR_RateNumber);
%% =====
```

The **Calibration** tab operates device and cable compensation. Open Circuit or Short Circuit compensations are available. Compensation can be operated either in a given frequency (**This Frequency**) or in the entire frequency spectrum (**All Frequency**). An example of a MATLAB function for compensation:

```
% Button pushed function: LCR_OpenCircuitCompensation_Button
function LCR_OpenCircuitCompensation_ButtonPushed(app, event)

% -----
% Do nothing if there is no device -----
% -----
while isempty(app.LCRBridge)
end;

% -----
% Display the state of compensation process -----
% -----
app.LCR_OpenCompensationState_CheckBox.Visible = 1;
app.LCR_OpenCompensationState_CheckBox.FontColor = 'Blue';
app.LCR_OpenCompensationState_CheckBox.Text = "Calibrating";
app.LCR_OpenCompensationState_CheckBox.Value = 0;
app.LCR_OpenCompensation_Done = 0;

% -----
% Wait for finishing running tasks -----
% -----
while writeread(app.LCRBridge, "*OPC?") == "0"
end;
```



```

% -----
% Compensation only this frequency -----
% -----
if app.LCR_CompensationThisFrequency_RadioButton.Value
    % Send the compensation request -----
    writeline(app.LCRBridge, "CALL 0");
    % Compensation done -----
    if writeread(app.LCRBridge, "CROP") == "0"
        app.LCR_OpenCompensationState_CheckBox.FontColor = 'Blue';
        app.LCR_OpenCompensationState_CheckBox.Text =
"Calibrated";
        app.LCR_OpenCompensationState_CheckBox.Value = 1;
        app.LCR_OpenCompensation_Done = 1;
    % Compensation failed -----
    else
        app.LCR_OpenCompensationState_CheckBox.FontColor = 'Red';
        app.LCR_OpenCompensationState_CheckBox.Text = "Failed";
        app.LCR_OpenCompensationState_CheckBox.Value = 0;
        app.LCR_OpenCompensation_Done = 0;
    end;

% -----
% Compensation all frequencies -----
% -----
elseif app.LCR_CompensationAllFrequencies_RadioButton.Value
    % Send the compensation request -----
    writeline(app.LCRBridge, "CALL 1")
    writeline(app.LCRBridge, "CROP");
    % Longer Timeout for longer compensation process -----
    app.LCRBridge.Timeout = 180;
    % Wait for finishing running tasks -----
    while writeread(app.LCRBridge, "*OPC?") == "0"
    end;
    % Compensation done -----
    if readline(app.LCRBridge) == "0"
        app.LCR_OpenCompensationState_CheckBox.FontColor = 'Blue';
        app.LCR_OpenCompensationState_CheckBox.Text = "Calirated";
        app.LCR_OpenCompensation_Done = 1;
    % Compensation failed -----
    else
        app.LCR_OpenCompensationState_CheckBox.FontColor = 'Red';
        app.LCR_OpenCompensationState_CheckBox.Text = "Failed";
        app.LCR_OpentCalibratedCheckBox.Value = 0;
        app.LCR_OpenCompensation_Done = 0;
    end;
end;
end
end

```

The primary benefit of the first part of the program in comparison with manual control is the possibility to save a large number of measurement results for further processing. This benefit is also greatly beneficial for tests that run for a long time, such as accelerated failure tests. During the first practical work, this part of the program is used to measure the dependence of resistance and reactance of composite specimens on time. The measurement results will be presented in the next subsection.

5.2.2 Second part of MATLAB program

Fig. 5.4 shows the user interface of the second part of the program which enables automatic measurement and data acquisition when measuring in a certain frequency spectrum. The **Start Frequency** and **Stop Frequency** drop-down lists enable selecting the measuring frequency spectrum. The **Name of curve** field is used to set the name of the measured characteristics. The **START** button triggers the measurement. The **CLEAR** and **SAVE** buttons are used to delete and save measured data. After the end of the measuring process, the measured data are displayed in text in the table on the bottom and graphically in graphs.

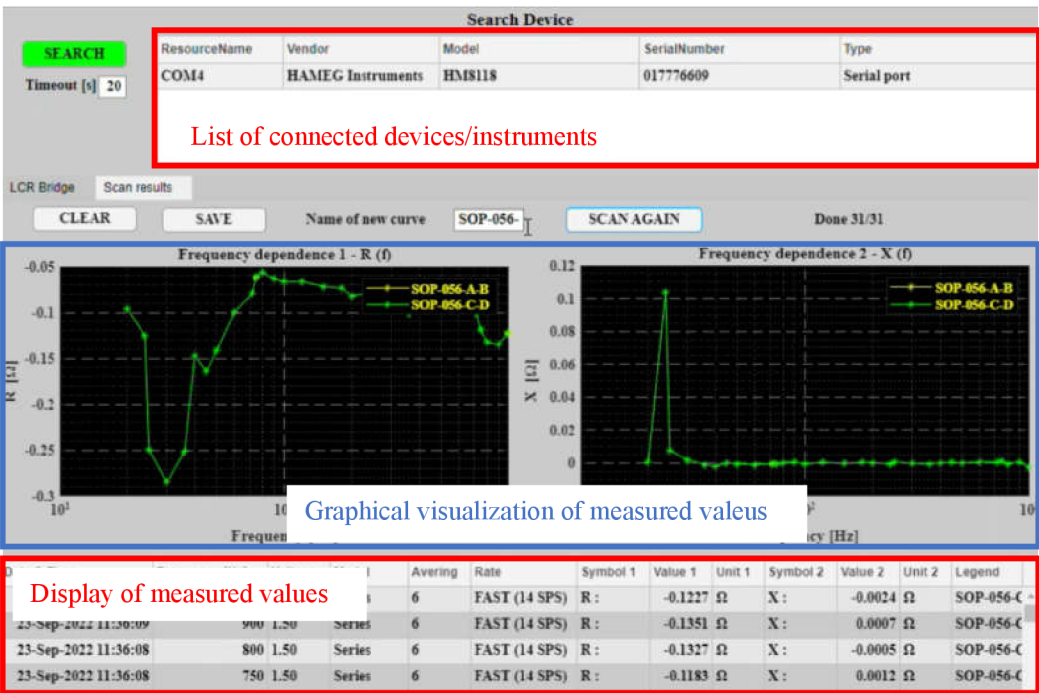


Fig. 5.4 The user interface of the program - the second part

This part of the program is very suitable for monitoring the behavior of specimens in a certain frequency spectrum. Graphical visualization of data enables simplified comparison among different specimens. In addition, it is also possible to save data for further processing. During the practical part of the thesis, this part of the program is used to measure the dependence of the behavior of the composite specimens on the frequency. The measurement results will be presented in the next subsection.

5.3 Experimental measurement

This subchapter describes results of impedance measurements of the specimens and frequency by using the realized automatically measuring station. The setup of the measuring station for impedance measurement of specimens is shown in Fig. 5.5.

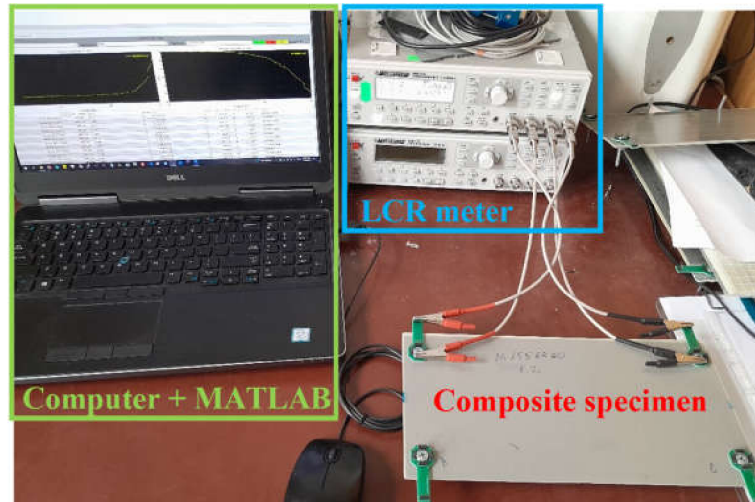


Fig. 5.5 Setup of realized automatically measuring station

5.3.1 Description of specimens

The measured specimens are produced by AVA with 7 glass-fiber laminate composite specimens and 1 carbon composite specimen. The geometry and dimensions of the specimens are shown in Fig. 5.6. For each specimen, 4 holes (A, B, C, D) are prepared for measurement.

Composite specimens made of glass laminate have an aluminized glass fabric layer (M3903452) or aluminum mesh (M1556860, M1712603, M3907280) layer as a conductive layer, in the places of holes (contacts for measurement), the conductivity is improved by an aluminum mesh (M1556860) or slice (NG1102101-001). Table 5-3 shows the designations and names of the conductive layers of individual specimens.

Table 5-3 Description of measured specimens

Designation	Name of specimen	Conductive mesh	Improving contact conductivity
M1556860-1	MRP18053112B no. 1	M1556860	NG1102101-001
M1556860-2	MRP18053112B no. 2	M1556860	NG1102101-001
M1712603-1	MRP18053112B no. 3	M1712603	NG1102101-001
M1712603-2	MRP18053112B no. 4	M1712603	NG1102101-001
SOP-056-2	SOP056DEA no. 2	M3903452	M1556860
SOP-056-4	SOP056DEA no. 4	M3903452	M1556860
SOP-057-3	SOP0571B4 no. 3	M3907280	M1556860

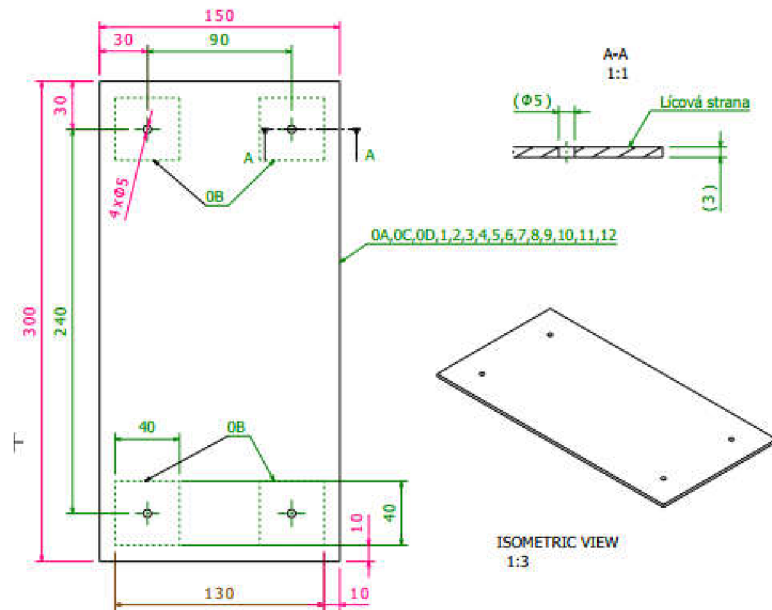


Fig. 5.6 Drawing of specimens prepared by AVA

During the manufacturing process, the holes are covered with epoxide resins which must be removed before impedance measurement. On this practical part, they are removed by manual grinding. It is better to apply high heat during grinding as the epoxide will be softer and the grinding process will have less effect on the conductive layer which is very thin. The connections between the measuring electrodes and the specimens are then realized by using contact printed circuit boards (PCB). The preparation procedures are shown in Fig. 5.7.

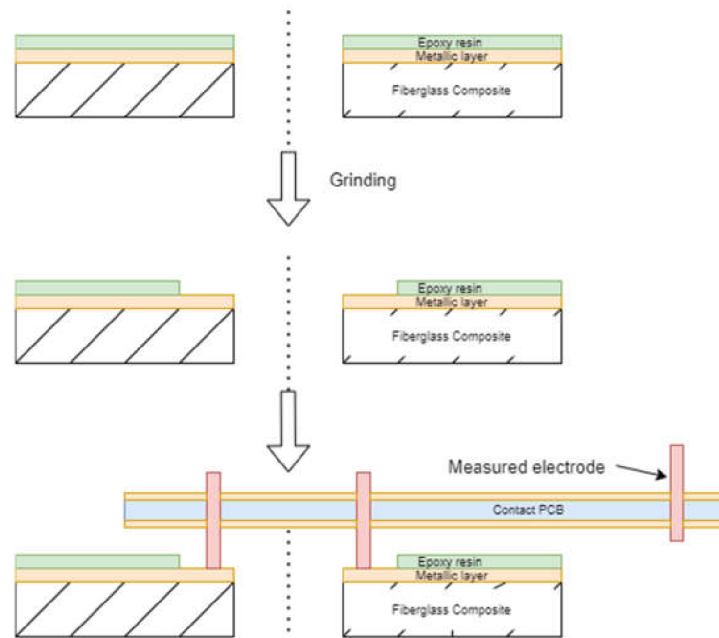


Fig. 5.7 Specimen preparation for measurement

5.3.2 Measured results – glassfiber composite

By using the proposed program, the dependence of impedance of individual specimens on the frequency is measured. For each specimen, the impedance between any two points is measured in both polarizations. In particular, there are 6 combinations from 4 points, so at each specimen, there are 12 measurements per frequency. For sufficient accuracy, the measurement is performed at the lowest speed and the measurement results are averaged from each of the 6 values. Since the impedances in all cases are in the order of $m\Omega$, the measuring frequency spectrum is chosen between 20 Hz and 10 kHz – see Table 5-2. It is obvious that the number of measurements is large, and it is necessary to measure and acquire data automatically by using the proposed program.

The measurement results of each specimen are then graphically visualized for analysis, for example, Fig. 5.8 shows the measured resistance and impedances of specimens M1556860-1 and M1556860-2. The inaccuracy of the measurements is also calculated and shown in the characteristics. It is possible to see that the electrical conductivity of the specimens does not depend on the polarization of the measurement. For example, the impedance between point A and point B is identical in both polarities of the measurement. Therefore, the conductivity of the composite specimens is isotropic. This conclusion is applied to all the measured specimens.

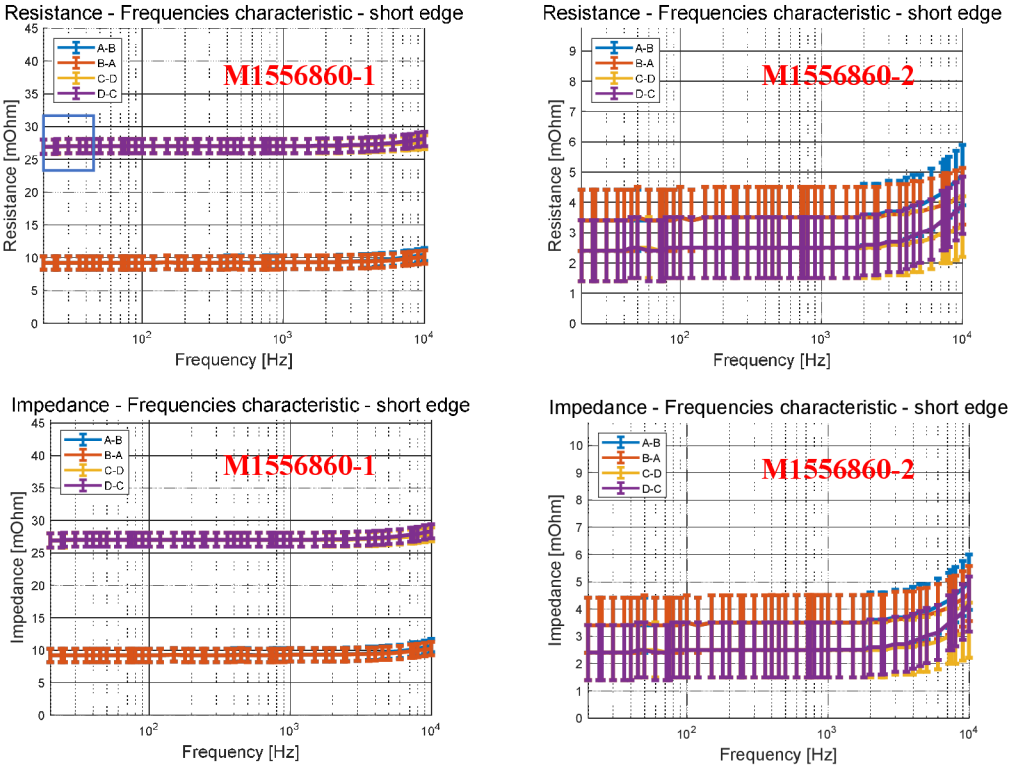


Fig. 5.8 Measured resistance and impedance of specimens of type M1556860

However, it is worth noting that there is a difference between the impedances of the 2 identical samples. While the impedance and resistance measured along the short edges (between A and B, as well as between C and D) of the M155860-2 specimen is smaller than 5 mΩ, the impedance and resistance measured along the short edge of M1556860-1 specimen are about 10 mΩ and 27 mΩ. The reason for these differences may be the imperfection of manual preparation before measurement. The conductive layers can be damaged, even removed, during manual grinding. Such damage is different at different points, and then affects the measurement results differently.

For the same reason, the measured values along symmetric paths, such as between A and B, and between C and D of specimen M1556860-1, are very different. These values should be similar for symmetrical reasons, as in the case of specimen M1556860-2. The additional possible reason for this difference is the imperfection of symmetry when the distance of symmetric points to the specimen's boundary is not identical. That imperfection causes the difference of boundary effect at the different electrodes, thus affecting the measured results.

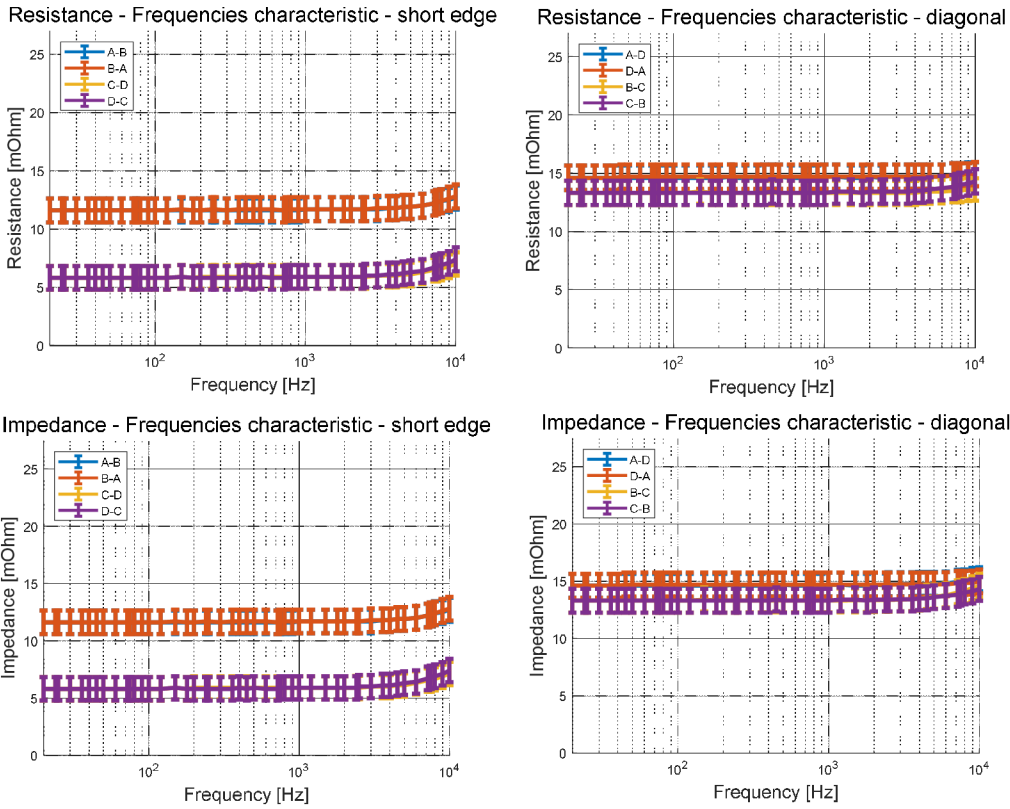


Fig. 5.9 Measured impedance and resistance of specimen SOP-057-3

It also can be seen that the effects of imperfect specimen preparation are different in different measured paths. For example, as shown in Fig. 5.9, the measured values of symmetric paths measured along the diagonal (between A and D, and between C and B) of specimen SOP-057-3 are similar and cover each other; however, the measured values of symmetric paths measured along the short edge (between A and B, and between C and D) are different (the values is different up to two times to the other).

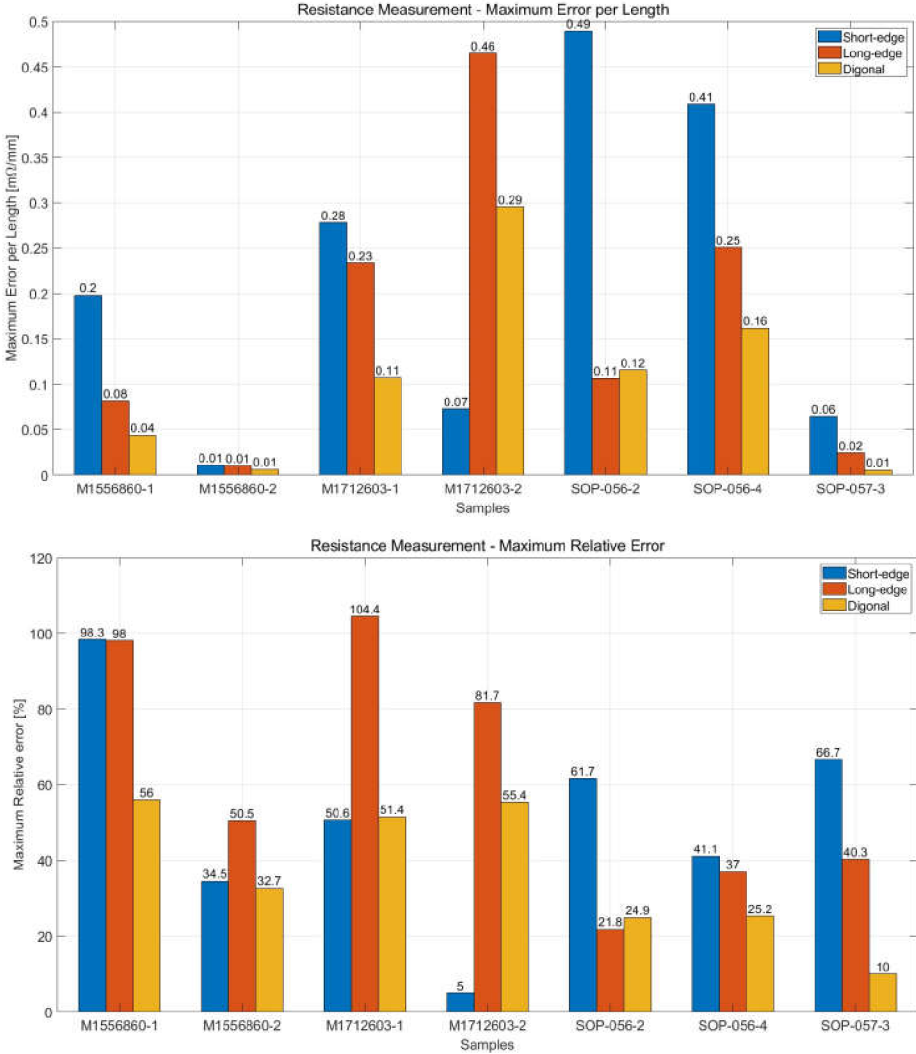


Fig. 5.10 Differences between measured resistance along symmetrical paths

Fig. 5.10 shows the differences between measured resistance values along symmetrical paths. It is clear from the results that the measured value along the short edge or long edge of the specimen appears unsuitable for measurement, as they show the highest absolute and relative errors. These errors are due to boundary effects which will be discussed more in the next part of the chapter.

Finally, the measured resistance and impedance of specimens prepared by AVA are compared to find the most suitable materials for manufacturing the dorsal cover of L-39NG aircraft. Fig. 5.11 shows the comparison of resistance measured between points B and C. The inaccuracy of the LCR instrument is also calculated and shown in the characteristics. Compared with the requirements defined by AVA, only the materials type M1556860 and SOP-057-3 are suitable. The other material types have much high resistance and impedance, which prevents them being selected as the materials for manufacturing the airframe.

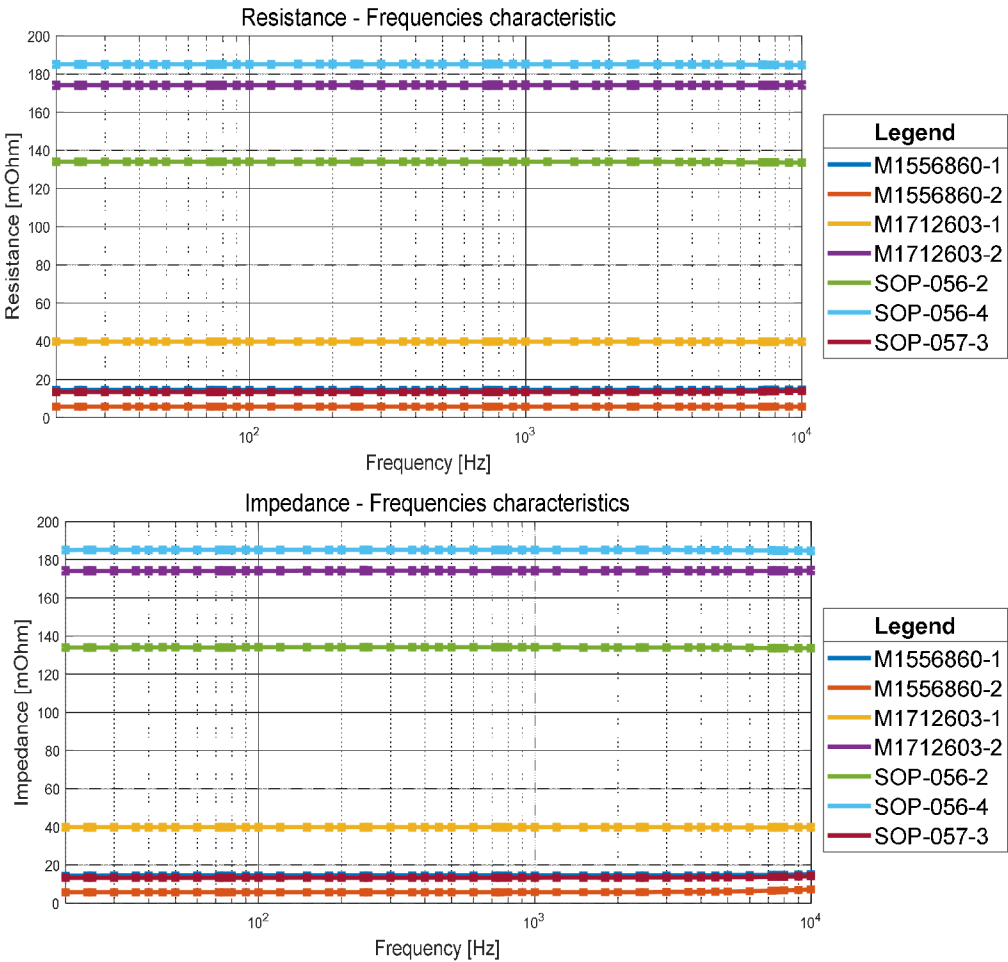


Fig. 5.11 Comparison of resistance measured between points B and C

The frequency dependence of the phase shift is also interesting and shown in Fig. 5.11. Almost all specimens have a "resistive" behavior with a phase around zero while the M1556860 specimens, which have the best impedance and resistance values, have a negative phase shift at high frequency (in the order of kHz). This property is remarkable for high-frequency applications, such as radar cover, or EMI protection.

Phase - Frequencies characteristics

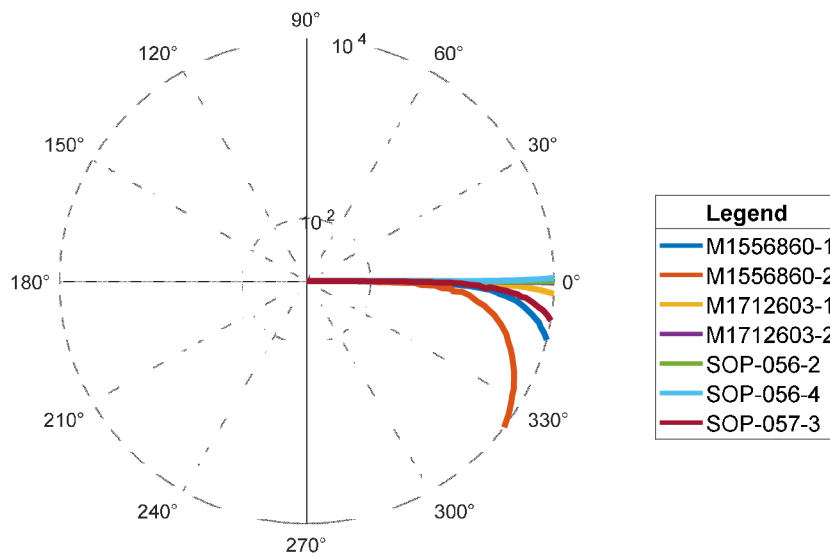


Fig. 5.12 Dependence of phase shift on frequency

All the measured results and comparisons of glassfiber composite specimens can be found in Appendix.

5.3.3 Measured result – carbon composite

The specimen made from carbon composite is also measured. The measured results however show that prepared carbon composite is not suitable for airframe manufacturing. The measured resistance value is in the range of 250-300 mΩ – as shown in Fig. 5.13, which is much greater than the required value defined by AVA.

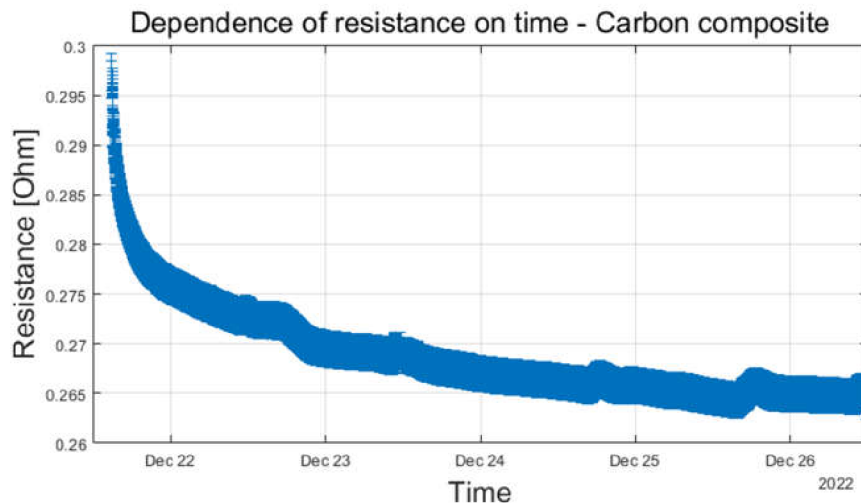


Fig. 5.13 Resistance of carbon composite specimen (linear representation)

However, an interesting behavior of carbon composite is observed. During the measurement time of 120 hours, the impedance and resistance values constantly decreased. The initial value was about 300 mΩ, decreased rapidly to about 290 mΩ in the first half hour, and then decreased to about 265 mΩ – as shown in Fig. 5.14. The logarithmic representation of the resistance's dependence on time shows that the decreasing resistance value can be approximated and considered as logarithmic decreasing with two different stages. In the range of this thesis, the interesting behavior of the carbon composite specimen was not studied more, because this specimen does not meet the basic requirement for aircraft airframe. However, this behavior was reported for further studies in future developments.

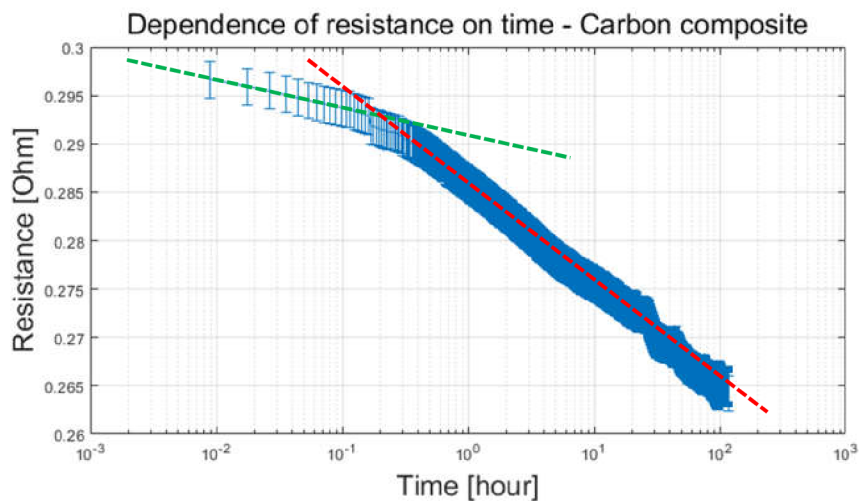


Fig. 5.14 Resistance of carbon composite specimen (logarithmic representation)

5.4 Chapter conclusion

5.4.1 Optimize selection of conductive layer

The glass fiber itself is an electrically non-conductive material; therefore, in order to be used for aircraft covers, the glass fiber composite must be modified by adding a conductive layer. The main goal of this part is to measure and compare various types of conductive layers to optimize the selection for use in L-39NG aircraft.

From the measured results, it is able to conclude that specimens of type M1556860 have the smallest impedance and resistance, which is an important criterion when choosing a material for aircraft primary structure (cover) regarding LSP. The SOP-057-3 type specimen may be acceptable, but more tests and measurements must be conducted. Other specimen types M1712630 and SOP-056 have high impedance and resistance (about tens to hundreds of mΩ) and are not suitable for the aircraft cover.

The SOP-056 specimens have conductive layer made from aluminized glass fiber M3903452 whose configuration is shown in Fig. 5.15. The fabric is composed of E-glass fiber half coated with pure aluminum. The aluminum content (by weight) is about 30-40%. Due to the small aluminum content, the aluminized glass fiber is used to reduce the weight; however, its electric conductivity does not meet the requirement for LSP. Therefore, the recommendation here is using aluminum mesh instead of aluminized glass fabric for the conductive layer of glass fiber composite.

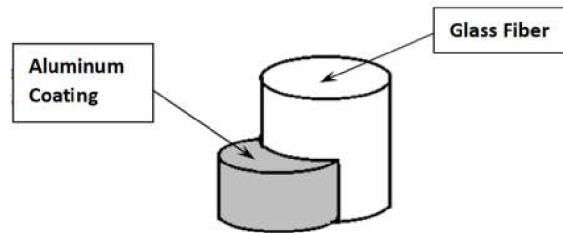


Fig. 5.15 Aluminum glass fiber M3903452 configuration

The other specimens have conductive layers made from aluminum expanded metal. Fig. 5.16 shows the structure and an example of an aluminum expanded metal used in aerospace application. The main parameters of an aluminum expanded metal are:

- material,
- material thickness,
- meshes per inch,
- screen opening size,
- open area,

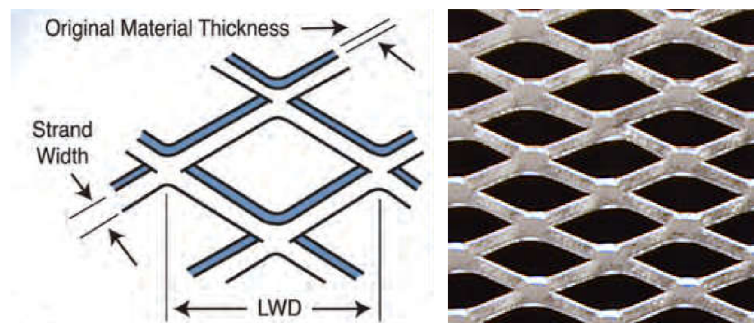


Fig. 5.16 Aluminum mesh – structure and example [52]

Table 5-4 shows the main parameters of aluminum expanded metal used in measured specimens. Comparing M1556860 and M1712603 meshes, which are made from the same material, it is obvious that material thickness has less effect on electrical conductivity of mesh than mesh density. M1556860 mesh has a smaller material thickness, but a larger mesh density result in better conductivity, as shown above.

Table 5-4 Main parameters of compared meshes

		M1556860	M1712603	M3907280
Material		Aluminum alloy 5056-0	Aluminum alloy 5056-0	Aluminum
Material thickness [mm]		0.053	0.102	0.102
Mesh density (per inch)	Warp	200	120	12-13
	Weft	200	120	22-23
Screen opening size [μm]		74	120	2032
Open area [%]		28-39	21-32	66-76

The material also has an important role. The M1556860 and M1712603 meshes are made from aluminum alloy 5056-0 (95% Al, 4% Mg), while the M3907280 mesh is made from aluminum. Comparing M1712603 and M3907280 meshes, which have the same material thickness, the mesh density of M1712603 is much greater than M3907280. However, the higher electrical conductivity of aluminum (35×10^6 S/m) than aluminum alloy 5056-0 (30×10^6 S/m) provides M3907280 mesh much better conductivity.

From the above analysis, it is able to partially conclude that for LSP, using aluminum mesh is preferred over aluminized glass fiber. The material for aluminum mesh is one of the most relevant factors. Pure aluminum will provide much better conductivity than aluminum alloys, in the same dimension and mesh density. To choose the dimension and mesh density of the aluminum mesh, the mesh density is much more important than material thickness.

Regarding the requirement of not affecting the operation of DME/TRANSPONDER, it is clear that the size of metallic mesh in the measured species is much smaller than the requirement limit (246 – 312 mm) (up to thousands of times). The effect of using metallic mesh for the operation of the DME/TRANSPONDER antenna can now be neglected.

5.4.2 Suggestion of specimen for future measurements

Specimens prepared by AVA were measured and compared. However, due to the inappropriate distribution of the prepared electrodes, the measured value can only be used for comparison between prepared samples and not for characterizing the used metallic meshes. The reason is the boundary effect when measured electrodes are located near the boundary of the specimen. For illustration, the distribution of current density in different locations of measuring electrodes is simulated and shown in Fig. 5.17. It is obvious that the boundary of the specimen causes the inhomogeneous distribution of current density thus measured value cannot characterize the properties of bare material.

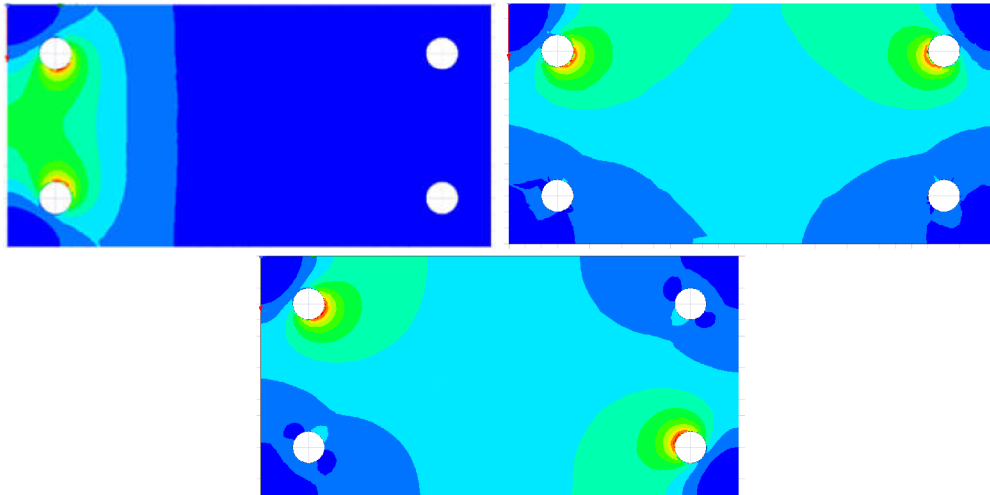


Fig. 5.17 Boundary effect – distribution of current density

Therefore, for further measurements in the future, specimens with other shapes must be used. For example, the specimen shape in Fig. 5.18 was simulated. The measured resistance value between electrodes is R_{12} , whose dependence on the dimension of the specimen (d is width, L is the length of the specimen) is shown in Fig. 5.19. The characteristic shows that in the cases when $d > L$, the measured resistance can be considered independent on the boundary effects. For example, the specimen can be prepared with the dimension of $d = 300$ mm, $L = 200$ mm. The simulated current density distribution is also shown to illustrate the effect of specimen's dimensions to the largeness of boundary effect.

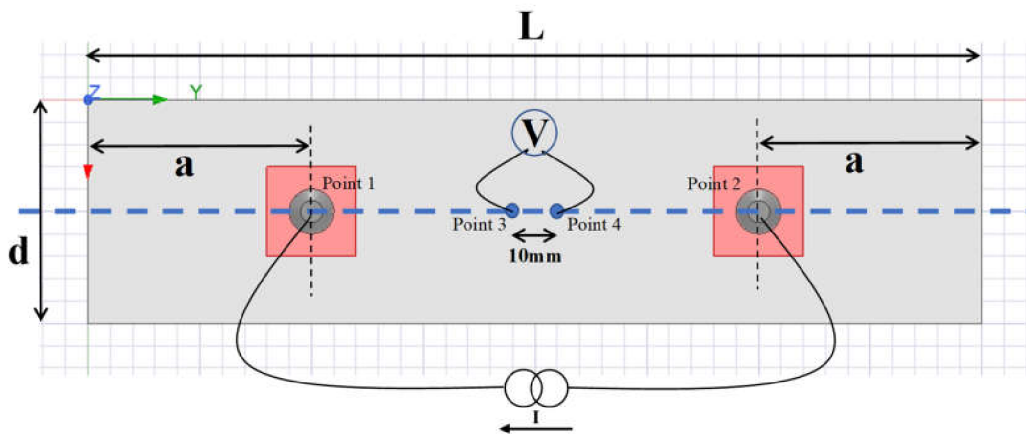


Fig. 5.18 Suggested shape of specimen and simulation setup

Dependence of R12 on L and d

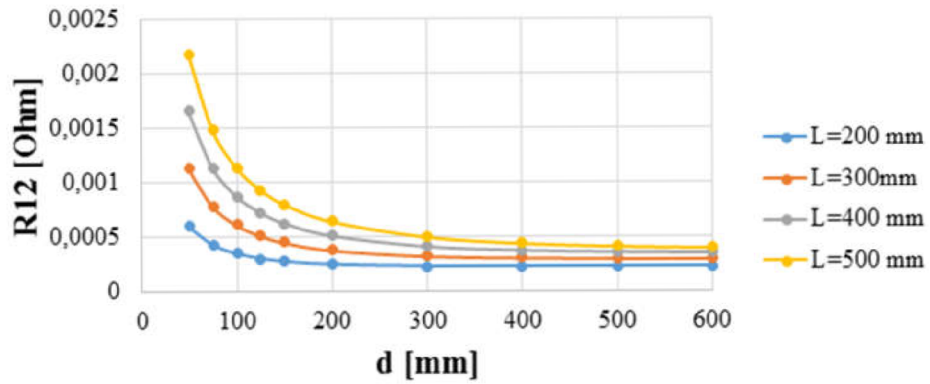


Fig. 5.19 Dependence of measured resistance on dimension of specimen

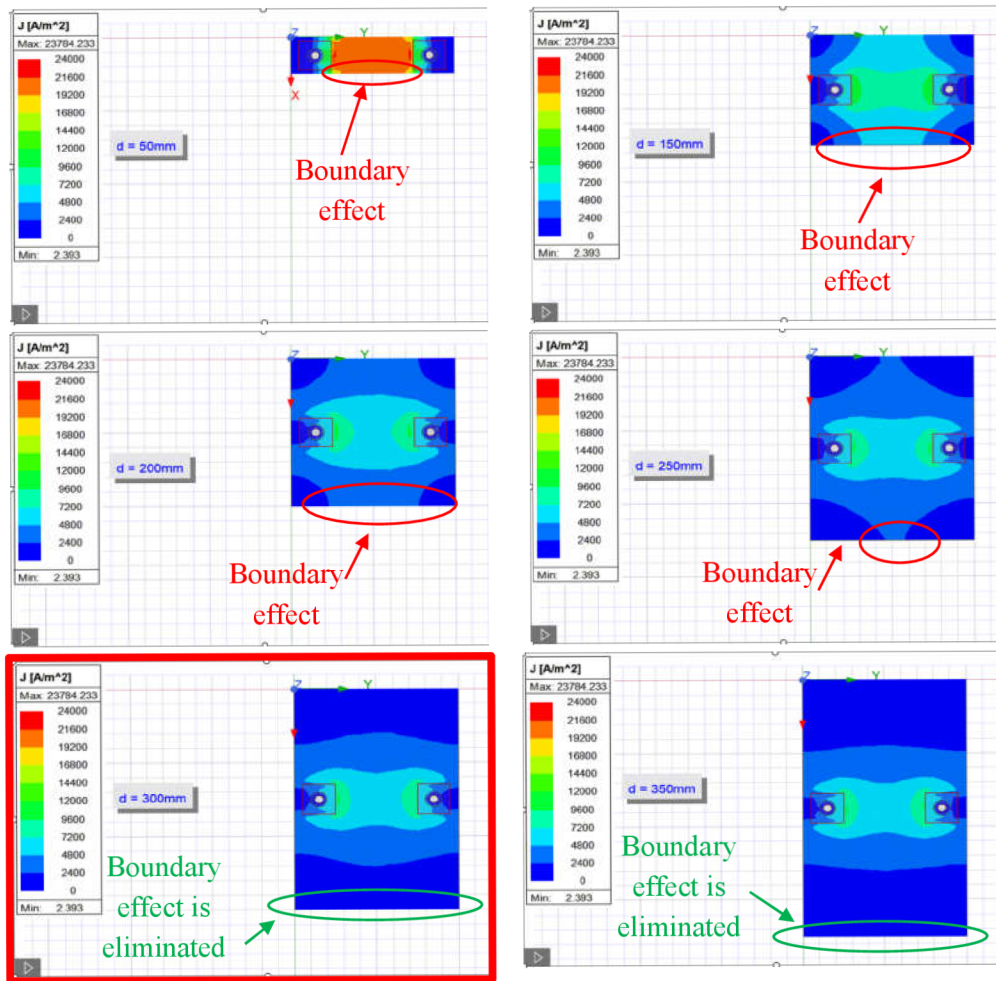


Fig. 5.20 Boundary effect in different specimen's dimensions

6. PRACTICAL LIGHTNING STRIKE TESTING

In order to provide as much knowledge as possible about the ability of the tested composite materials to protect the aircraft from lightning damage, the thesis includes not only impedance measurement but also lightning strike test of selected specimens. The test was conducted in the High voltage laboratory, Faculty of Electrical Engineering and Communication, Brno University of Technology.

6.1 Test standard and test system

The overview of aircraft LSP test standards and specifications was discussed in subchapter 3.2.1. As presented, LSP requirements for equipment are provided in standards STANAG 4237, ED-84/ARP 5412, and RTCA/DO-160. The selected standard is RTCA/DO-160G, which is published by the Radio Technical Commission for Aeronautics (RTCA) and is recognized by the International Organization for Standardization (ISO) as international standard ISO-7137. The specification for lightning direct effects testing is presented in section 23 of this standard, which is related to determining the ability of externally mounted equipment to withstand the direct effects of a lightning strike. The flowchart for the selection of High Voltage and High Current tests according to RTCA/DO-160 is shown in Fig. 6.1. In the case of testing in the range of this thesis, the material specimens are covered by resin, so the first tests must be high voltage tests [53].

The high voltage tests were conducted using the Heafely SGDA impulse test system which is designed to generate impulse voltages simulating lightning strokes and switching surges. The system has 10 stages and is capable of delivering up to 100 kV with 10 kJ energy per stage. The basic blocks and principles of SGDA high voltage impulse test system is illustrated in Fig. 6.2. The functional block of the system can be divided into 2 subsystems. The first one, or test subsystem, includes:

- charging rectifier,
- impulse generator, contains a number of capacitors
- control system,
- divider.

The second one, which is intended for additional measurement, is named accessories subsystem and is composed of

- chopping gap,
- shunt,
- measuring system [54].

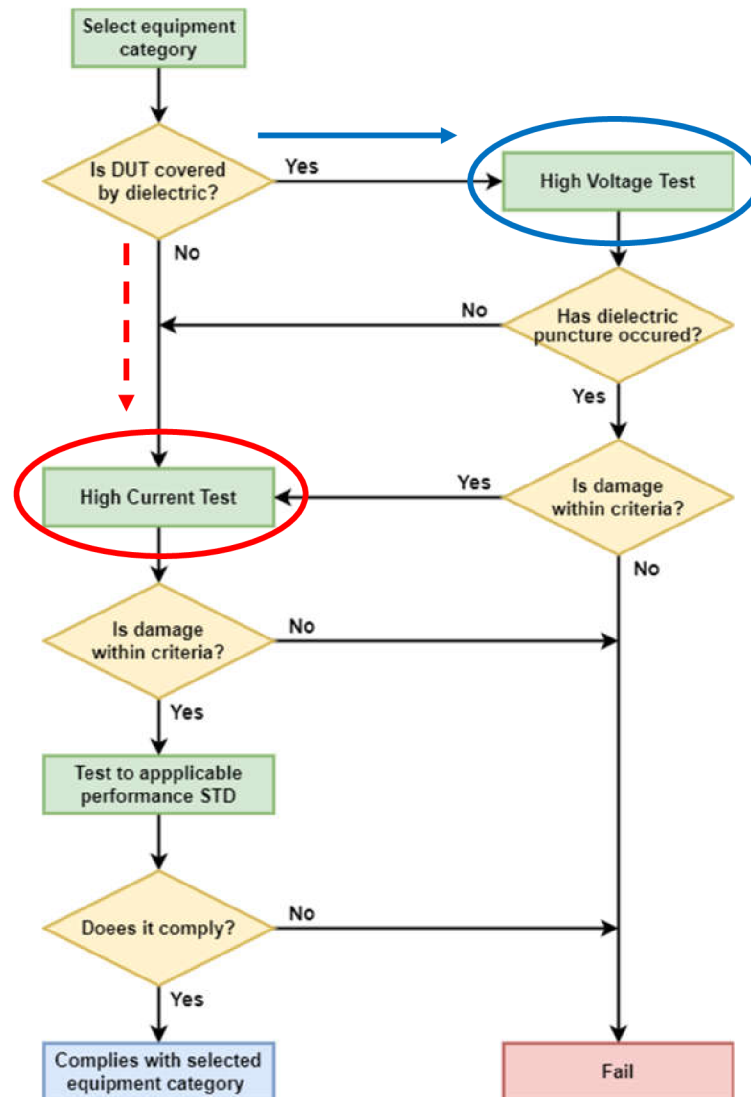


Fig. 6.1 Flowchart for High Voltage and High Current Tests [53]

The function of the SGDA test system is divided into 2 phases. In the first phase, or the charging phase, the impulse generator is charged through the charging rectifier unit. All the capacitors are connected in parallel via the charging resistor. When the final charging voltage is reached, the system changes to the second phase or discharging phase. In the second phase, all capacitors are connected in series, so the charging voltage is multiplied. The required value of impulse voltage is achieved by using the divider unit. The waveform of generated impulse can be defined by resistors connected in parallel and in series with capacitors (wave shaping resistors) [54].

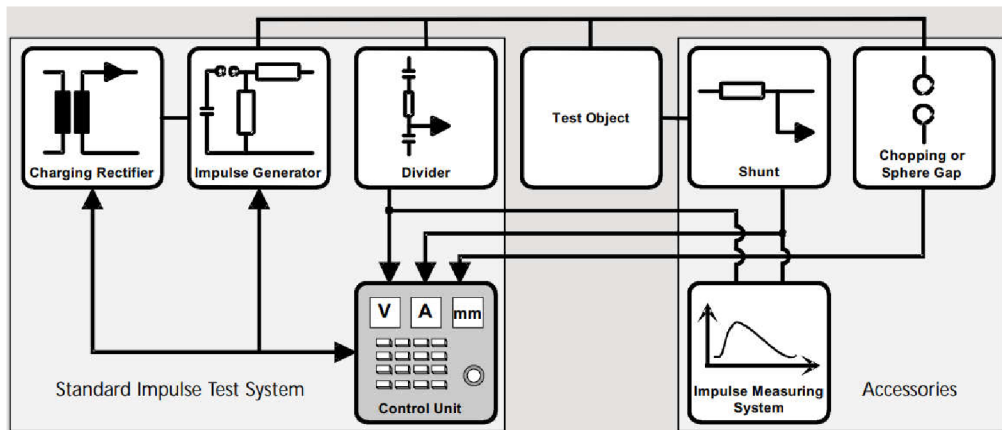


Fig. 6.2 Principle of SGDA high voltage impulse test system [54]

The setup of the lightning strike test is illustrated in Fig. 6.3. The specimens under the test were types M1712603. The ball electrode with a diameter of 7mm was used. Two types of discharge – contact discharge and air discharge were applied. The set test voltage was increased from 20 kV to 200 kV. The detailed setup value and the result will be presented in the next part of this chapter.

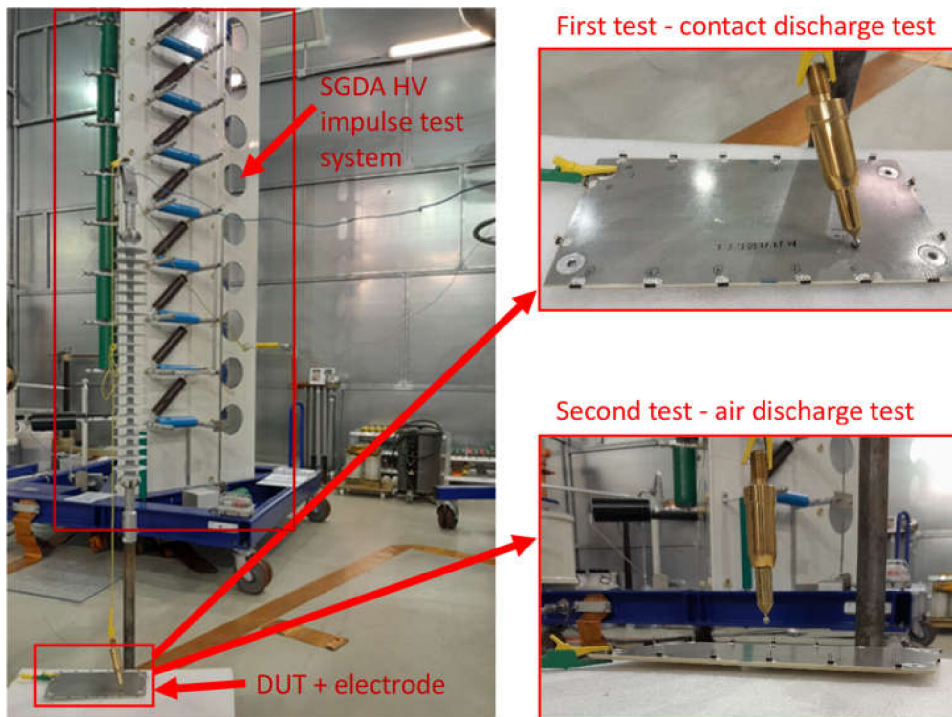


Fig. 6.3 Lightning strike test setup

6.2 Lightning strike to protected surface

The first tests were set up in such a way that there was an impulse test impact on the surface of the specimens, which is protected by a metal . Tests were conducted in both type- contact discharge and air discharge.

6.2.1 Contact discharge test

The contact discharge test was conducted with the set voltage $V_{set} = +20$ kV. The test impulse voltage waveform is shown in Fig. 6.4, where V_p reaches peak voltage; t_1 is time to voltage reach the peak value; and t_2 is time to voltage decrease to half of peak value. The wave form meets the requirement of V_{90} method defined in RTCA/DO-160G standard.

The damages caused by contact discharge test are also shown in the Fig. 6.4. The metallic mesh was molten due to the thermal effects of lightning strike. The mesh was degraded but not completely destroyed (the wire was not broken)

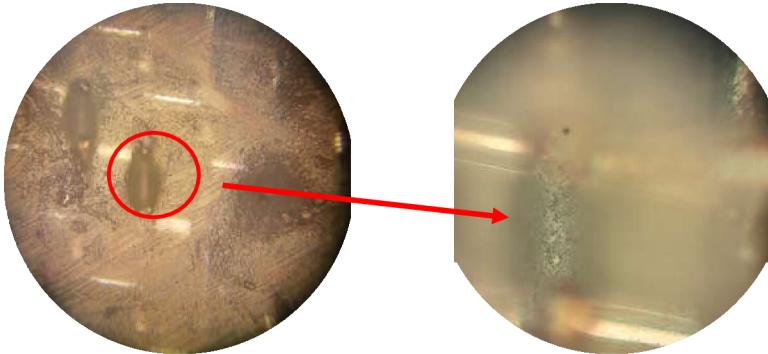
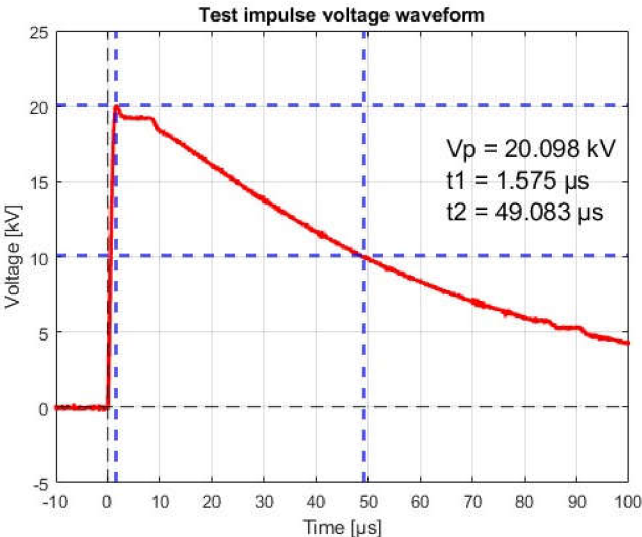


Fig. 6.4 Test impulse voltage wave form and damages – contact discharge test

6.2.2 Air discharge test

The air discharge tests were conducted with set voltages of +25 kV, +80 kV, -80 kV, and +400kV. However, the corresponding reached peak voltage were +25.3 kV, +25.4 kV, -27.3 kV, and +64.4 kV. In all cases, the strike only causes the degradation of the resin layer and small damage (a few windows) of metallic mesh, any puncture or large damage was not created.

Fig. 6.5 and Fig. 6.6 shows the test waveform and corresponding damage in the case of set voltage +80 kV and -80 kV. The bare visual comparison shows that negative voltage causes larger surface damage. The observation under the microscope, however, shows that the negative voltage causes mainly matrix degradation. Larger metallic mesh damage was caused by a positive voltage. The molten of metallic wire in the case of positive voltage (in Fig. 6.5) is also more significant, the wire was almost broken, only a thin layer remained, and a relatively large amount of metal flowed toward the ends of the wire. In the case of negative voltage (in Fig. 6.6), the metallic wire was also molten, however, a relatively large metal amount still remains in its original position.

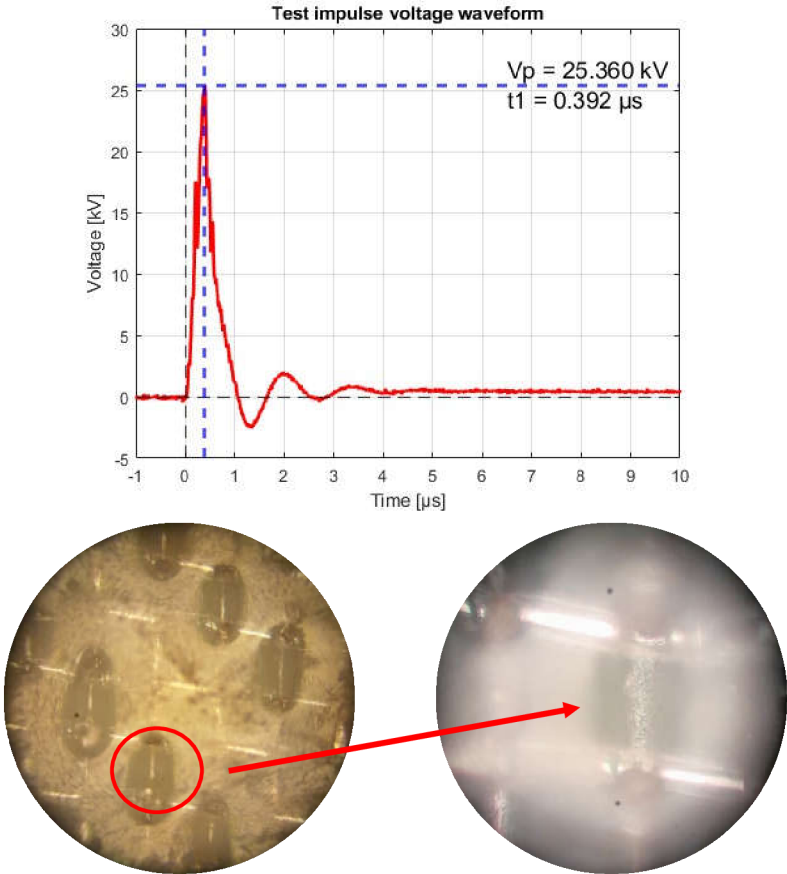


Fig. 6.5 Test impulse voltage wave form and damage – air discharge, +80 kV

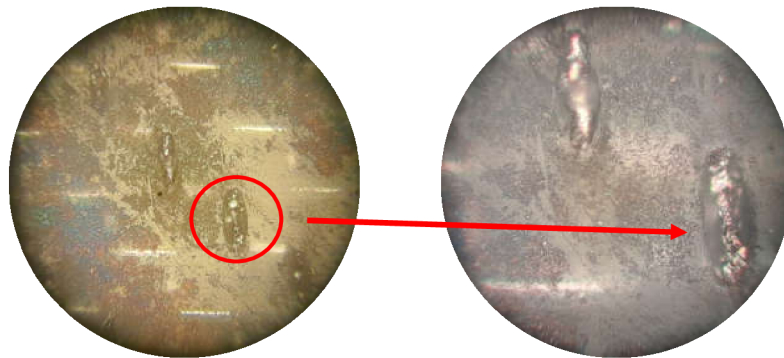
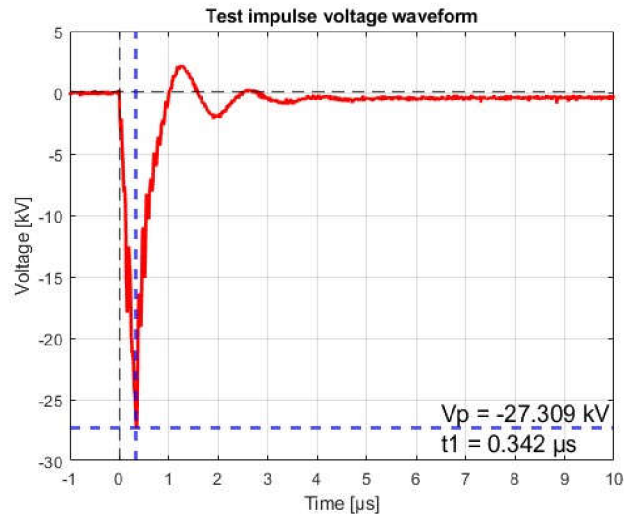


Fig. 6.6 Test impulse voltage wave form and damages – air discharge , -80 kV

6.3 Lightning strike to unprotected surface

The lightning strike to the unprotected surface was conducted with the set voltage of +400 kV. The reached peak voltage was +142 kV – as shown in Fig. 6.7. Fig. 6.8 shows the significant degradation of the matrix layer at the entry point caused by the heat effect of the lightning strike. The large damaged area on the unprotected surface clearly proves the importance of the metallic layer.

Since the surface struck by lightning is not protected by the metal layer, the lightning current flows to the nearest electrode on the boundary of the specimen to return to the ground through the metal layer on the second surface. This electrode was signed as the exit point in Fig. 6.8. The lightning current also caused damage at the exit point, damaging the conductive epoxy layer prepared for another test in the next chapter.

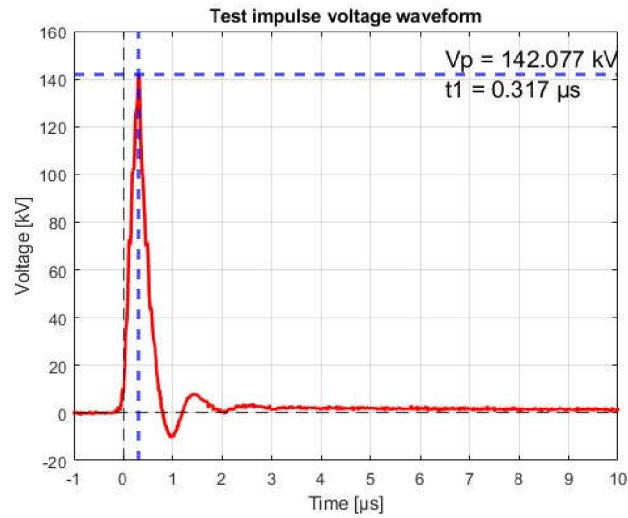


Fig. 6.7 Test impulse voltage wave form – air discharge test, $U_{set} = 400 \text{ kV}$

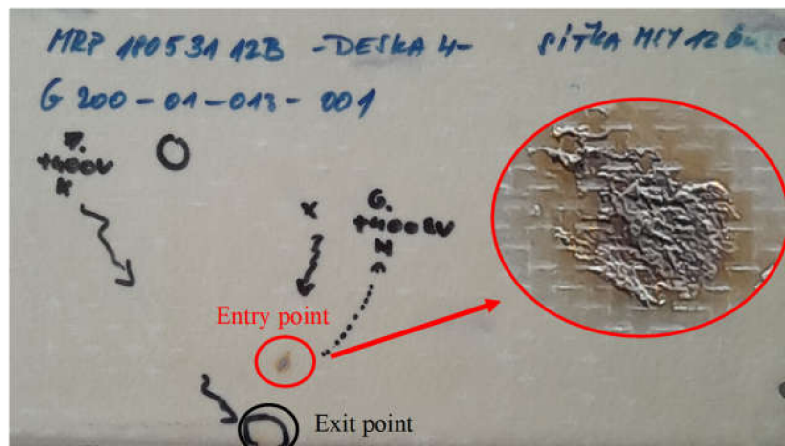


Fig. 6.8 Damage caused by lightning strike to unprotected surface

6.4 Chapter conclusion

This chapter presents the practical lightning strike testing for the selected specimen. Lightning strike tests were conducted in the High voltage laboratory using the Heafely SGDA impulse test system and were set up based on the standard RTCA/DO-160. The damages in the specimen were then observed under the microscope to compare the effect of lightning strikes in different setups. The results prove the importance of the metallic layer in LSP. However, unfortunately, the test voltage was not able to reach the requirement value defined in RTCA/DO-160. Therefore, it is important to use another test system, for example, a high current test system, in the future to conduct the lightning strike test in composite specimens.

7. DEVELOPMENT OF EIT/ERT METHOD

As discussed in Chapter **Error! Reference source not found.**, the surface damage or visible damages often have small areas; however, the core damages or hidden damages can be much and more serious. Hidden damage in structures can only be detected by Non-destructive Testing (NDT) methods. Therefore, this chapter focuses on the development of the Electrical Impedance/Resistance Tomography (EIT/ERT) method, which is used as one of the most interesting and promising NDT methods for aircraft structures. Developed method will be applied to the specimens under the lightning strike test, to verify the ability of damage localization.

7.1 State of art – NDT and EIT/ERT method

Non-destructive testing can be referred to as an independent scientific discipline that combines methods of assessing integrity of materials for surface and/or more importantly internal defects without destroying materials or their suitability for service. In recent decades, there has been an explosion of interest in this field. The importance and the necessity of NDT have been constantly growing since the demand for structural health monitoring, which is related to the safe use of structure, has rapidly increased. The aerospace industry is one of the fields that have the highest requirements for operation safety. Thus, it is clear that NDT is one of the most attractive and important developing fields in aerospace industry [55]–[57].

Czech aerospace industry has been quickly and early responded to the trend of aerospace NDT development. A number of NDT methods have been used by Czech Aerospace Research Centre (VZLU) and AVA. A number of activities on the R&D of this field have been also conducted in the cooperation between VZLU, AVA, Honeywell Technology Solutions and Czech Technical University in Prague (CVUT). The recently used NDT methods are:

- visual testing,
- magnetic particle Testing,
- ultrasonic Testing,
- radiographic Testing [55]–[60].

In addition to these NDT methods, there is another attractive method which has been applied to several fields, including medical imaging, biotechnology, chemical engineering, nanotechnology, civil engineering, geographical mapping, and so on. This method is called Electrical Impedance/Resistance Tomography (EIT/ERT) and essentially based on assessing the impedance of the object from the voltage and current values measured on the surface (predominantly in the boundary) of the object. The process of evaluating the electrical impedance from the measured values by using the finite element method (FEM) is called tomography, or image reconstruction [61]–[67].

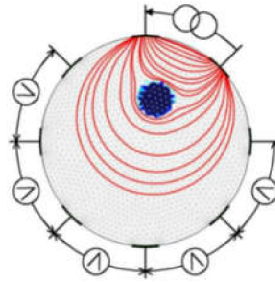


Fig. 7.1 Basic principle of EIT/ERT method [66], [67]

The basic principle of the EIT/ERT method is shown in Fig. 7.1. The object under test is stimulated by a small alternative (in case of EIT) or direct (in case of ERT) current, which is connected to two electrodes (most commonly, two electrodes side by side). The drop voltages between remaining electrodes are measured, so the number of acquired measured values is given by the number of electrodes. For example, in a 16-electrode EIT/ERT system, the number of acquired values is 208 voltages (13 voltage measurements per stimulus multiplied by 16 stimulus electrode couple). The resolution of reconstructed tomography/image depends on the acquired data, and thus depends on the number of electrodes. It is shown in a number of researches that the distribution of electrodes on the evaluated object also affects the reconstruction results [61]–[67].

It is obvious that the EIT/ERT method can be used as one of the NDT methods, which visualizes the surface and/or the internal damages in the reconstructed image. The object's structural damage causes a local change in the object's electrical impedance/resistance. As a result, theoretically, reconstructed tomography will clearly show location of the structural damage, as illustrated in Fig. 7.2. In practice, the resolution of reconstructed image which depends on the number and distribution of electrodes will affect the accuracy of damage localization.

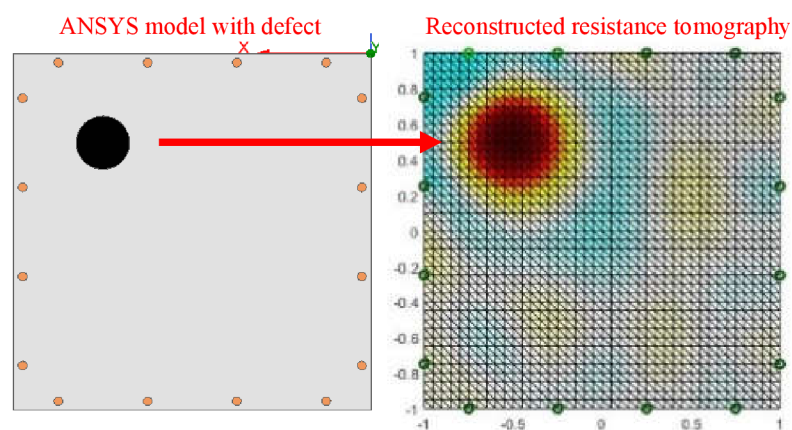


Fig. 7.2 Structural damage visualization using ERT/EIT method (simulation data)

7.2 Proposed LCR meter based EIT system

From the principle of the EIT/ERT method and the principle of impedance measurement method using the auto-balancing bridge, an idea that the LCR meter is able to be used for EIT/ERT measurement is offered. The main advantage of this idea is the ability to achieve high accuracy measured value with high signal to noise ratio (SNR) and wide dynamic measurement range, due to using a precise measuring instrument dedicated to impedance measurement. A similar idea, which used an LCR meter for electromagnetic tomography was introduced in [68].

7.2.1 Prepare of specimens

For EIT/ERT measurement, a number of electrodes must be implemented in the surface of the evaluated object; in this case, they are specimens under the lightning strike test. The specimen surface is covered with a layer of resin which is not electrically conductive. Therefore, in the first step, the resin layer on the specimen surface must be ground in the location of electrodes. Hot air from a soldering station was locally applied during grinding to soften the resin and reduce the risk of mechanical damage to the thin metallic layer.

The connection between electrodes and specimen must have as low as possible contact resistance, and as high as possible mechanical strength. The EPO-TEK H21D two-component silver-filled epoxy is used to implement electrodes. Because of being designed for chip bonding in microelectronics, this epoxy provides low volume resistivity which is necessary for low contact resistance between electrodes and specimen surface. The H21D epoxy can be cured in a temperature of 80°C in 90 minutes. The low curing temperature eliminates the risk of matrix degradation of composite specimens.

Because the contact resistance increases as the thickness of the conductive epoxy layer increases, it is important to apply an as thin as possible layer of conductive epoxy between the specimen surface and electrodes. Such a thin layer; however, does not provide mechanical strength enough connection. Therefore, conductive epoxide is applied two times. In the first time, a thin layer is applied between electrodes and the specimen surface to provide small contact resistance. After curing, more epoxy is added to the connection to maintain the mechanical strength.

The summary of the main steps of realizing conductive connection is:

- grinding the resin layer on the specimen surface,
- applying as thin as possible conductive epoxy layers to the specimen surface,
- implementing electrodes to applied thin epoxy layers,
- curing specimen with conductive epoxy and electrode,
- adding more epoxy to the connection,
- curing specimen with additional epoxy.

7.2.2 Measurement setup

The setup of the LCR meter-based EIT system is shown in Fig. 7.3. The four terminals of LCR are connected to the electrodes of the evaluated object in the configuration that the two terminals Lc and Hc are connected to stimulus electrodes, while Lp and Hp are used to measure drop voltage between remain electrodes (measured electrodes). A current with constant amplitude and frequency will be applied to the evaluated object through Lc and Hc terminals. The LCR meter measures the impedance of DUT by measuring the voltage between Lp and Hp terminals. Thus, based on the impedance results, it is easy to compute back the voltage between Lp and Hp terminal, which is, in our case, the drop voltage between electrodes when the object is stimulated by a current.

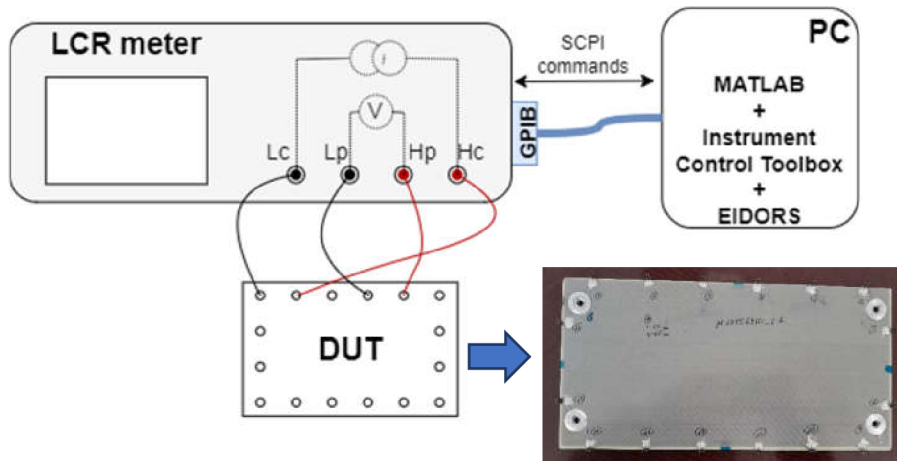


Fig. 7.3 LCR meter-based EIT system

The LCR meter is driven by the MATLAB program, similar to the program for impedance measurement presented in Chapter 4.2. The MATLAB program, in this case, is also in charge of reconstructing the impedance/resistance tomography of the object and visualizing the result. To reconstruct the tomography, the MATLAB-based open-source software EIDORS [69] is used. The basic operation of EIDORS is shown in Fig. 7.4

As shown in Fig. 7.4, the first step to working with EIDORS is to create finite element FEM model of evaluated object. The EIDORS, in its prepackaged libraries, provides a number of common FEM models, such as circular model, square model, cylinder model, and biomedical model. However, these common models cannot be used for the specimens provided by AVA. Therefore, it is necessary to modify the prepackaged FEM model to the model suitable for provided specimens. The prepacked square model is chosen to be modified. The main modifications are: change the shape of the FEM model (square \rightarrow rectangle), optionalize the location of electrodes (which is fixed in the prepacked model).

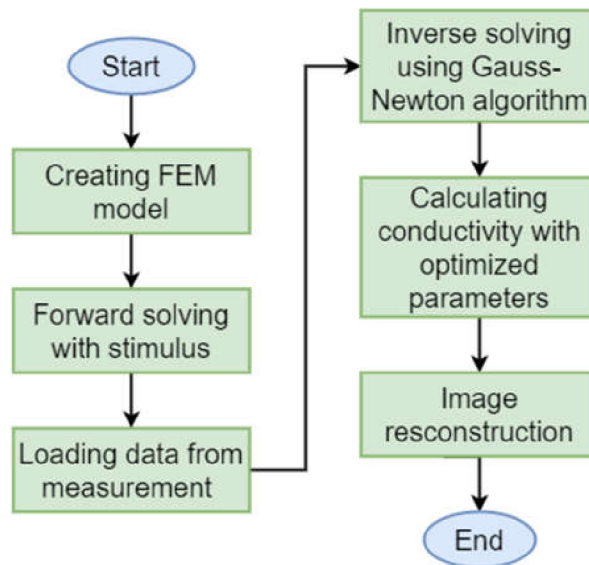


Fig. 7.4 Flowchart of EIDORS basic operation [70]

After modification, the FEM model is verified by using data simulation in Ansys Maxwell software. The result is shown in Fig. 7.5. Clearly, the modified FEM model fulfills the requirement that the damage can be localized.

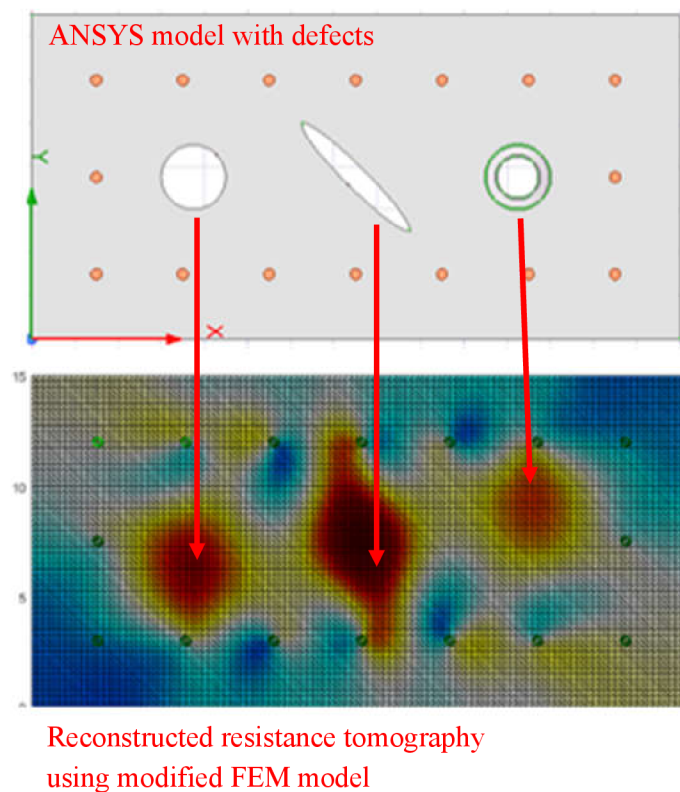


Fig. 7.5 Functional verification of modified FEM model

7.2.3 Functional verification and measurement result

To verify function of the entire proposed system, the specimen with a defect caused by the lightning strike test was used. As shown in Fig. 7.6, the lightning strike caused damage in the location of electrode 3. The lightning strike damaged the electrode, the conductive epoxy layer, and, particularly, the metallic mesh.

The reconstructed impedance tomography is shown in Fig. 7.7, which clearly proves the ability of damage localization. The red zone indicating the specimen damage locates next to electrode 3, which is in agreement with the damage indicated in Fig. 7.6.

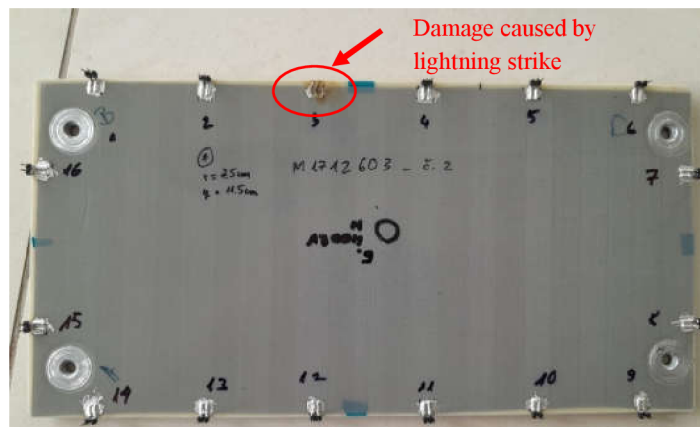


Fig. 7.6 Specimen with defect cause by lightning strike

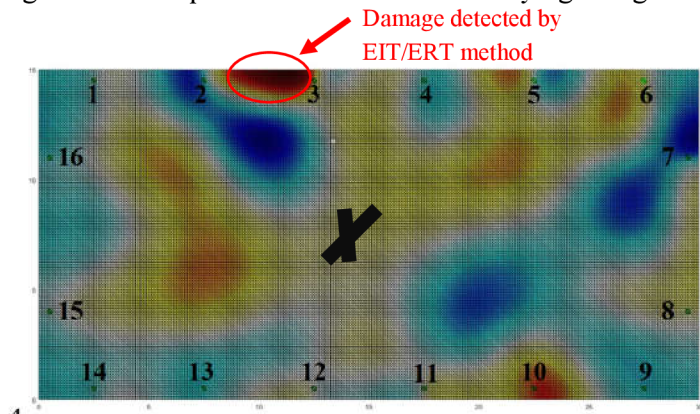


Fig. 7.7 Damage localization using EIT/ERT method

The small inaccuracy in results can be caused by several reasons. Firstly, the number of used electrodes is small, so tomography's resolution is not high enough, which leads to some displacement of indicated damage. Secondly, the damage, unfortunately, is produced in the location of the electrode, which reduces the number of effective electrodes (electrode 3 cannot be used) and changes their distribution. In addition, the image reconstruction algorithms, inaccuracy of measurement, and instability of the instrument also can be further reasons.

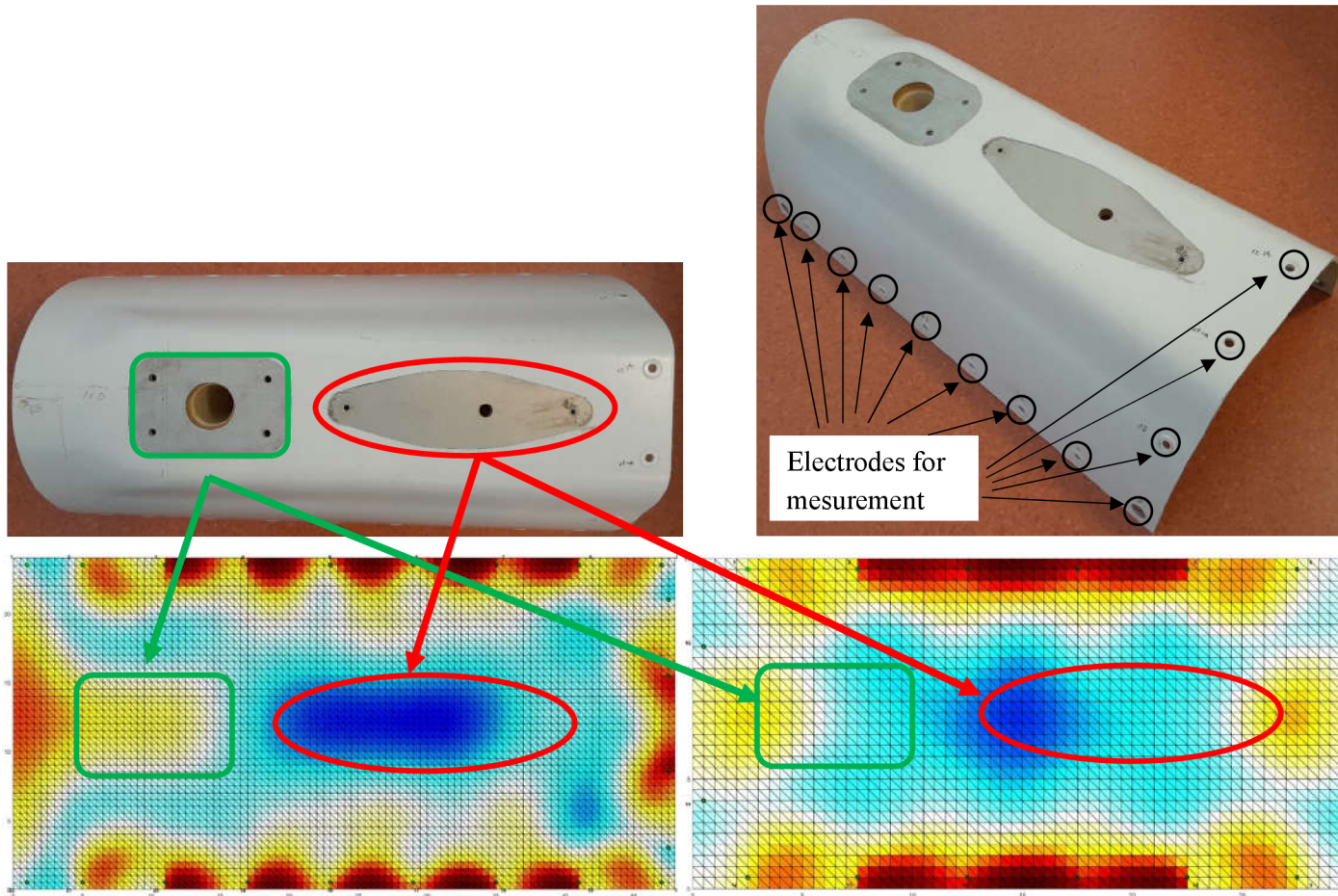


Fig. 7.8 L-39NG dorsal cover (above) with 22 (below, left) and 16 (below, right) electrodes tomography

The L-39NG dorsal cover is also tested using the proposed LCR meter-based EIT system. Measurements were carried out with two electrode configurations: 22 electrodes and 16 electrodes. The rivets prepared to attach the dorsal cover to the airframe are used as electrodes. The objective of this measurement is to verify the applicability of the proposed system to the aircraft structure. The results are shown in Fig. 7.8.

It is clear that the number of electrodes used seriously affects the reconstruction results. In the case of using 22 electrodes, the reconstruction tomography clearly shows the location of the aluminum plates, which are used for the installation of the DME/TRANSPONDER antenna and flash beacon. However, the reconstructed tomography from the measurements of the 16 electrodes could not locate these aluminum plates. Results can be improved using better electrode distribution, however, for NDT testing of an active airframe, it is imperative to use existing studs to measure, otherwise, the airframe's function and safety can be significantly affected.

Disadvantages of this system are the long measurement process, requiring an LCR meter, and manual switching of measured electrodes. Thus, it is not suitable for in-flight measurement. However, for use in the aircraft structure maintenance process, it provides, as discussed above, high precision, and a wide dynamic measurement range with a low-cost and short-time R&D process. The development of an electronic system that fulfills the EIT function will be presented in the next part of this chapter.

7.3 Development of FPGA-based EIT/ERT system

The main motivation for this development is to realize an electronic system, which can be used for in-flight structure health monitoring, based on EIT/ERT method. A number of electronic EIT/ERT systems are presented, most of them use a unique analog-to-digital converter (ADC) to measure the voltage between electrodes. An electronic multiplexor selects the measured electrodes, and the selected voltage is amplified before being measured by ADC. Then, the electronic multiplexor switches the measured electrodes to the next ones, and the process continues until the voltages between all electrodes are measured. Such a system has a shorter measurement time period than manual multiplexing; however, the measurement process is still in sequence, which is longer than it in parallel. In addition, the "on" resistance of multiplexors can never be zero, affecting the measured voltage values and image reconstruction result. The high-speed switching process of multiplexors can also cause EMI to other electronic systems.

7.3.1 Basic concept

From these discussed disadvantages of conventional electronic EIT/ERT systems, in the range of this thesis, an FPGA-based EIT/ERT system was developed in the beginning stage. The main idea of this development is to use an FPGA, with an

array of ADCs, instead of a unique ADC. The advantages are measuring processes are conducted in parallel, which increases the measurement speed. Multiplexors are not used, so the issues of their “on” resistance and EMI caused by switching processing are removed. The block diagram of the developed system is shown in Fig. 7.9. The ADC array is driven by a unique clock signal, maintaining synchronization between ADCs. Data between the ADC array and FPGA are transferred parallel, each path transfers data from and/or to one ADC in the array.

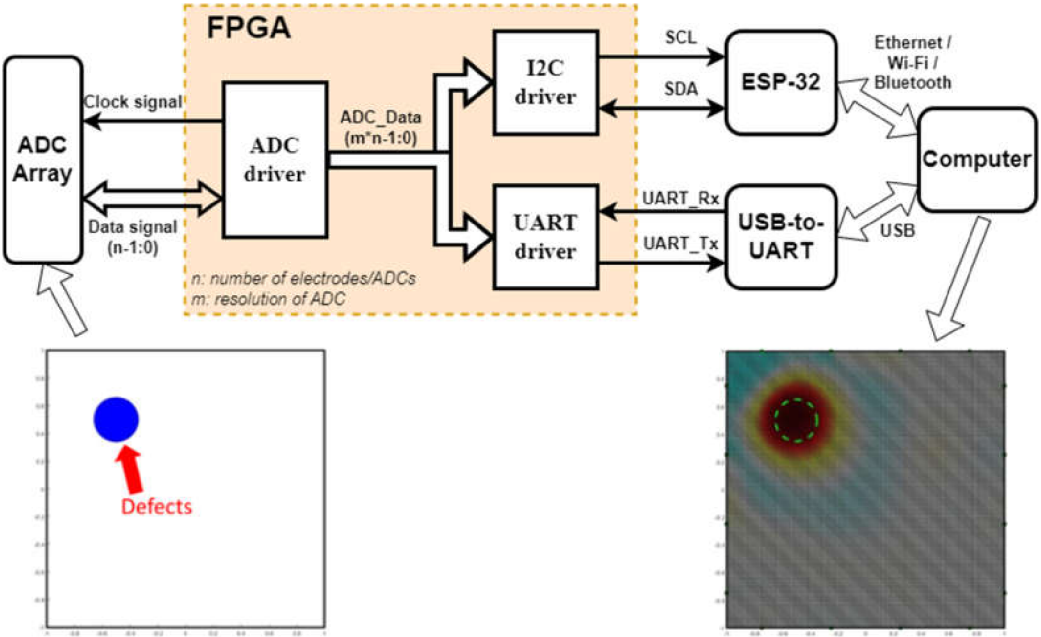


Fig. 7.9 Block diagram of developed EIT/ERT system

To transfer data between FPGA and computer, two options are developed. The first one uses a Universal Asynchronous Receiver/transmitter (UART) interface, with a USB-to-UART bridge (CP2102, CH340G, or similar chip). This option is simple and friendly because it is compatible with USB ports in any computer. However, the data transfer speed is limited by the Baud rate of the UART interface. The second option is high-speed transfer using an ESP-32 microcontroller. The data can be transferred between FPGA and microcontroller via Inter-Integrated Circuit (I2C) protocol, Serial Peripheral Interface (SPI) protocol, or any other protocol. The microcontroller, then, transfers data to the computer via Ethernet or Wi-Fi protocol, making the transfer at high speed. It is important to note that such data transmission between FPGA and computer is suitable for beginning developed stages when the system is developed and verified in the laboratory. For further developed stages, transmission compatible with aircraft standards must be considered.

The selected ADC for the system is differential 24-bit sigma-delta ADC HX711. Each HX711 ADC contains 2 differential input channels (channel A and B) with an internal integrated low-noise Programmable Gain Amplifier (PGA) providing a programmable gain of 128 or 64 for channel A and a fixed gain of 32 for channel B. The full-scale differential input voltage with supply voltage 3,3 V; therefore, is ± 13 mV or ± 26 mV (for channel A), and ± 52 mV (for channel B). The interface to control and communicate with HX711 is a serial interface via 2 ports - PD_SCK for the clock signal, and DOUT for the data signal. The input channel with the corresponding gain is selected by the number of pulses transmitted via the PD_SCK port. The output data rate is optional and selected by connecting the RATE port to the ground (10 samples per second) or to the power supply voltage (80 samples per second). The circuit diagram of HX711 ADC is shown in Fig. 7.10

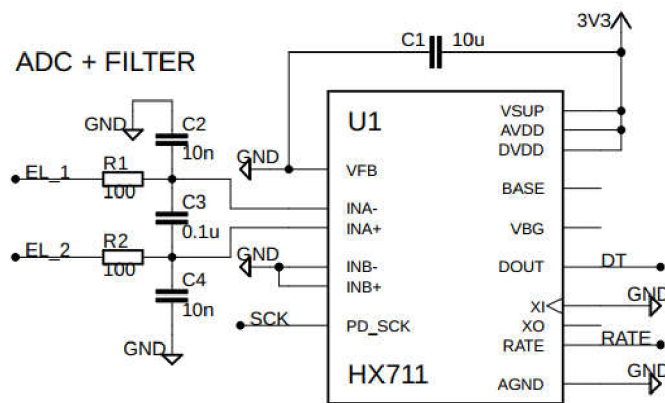


Fig. 7.10 HX711 ADC circuit diagram

7.3.2 VHDL design

The VHDL description of the system can be separated into 3 drivers, as shown in Fig. 7.9. The first driver is an ADC driver, which controls and obtains measured data from the ADC array connected to the investigated object. The second one is an I2C driver, which sends the acquired data to the microcontroller ESP-32 via an I2C bus. The I2C driver is also developed for controlling other ADCs with higher sample rates in the future. The last one is the UART driver, which sends the acquired data to a computer via the UART bus. All the drivers were described in VHDL as Finite State Machine (FSM).

Fig. 7.11 shows the state diagram of the driver controlling the HX711 ADC. This FSM is simple with only 3 states. When no action is required, FSM is in state Idle. If ADC data is ready for being read, the SCK bus is pulled down by ADC, and FSM changes to state Read. After reading 24-bit ADC data, from MSB to LSB, the FSM changes to state Setup, the driver sends SCK pulse to configure ADC (select input channel with corresponding gain) for the next conversion and returns to state Idle.

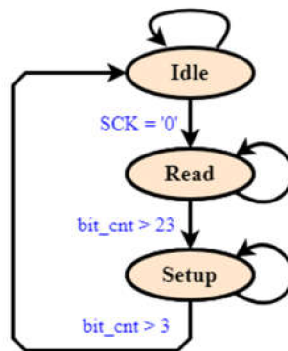


Fig. 7.11 State diagram of HX711 driver

Fig. 7.12 shows the state diagram of the I2C driver, which is used for both communication between FPGA and microcontroller and controlling other ADCs with higher data rates in the future, for example, ADC ADS1115. When no action is required, the FSM is in state Idle, and both SCL and SDA lines are at the high level. As soon as the start signal is pulled up, FSM changes to the state Start, and SDA is pulled down while SCL is still at a high level. After holding time is defined, FSM changes to state Addr, the driver sends the 7-bit address of the I2C slave with the bit R/\bar{W} to require Read or Write to Slave, then changes to the state ACK_Addr. If the address is accurate, the slave sends an acknowledge (ACK) signal by pulling down the SDA line. If it is required to write to slave, the FSM changes to state Write and sends data in each set of 8 bits. After receiving the ACK signal from the slave, the driver changes to state Stop, sets the SCL line to the high level, and the SDA line to low level; then returns to state Idle.

If it is required to read data from the slave, the driver will change to the state Read. However, in some cases, the I2C slave needs more time to manage data and cannot respond to the I2C master timely. In this case, the I2C slave can pull down the SCL line, perform a “clock stretching” and force the master into a waiting state. In this case, the driver will remain on state Stretching until the SCL line is released to the high level. After that the driver changes to state Read, reads data in a set of 8 bits, then changes to state ACK_Read, and sends an ACK signal to the slave by pulling the SDA line low. After sending the ACK signal, the driver changes to state Stop and returns to state Idle.

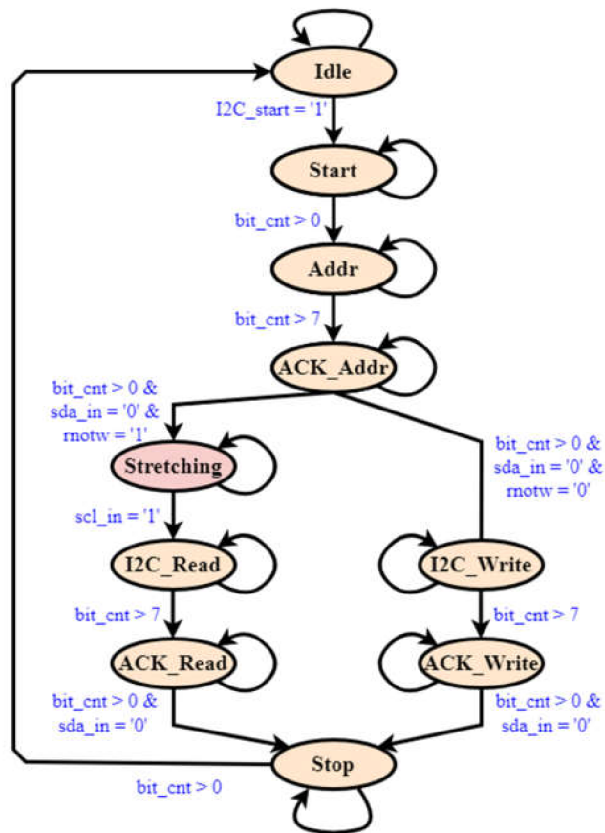


Fig. 7.12 State diagram of I2C driver

The state diagram of the UART driver is shown in Fig. 7.13. The driver will remain in state Idle if no action is required. Once it is required to send data, the driver changes to state TX_Start and pulls down the TX line. The driver, then, sends the data bit from LSB to MSB in turn, in a set of 8 bits. After sending 8 bits, the driver changes to state Stop, pulls the TX line high, and continues to send all the data before returning to state Idle. If the RX line is pulled down, the driver receives a request to read the data. The driver then reads data from LSB to MSB in a set of 8 bits, then returns to state Idle and waits for the next request of receiving data.

In our design, the data is sent and received in a set of 8 bits, the parity bit after each set of 8 data bits is not used, and a Stop bit(s) size is 1 bit. This configuration is called 8N1 UART configuration, which is the most common configuration of UART data transmission. To transmit data successfully, both the transmitting and receiving sides must have the same configuration and baud rate.

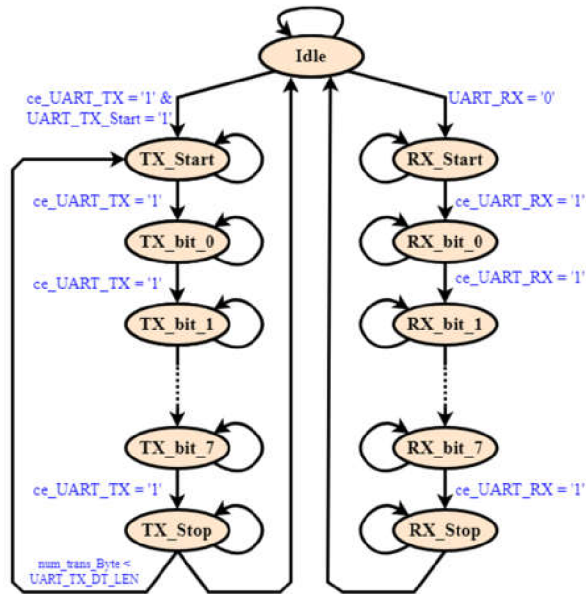


Fig. 7.13 State diagram of UART driver

7.3.3 Functional verification

The measurement setup to verify the function of developed system is shown in Fig. 7.14. The evaluated specimen was prepared using bronze board, which is produced for PCB. To create damage in the specimen, a hole was created in the board by mechanical drilling. For stimulus and measuring the specimen, 16 electrodes were implemented by soldering. The specimen is shown in Fig. 7.15.

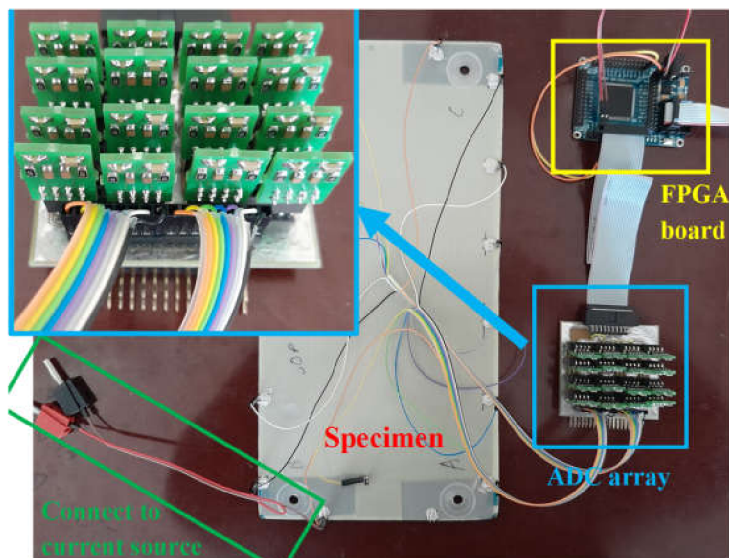


Fig. 7.14 Measurement setup of FPGA-based EIT/ERT system



Fig. 7.15 Specimen for functional verification of FPGA-based developed system

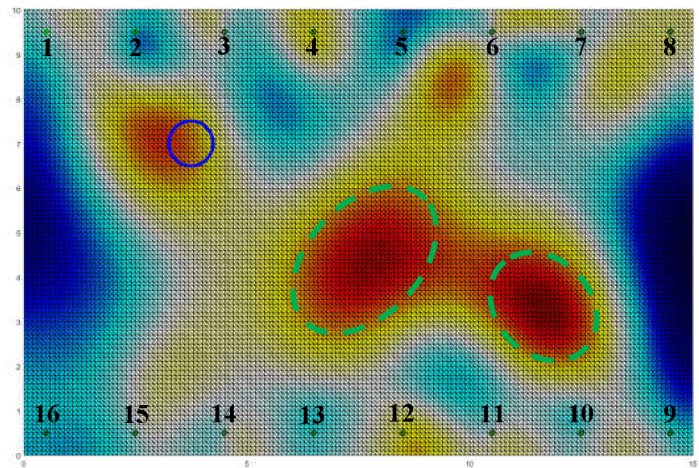


Fig. 7.16 Tomography of specimen - measured by FPGA

The image reconstruction result is shown in Fig. 7.16. The damage was approximately localized (the blue circle indicates the location of damage in the specimen). However, the reconstructed image also shows the “virtual” damages (signed by green dashed circles), which are not in the specimen.

The specimen with damage caused by lightning strikes, which was presented in the previous part of the chapter and measured by the LCR meter was also tested with the FPGA-based system. However, the result can be seen in Fig. 7.17, was not meet the requirement. The damage was not localized as to be expected.

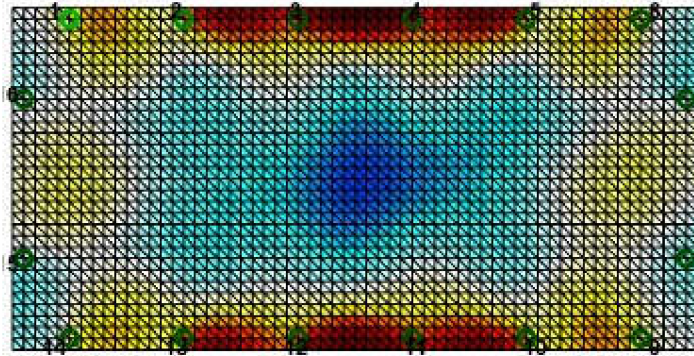


Fig. 7.17 Tomography of specimen with lightning strike damage - measured by FPGA

The reason of unprecise damage indicating can be the inaccuracy of ADC (for example, offset, gain error, and so on) and/or the uncorrelation between ADCs in the ADC arrays. In addition, the measured voltage values were in the range of several tens of microvolts, which is much smaller than the full-scale input range of ADC (several tens of millivolts). Therefore, in the next stage of development, it is important to amplify the voltage before the measurement, to effectively use the full input range of the ADCs.

7.4 Chapter conclusion

This chapter presents the development of the EIT/ERT method as an NDT method for aircraft structure. The study about the state of the art of NDT and EIT/ERT methods is briefly presented as the introduction of the development. An EIT/ERT system using an LCR meter is proposed and used for the NDT test of the composite specimen, which is damaged during the lightning strike test. The main advantages of the LCR meter-based system are high accuracy, high SNR, and wide dynamic measurement range, due to using a dedicated measuring instrument. The image reconstruction result shows that the proposed system is able to approximately localize the damage in the specimen. However, the LCR-based system is more suitable for use in the maintenance process of aircraft structures because of requirements of manual switching electrodes, and long measurement time. For use as an in-flight structure health monitoring system, the EIT/ERT must be developed as a stand-alone electronic system.

The first developed stages of an electronic system for EIT/ERT measurement are also presented. The idea is to use FPGA with an ADC array, to parallelize the measuring process, so the measurement time can be reduced. The developed system also avoids using multiplexors to eliminate the effect of their “on” resistance and the EMI issues caused by their high-speed switching. The development stages presented in the thesis focus mainly on developing VHDL design for parallel driving the ADC array and acquiring measured data from these ADCs, as well as for transferring data between

FPGA and computer and other peripherals. The developed system is also verified by a specimen made from a PCB bronze board, with damage created by drilling. The result shows that the reconstructed image not only approximately localizes the damage but also indicates “virtual” damages which are not in the evaluated specimen. The next development stages will be to improve the accuracy of measurement and verify the system’s ability to localize the damage caused by lightning strikes on composite specimens.

8. CONCLUSION

As discussed in Chapter 2, in recent decades, composite materials are preferred to be used as an alternative to standard metals in the aircraft industry due to their outstanding mechanical properties and thermal stability. Conventional composite materials; however, have limitations in electrical conductivity which is related to the issues of electrical energy distribution, EMI shielding, and especially lightning strike protection in aircraft, as discussed in Chapter 3.

This thesis; therefore, focuses on the measurement and testing of electrical properties of composite materials, which are used for manufacturing of the L-39NG aircraft dorsal cover. For that reason, the main tasks done in this thesis are summarized as follows:

- Preparing composite specimens for measuring and testing: composite specimens were covered by nonconductive epoxide; thus, it is necessary to remove the epoxide layer in a suitable way before any testing and measuring.
- Testing conductivity of composite materials: the first important test was to estimate the range of the measured material's conductivity, which could be considered as a basis for proposing suitable methodologies and methods for further activities.
- Comparing to select the suitable impedance measurement method and instrument: from the estimated conductivity of the measured material and the comparing of impedance measurement method (discussed in Chapter 3), the suitable measurement method (auto-balancing bridge method) and instrument (LCR meter) were selected.
- Proposing a methodology to measure composite specimens prepared by AVA: the impedance between any two electrodes of each specimen was measured, in both polarizations, in order to fully verify the electrical impedance and conductivity of the specimen.
- Design of automatic measuring station using MATLAB environment and SCPI standard for GPIB and RS-232 interface: the main task of the thesis was the design and realization of measuring station. The measuring station was detailly described in Chapter 5.
- Measurement impedance of composite materials: using the above realized measuring system and proposing methodology, the impedance of specimens was measured.
- Analyzing the measurement results, regarding the requirements defined by AVA: the measurement results were analyzed, including their inaccuracy. The analysis was conducted concerning requirements defined by AVA. The detailed analysis was presented in Chapter 5 and was reported to AVA.

- Proposing possible optimization of material selection: based on the analysis and comparing measured results between different specimens, and the parameters of corresponding conductive layers, the possible optimization of material selection was proposed in Chapter 5.
- Analysis the compatibility of the measured conductive layer with the DME/TRANSPONDER antenna: measured conductive layers were analyzed even regarding compatibility with the DME/TRANSPONDER antenna.
- Proposing possible optimization of specimens' dimensions: based on the distribution of current density modeled in Ansys software, the possible optimization of specimens' dimensions was proposed for further measurements and testing for following tasks in the future.
- Testing the lightning strike protection ability: to provide more knowledge about the lightning strike protection ability of the used conductive layer, the lightning strike test was also conducted. The test was described in detail in Chapter 6.
- Analyzing damages caused by lightning strikes with different parameters: The damages caused by lightning strikes with different parameters were observed under the microscope and compared in Chapter 6.
- Proposing the NDT method for detecting the hidden damages caused by lightning strikes: As discussed in Chapter 3, the hidden damages of composite caused by lightning strikes were more serious than visible ones. Therefore, a new NDT method, EIT/ERT method, was proposed and verified for detecting hidden damages. A detailed description of the method and achieved results were introduced in Chapter 7.

Therefore, in conclusion, all the tasks of the thesis have been achieved. In detail:

- **The measuring station for testing the L-39NG aircraft dorsal conductive layer was designed and realized:** the measuring station was designed and realized in the development environment MATLAB with using of the Instrument control toolbox, and SCPI standard. The selected measuring instrument was the R&S HM8118 LCR meter. The physical layer between the controlling computer and the instrument was implemented by the GPIB and RS-232 interfaces. The measuring station enabled remote control measuring instruments to conduct measurements automatically, and automatically acquired measured data for storage, visualization, and analysis. The measuring system was also designed for quickly comparing and analyzing the impedance of measured specimens due to the graphical user interface.
- **The electrical properties of composite specimens' conductive layer were experimentally verified:** using the realized measuring system, the electrical

properties of composite specimens' conductive layer were measured. The measured results provided the basis for proposing optimization of materials selection. However, due to the inappropriate distribution of the prepared electrodes, the measured value could only be used for comparisons between the used conductive layer, not for their characteristics. From the modeling of the current density distribution, the possible optimization of specimens' dimensions was proposed for further measurements and testing in the following activities.

- **Possible optimizations of material selection were suggested:** On the basis of - measured results' comparison with parameters of the used conductive layer, the impacts of each parameter on the resulting conductivity of composite specimen were analyzed. The compatibility of the measured conductive layer with the DME/TRANSPONDER antenna was also analyzed. These provided analyses offered possible optimizations to select suitable materials for manufacturing the dorsal cover of L-39NG aircraft.

In addition, the thesis also provided results of the lightning strike test, which is important to verify the material's ability for lightning strike protection. This ability is one of the most important criteria for selecting materials for manufacturing aircraft structures. Furthermore, the thesis presented the development of systems for NDT testing of composite aircraft structures. The first one was developed by using an LCR meter, thus being suitable for use in the maintenance of aircraft structures. This system's ability to localize the damage was verified. The second system, which was basically the FPGA-based electronic system expected to be used as a structural health monitoring system using EIT/ERT method, was developed in the first stages.

The follow-up work will be to use the developed measuring system to measure the new composite structure prepared by AVA. In the range of the thesis, the carbon composite did not meet the requirement of electrical conductivity. The new carbon composite specimen must be tested to find the most suitable material for manufacturing L-39NG dorsal cover. The FPGA-based EIT/ERT system also needs improving to be able to be used as a structural health monitoring system to detect damage in the composite structures.

LITERATURE

- [1] F. C. (Flake C.) Campbell, “Structural composite materials,” p. 612, 2010, Accessed: Apr. 08, 2023. [Online]. Available: https://books.google.com/books/about/Structural_Composite_Materials.html?id=D3Wta8e07t0C
- [2] S. K. Mazumdar, *Composites manufacturing : materials, product, and process engineering*. CRC Press, 2002. Accessed: Apr. 08, 2023. [Online]. Available: <https://www.routledge.com/Composites-Manufacturing-Materials-Product-and-Process-Engineering/Mazumdar/p/book/9780849305856>
- [3] A. A. Baker and M. L. Scott, “Composite Materials for Aircraft Structures, Third Edition,” *Composite Materials for Aircraft Structures, Third Edition*, Sep. 2016, doi: 10.2514/4.103261.
- [4] B. Esp, “Practical Analysis of Aircraft Composites,” p. 737, 2017.
- [5] B. Kročová, “Částicové kompozity vyztužené krátkými vlákny”, Accessed: Apr. 08, 2023. [Online]. Available: <http://dspace.vutbr.cz/handle/11012/6380>
- [6] F. Smith, “The Use of composites in aerospace: Past, present and future challenges,” 2013.
- [7] B. Alemour, O. Badran, and M. R. Hassan, “A review of using conductive composite materials in solving lightning strike and ice accumulation problems in aviation,” *Journal of Aerospace Technology and Management*, vol. 11, 2019, doi: 10.5028/JATM.V11.1022.
- [8] S. P. Rawal, M. S. Misra, and R. G. Wendt, “Composite Materials for Space Applications,” Virginia, Aug. 1990.
- [9] C. Soutis, “Fibre reinforced composites in aircraft construction,” *Progress in Aerospace Sciences*, vol. 41, no. 2, pp. 143–151, 2005, doi: 10.1016/J.PAEROSCI.2005.02.004.
- [10] L. Zhang, X. Wang, J. Pei, and Y. Zhou, “Review of automated fibre placement and its prospects for advanced composites,” *J Mater Sci*, vol. 55, no. 17, pp. 7121–7155, Jun. 2020, doi: 10.1007/S10853-019-04090-7.
- [11] A. Krzyzak, E. Kosicka, M. Borowiec, and R. Szczepaniak, “Selected Tribological Properties and Vibrations in the Base Resonance Zone of the Polymer Composite Used in the Aviation Industry,” *Materials 2020, Vol. 13, Page 1364*, vol. 13, no. 6, p. 1364, Mar. 2020, doi: 10.3390/MA13061364.
- [12] Y. Xu, J. Zhu, Z. Wu, Y. Cao, Y. Zhao, and W. Zhang, “A review on the design of laminated composite structures: constant and variable stiffness design and topology optimization,” *Adv Compos Hybrid Mater*, vol. 1, no. 3, pp. 460–477, Sep. 2018, doi: 10.1007/S42114-018-0032-7.
- [13] R. Deo, J. Starnes, and R. Holzwarth, “Low-Cost Composite Materials and Structures for Aircraft Applications,” 2003.

- [14] “New Russian Stealth Material can absorb 95% Electronic Radiation.” https://www.defensemirror.com/news/33924/New_Russian_Stealth_Material_can_absorb_95_Electronic_Radiation#.ZEMU6HZByUk (accessed Apr. 22, 2023).
- [15] S. Pervaiz, T. A. Qureshi, G. Kashwani, and S. Kannan, “3D printing of fiber-reinforced plastic composites using fused deposition modeling: A status review,” *Materials*, vol. 14, no. 16, Aug. 2021, doi: 10.3390/MA14164520.
- [16] “F-16.net - The ultimate F-16, F-35 and F-22 reference.” <https://www.f-16.net/f-35-news-article2671.html> (accessed May 23, 2023).
- [17] “L-39NG Program | AERO Vodochody AEROSPACE a.s.” <https://www.aero.cz/en/aircraft/programs/l-39ng/> (accessed Apr. 22, 2023).
- [18] “PROVING THE AIRFRAME STRENGTH OF THE L-39NG TRAINER JET Aerospace Testing International : 2022 Showcase.” <https://ati.mydigitalpublication.co.uk/articles/proving-the-airframe-strength-of-the-l-39ng-trainer-jet> (accessed Apr. 22, 2023).
- [19] J. Václavík, “Vývoj a zkoušky kompozitního vzduchovodu,” *TRANSFER*, vol. 32, pp. 16–20, 2019, Accessed: Apr. 22, 2023. [Online]. Available: www.vzlu.cz.
- [20] J. Václavík, “Vývoj kompozitního vzduchovodu pro letoun L-39NG,” *TRANSFER*, vol. 27, pp. 28–34, 2016, Accessed: Apr. 22, 2023. [Online]. Available: www.vzlu.cz
- [21] “Nový český proudový letoun Aero L-39NG absolvoval svůj první let – CZECH AIR FORCE.” <https://czechairforce.com/news/novy-cesky-proudovy-letoun-aero-l-39ng-absolvoval-svuj-prvni-let/> (accessed May 22, 2023).
- [22] “Slavnostní roll-out nového letounu L-39NG, který získá i pardubické Centrum leteckého výcviku – CZECH AIR FORCE.” <https://czechairforce.com/news/slavnostni-roll-out-noveho-letounu-l-39ng-ktery-ziska-i-pardubicke-centrum-leteckeho-vycviku/> (accessed May 22, 2023).
- [23] T. K. Eismín, *Aircraft Electricity and Electronics, Sixth Edition*. McGraw-Hill Education, 2014. Accessed: May 13, 2023. [Online]. Available: <https://www.accessengineeringlibrary.com/content/book/9780071799157>
- [24] S. Dominiak, J. Wassner, S. Gastel, and J. Späh, “POWER LINE DATA BUS (PLUS),” 2019.
- [25] “Distribution of power supplies (part 1).” https://www.industrial-electronics.com/aircraft_8.html (accessed May 13, 2023).
- [26] R. Dureja, E. W. D. Rozier, and K. Y. Rozier, “A Case Study in Safety, Security, and Availability of Wireless-Enabled Aircraft Communication Networks *”, Accessed: May 13, 2023. [Online]. Available: <https://nuxmv.fbk.eu/>.
- [27] “The Software Discrepancies That Caused A Multibillion-Euro Delay To The Airbus A380 Program.” https://simpleflying.com/airbus-a380-program-software-discrepancies-delay-story/?newsletter_popup=1 (accessed May 13, 2023).
- [28] A. Bigand, “Damage assessment on aircraft composite structure due to lightning constraints,” 2020. Accessed: May 13, 2023. [Online]. Available: <http://www.theses.fr/2020ESAE0027>

- [29] P. Rafael Sousa Martins, “Experimental and theoretical studies of lightning arcs and their interaction with aeronautical materials,” Université Paris-Saclay, 2016. Accessed: May 14, 2023. [Online]. Available: <https://theses.hal.science/tel-01434344>
- [30] D. Morgan, C. J. Hardwick, S. J. Haigh, and A. J. Meakins, “The Interaction of Lightning with Aircraft and the Challenges of Lightning Testing Lightning Hazards to Aircraft and Launchers The Interaction of Lightning with Aircraft and the Challenges of Lightning Testing”, Accessed: May 14, 2023. [Online]. Available: <https://hal.science/hal-01184419>
- [31] BARDIA KIASAT, ABEEB FAJOBI OLAMILEKAN, ADAM BIN MOHD FIKRI, NADIA SYUHADA BINTI JANUDIN, and FITRIATI KAMARIL ISWARDHANI BINTI ROHADI SILO EDIPRONO, “Damage Caused by Electromagnetic Radiation on Aircraft Structure Composite Material .,” Feb. 2018. Accessed: May 14, 2023. [Online]. Available: https://www.academia.edu/36636653/Damage_Caused_by_Electromagnetic_Radiation_on_Aircraft_Structure_Composite_Material
- [32] C. Karch, M. Calomfirescu, M. Rothenhäusler, C. Brand, and H. Meister, “FFS: Lightning Strike Protection of Radomes – An Overview,” 2017.
- [33] C. Karch, C. Paul, and F. Heidler, “Lightning Strike Protection of Radomes,” *EMC Europe 2019 - 2019 International Symposium on Electromagnetic Compatibility*, pp. 650–655, Sep. 2019, doi: 10.1109/EMCEUROPE.2019.8871944.
- [34] “The History of Lightning Protection Technology for Aircraft.” <https://weatherguardaero.com/lightning-protection-technology-aircraft/> (accessed May 16, 2023).
- [35] C. C. Goodloe, “Lightning Protection Guidelines for Aerospace Vehicles,” 1999.
- [36] “Electromagnetic Compatibility in the Defense Systems of Future Years,” 2002.
- [37] “MIL-B-5087 B BONDING ELECTRICAL LIGHTNING PROTECTION.” http://everyspec.com/MIL-SPECS/MIL-SPECS-MIL-B/MIL-B-5087B_2295/ (accessed May 16, 2023).
- [38] A. Katunin, K. Krukiewicz, A. Herega, and G. Catalanotti, “Concept of a Conducting Composite Material for Lightning Strike Protection,” *Advances in Materials Science*, vol. 16, no. 2, pp. 32–46, Jun. 2016, doi: 10.1515/ADMS-2016-0007.
- [39] “Lightning Strikes: Protection, Inspection, and Repair.” https://www.boeing.com/commercial/aeromagazine/articles/2012_q4/4/ (accessed May 17, 2023).
- [40] L. Chemartin, P. Lalande, C. Delalondre, B. G. Cheron, H. Andreu, and C. Andre, “3D SIMULATION OF ELECTRIC ARC COLUMN FOR LIGHTNING AEROPLANE CERTIFICATION,” *High Temperature Material Processes: An International Quarterly of High-Technology Plasma Processes*, vol. 12, no. 1–2, pp. 65–78, 2008, doi: 10.1615/HIGHTEMPMATPROC.V12.I1-2.60.

- [41] L. Chemartin *et al.*, “Direct Effects of Lightning on Aircraft Structure: Analysis of the Thermal, Electrical and Mechanical Constraints,” *Aerospace Lab*, no. 5, pp. 1–15, Dec. 2012, Accessed: May 14, 2023. [Online]. Available: <https://hal.science/hal-01184416>
- [42] M. D. Coutellier, “Développement d’un modèle mécanique pour la prédiction des dommages de panneaux composites aéronautiques soumis à un choc foudre,” <http://www.theses.fr>, Mar. 2016, Accessed: May 14, 2023. [Online]. Available: <http://www.theses.fr/2016ESAE0004>
- [43] Y. Li, R. Li, L. Lu, and X. Huang, “Experimental study of damage characteristics of carbon woven fabric/epoxy laminates subjected to lightning strike,” *Compos Part A Appl Sci Manuf*, vol. 79, pp. 164–175, Dec. 2015, doi: 10.1016/J.COMPOSITESA.2015.09.019.
- [44] Y. Hirano *et al.*, “Lightning damage suppression in a carbon fiber-reinforced polymer with a polyaniline-based conductive thermoset matrix,” *Compos Sci Technol*, vol. 127, pp. 1–7, Apr. 2016, doi: 10.1016/J.COMPSCITECH.2016.02.022.
- [45] “This is what you should know about Boeing 787 lightning protection | Mainblades.” <https://mainblades.com/article/this-is-what-you-should-know-about-boeing-787-lightning-protection/> (accessed May 17, 2023).
- [46] Keysight, “Keysight Technologies Impedance Measurement Handbook A guide to measurement technology and techniques 4th Edition Application Note”.
- [47] R. Dosoudil, “DETERMINATION OF PERMEABILITY FROM IMPEDANCE MEASUREMENT USING VECTOR NETWORK ANALYZER,” 2012.
- [48] “R&S@HM8118 Programmable LCR-Bridge Benutzerhandbuch User Manual”.
- [49] “Introduction to SCPI Language.” https://rfmw.em.keysight.com/spdhelpfiles/33500/webhelp/us/content/___I_SCPI/0%20scpi_introduction.htm (accessed May 02, 2023).
- [50] “2. Introducing SCPI Commands | Rohde & Schwarz.” https://www.rohde-schwarz.com/cz/driver-pages/remote-control/remote-programming-environments_231250.html (accessed May 02, 2023).
- [51] “Standard Commands for Programmable Instruments (SCPI) Volume 1: Syntax and Style,” 1999, Accessed: May 02, 2023. [Online]. Available: <http://ourworld.compuserve.com/homepages/acea/>
- [52] “Products.” <https://www.aero-consultants.co.uk/productpage.php?product=13210&category=372&name=Expanded+Metals> (accessed May 07, 2023).
- [53] “RTCA DO-160G for Airborne Equipment | DO-160.” <https://do160.org/rtca-do-160g/> (accessed May 16, 2023).
- [54] “Medium Impulse Voltage Generator - Haefely Catalogs | Technical Documentation .” <https://pdf.directindustry.com/pdf/haefely-ag/medium-impulse-voltage-generator-type/17027-501765.html> (accessed May 17, 2023).

- [55] S. Kumar and D. Mahto, "Recent Trends In Industrial And Other Engineering Applications Of Non Destructive Testing: A Review," 2013, Accessed: May 18, 2023. [Online]. Available: <http://ssrn.com/abstract=2770922http://www.ijser.org>
- [56] Petr Bělský, "Ultrazvuková nedestruktivní kontrola kompozitních konstrukcí ve VZLÚ," *TRANSFER*, vol. 21, pp. 11–17, 2014, Accessed: May 18, 2023. [Online]. Available: www.vzlu.czup
- [57] S. K. Dwivedi, M. Vishwakarma, and P. A. Soni, "Advances and Researches on Non Destructive Testing: A Review," *Mater Today Proc*, vol. 5, no. 2, pp. 3690–3698, 2018, doi: 10.1016/J.MATPR.2017.11.620.
- [58] P. Raso and T. Marczi, "Algorithm for the signal evaluation of L39-NG Aircraft Ultrasonic Guided Wave SHM Sensor System", Accessed: May 18, 2023. [Online]. Available: <http://www.ndt.net/?id=23220>
- [59] T. Marczi and P. Rášo, "Design of UGW SHM Sensor System for L-39NG Aircraft", Accessed: May 18, 2023. [Online]. Available: <http://www.ndt.net/?id=23219>
- [60] K. Doubrava, M. Dvořák, N. Schmidová, T. Kostroun, J. Václavík, and M. Růžička, "EXPERIMENTAL ANALYSIS OF COMPOSITE JET ENGINE AIR INLET," in *Danubia-Adria Symposium on Advances in Experimental Mechanics*, 2019. Accessed: May 18, 2023. [Online]. Available: <http://www.aero.cz/en/media/news/l-39ng->
- [61] T. K. Bera, "Applications of Electrical Impedance Tomography (EIT): A Short Review," pp. 22–24, 2011, doi: 10.1088/1757-899X/331/1/012004.
- [62] S. Mansouri, Y. Alharbi, F. Haddad, S. Chabcoub, A. Alshrouf, and A. A. Abd-Elghany, "Electrical Impedance Tomography – Recent Applications and Developments," *J Electr Bioimpedance*, vol. 12, no. 1, p. 50, 2021, doi: 10.2478/JOEB-2021-0007.
- [63] D. I. J. Dědková, "IMAGE RECONSTRUCTION METHODS BASED ON ELECTRICAL IMPEDANCE TOMOGRAPHY," Brno University of Technology, 2007.
- [64] M. Cheney, D. Isaacson, and J. C. Newell, "Electrical Impedance Tomography *," *Society for Industrial and Applied Mathematics*, vol. 41, no. 1, pp. 85–101, 1999, Accessed: May 19, 2023. [Online]. Available: <http://www.siam.org/journals/sirev/41-1/33361.html>
- [65] A. Adler and A. Boyle, "Electrical Impedance Tomography".
- [66] N. Nam Pham, J. Leuchter, and Q. Huy Dong, "FPGA-based measurement instrument for the ERT applications of aerospace composite materials," *Proceedings of the 2022 20th International Conference on Mechatronics - Mechatronika, ME 2022*, 2022, doi: 10.1109/ME54704.2022.9983440.
- [67] J. Cagaň, "Hardware implementation of electrical resistance tomography for damage detection of carbon fibre-reinforced polymer composites," *Struct Health Monit*, vol. 16, no. 2, pp. 129–141, 2017, doi: 10.1177/1475921716666004.

- [68] Z. Cui, Y. Chen, P. Zou, C. Wang, and H. Wang, "Development of electromagnetic tomography system using LCR meter," I2MTC 2018 - 2018 IEEE International Instrumentation and Measurement Technology Conference: Discovering New Horizons in Instrumentation and Measurement, Proceedings, pp. 1–5, Jul. 2018, doi: 10.1109/I2MTC.2018.8409703.
- [69] "EIDORS." <https://eidors3d.sourceforge.net/index.shtml> (accessed May 20, 2023).
- [70] R. Basak and K. A. Wahid, "An In Situ Electrical Impedance Tomography Sensor System for Biomass Estimation of Tap Roots," *Plants* 2022, Vol. 11, Page 1713, vol. 11, no. 13, p. 1713, Jun. 2022, doi: 10.3390/PLANTS11131713.

SYMBOLS AND ABBREVIATIONS

Abbreviations:

ACK	Acknowledgement
ADC	Analog-to-Digital Converter
AVA	AERO Vodochody AEROSPACE a.s.
CTE	Coefficient of Thermal Expansion
DUT	Device Under Test
EIT/ERT	Electrical Impedance/Resistance Tomography
EMI	Electromagnetic Interference
EM coupling	Electromagnetic coupling
EUROCAE	European Organization for Civil Aviation Equipment
FAA	Federal Aviation Administration
FEM	Finite Element Method
FPGA	Field Programmable Gate Arrays
FSM	Finite State Machine
GUI	Graphical User Interface
IEEE	Institute of Electrical and Electronics Engineers
ISO	International Organization for Standardization
I2C	Inter-Integrated Circuit protocol
LSB	Least Significant Bit
LSP	Lightning Strike Protection
MSB	Most Significant Bit
NDT	Non-destructive Testing
PCB	Printed Circuit Board
RTCA	Radio Technical Commission for Aeronautics
SAE	Society of Automotive Engineers
SCPI	Standard Commands for Programmable Instrument
SNR	Signal-to-Noise Ratio
UART	Universal Asynchronous Receiver/Transmitter
VHDL	Very High Speed Integrated Circuit Hardware Description Language
VNA	Vector Network Analyzer
VZLU	Czech Aerospace Research Center

Symbols:

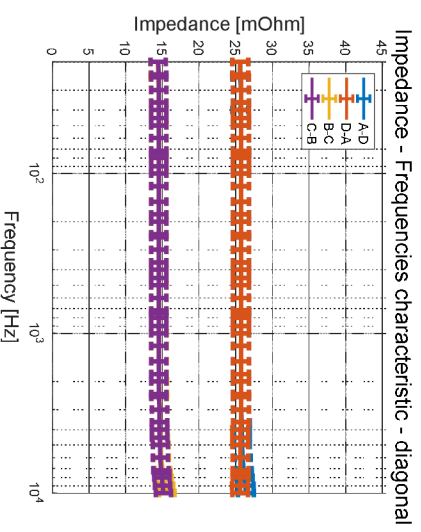
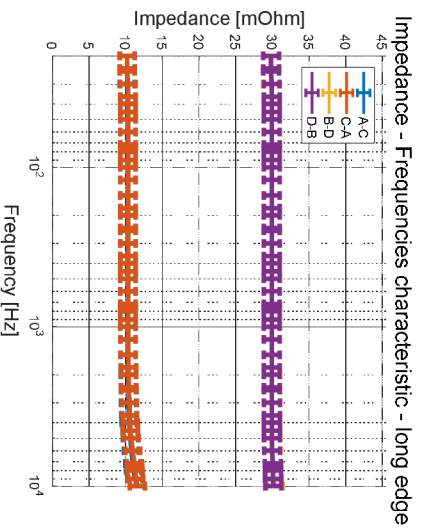
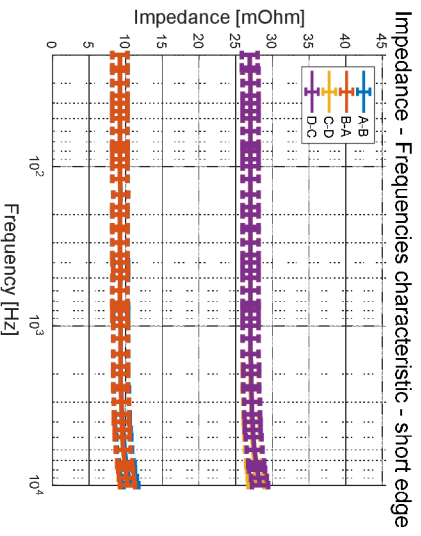
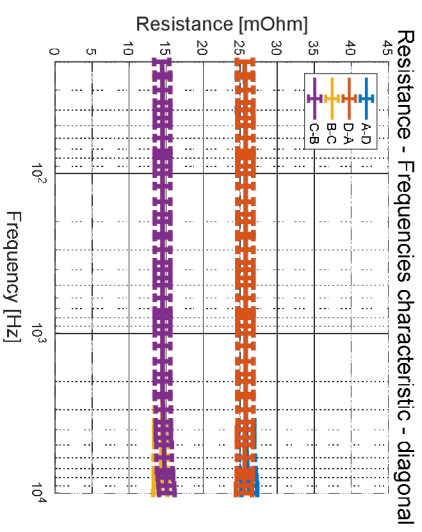
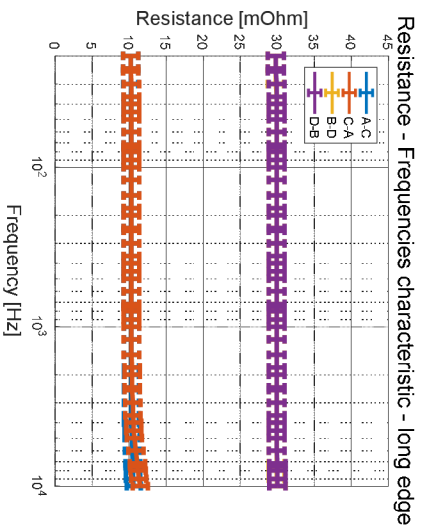
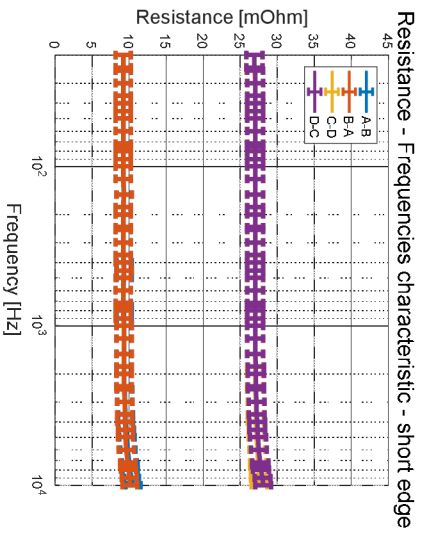
V	voltage	(V)
I	current	(A)
Z	impedance	(Ω)
R	resistance	(Ω)

LIST OF APPENDICES

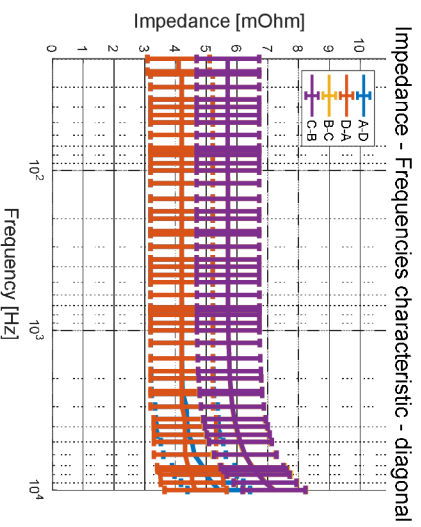
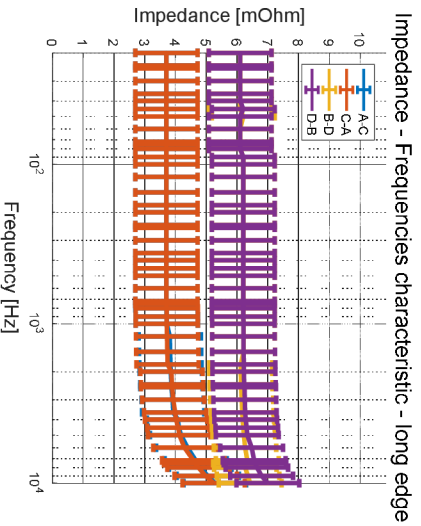
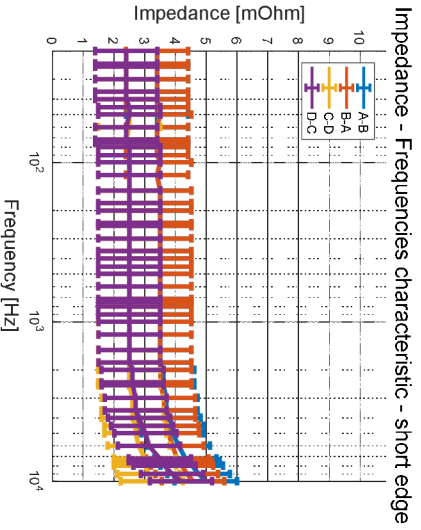
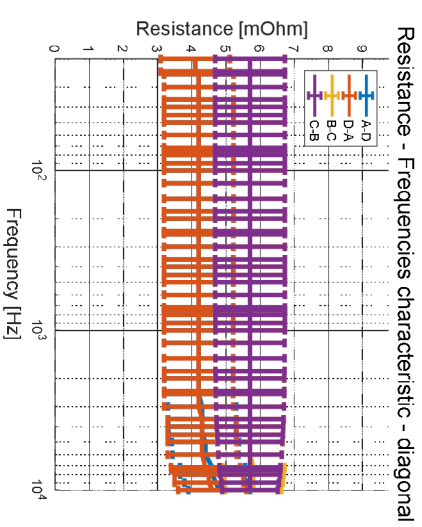
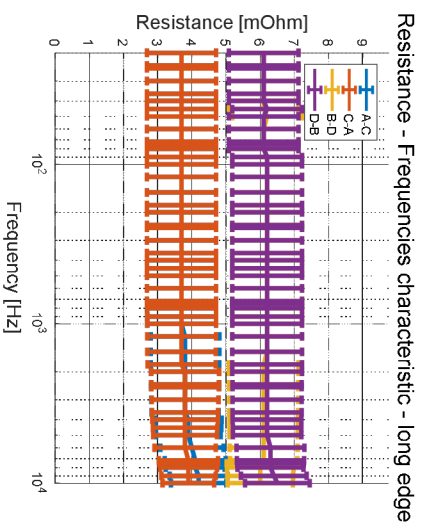
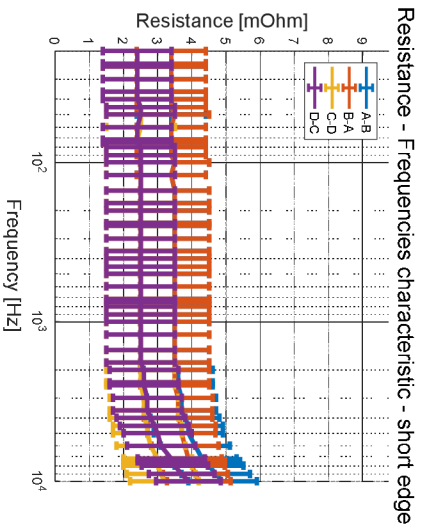
APPENDIX A – IMPEDANCE OF INDIVIDUAL SAMPLES.....	98
APPENDIX B – SAMPLE IMPEDANCE COMPARISON.....	106
APPENDIX C – LIGHTNINGS TRIKE TESTS	113

Appendix A - Impedance of individual samples

SampleM1556860-1

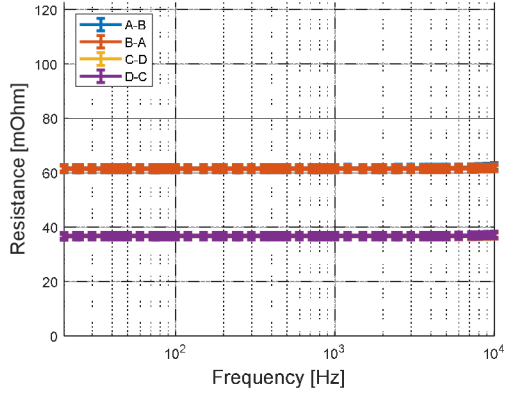


SampleM1556860-2

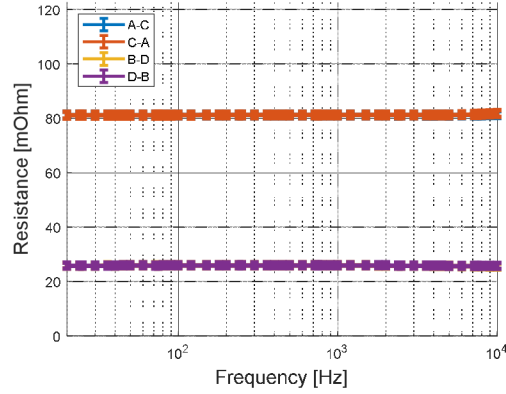


SampleM1712603-1

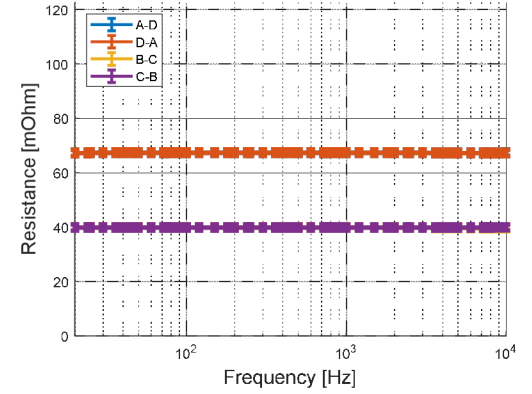
Resistance - Frequencies characteristic - short edge



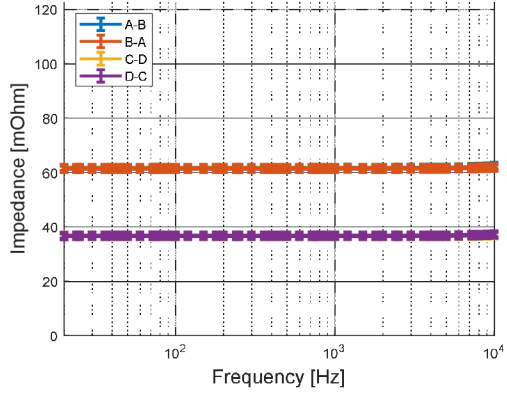
Resistance - Frequencies characteristic - long edge



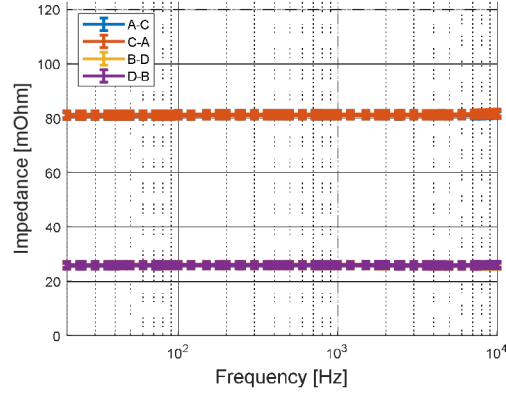
Resistance - Frequencies characteristic - diagonal



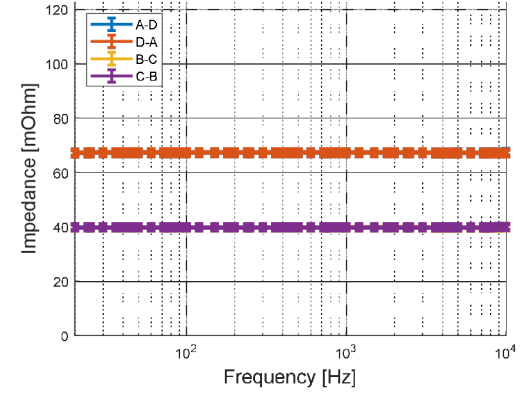
Impedance - Frequencies characteristic - short edge



Impedance - Frequencies characteristic - long edge

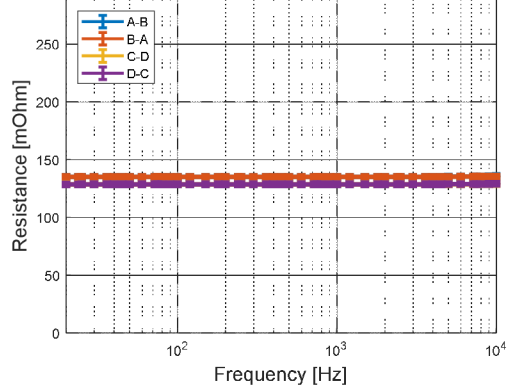


Impedance - Frequencies characteristic - diagonal

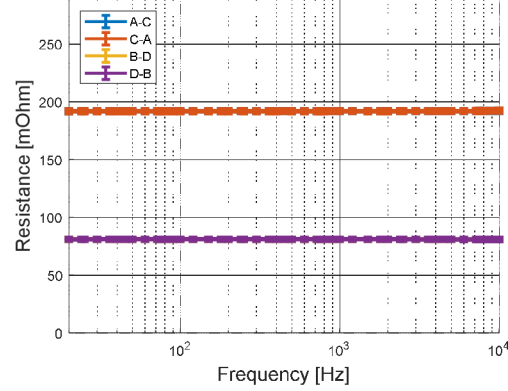


SampleM1712603-2

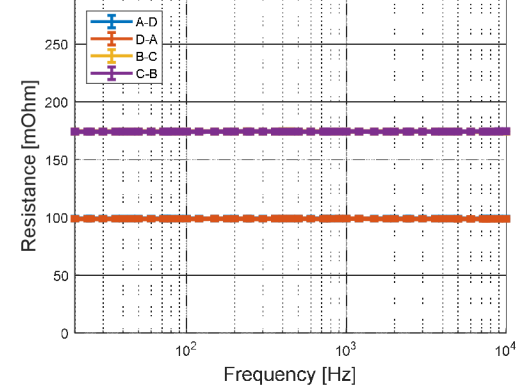
Resistance - Frequencies characteristic - short edge



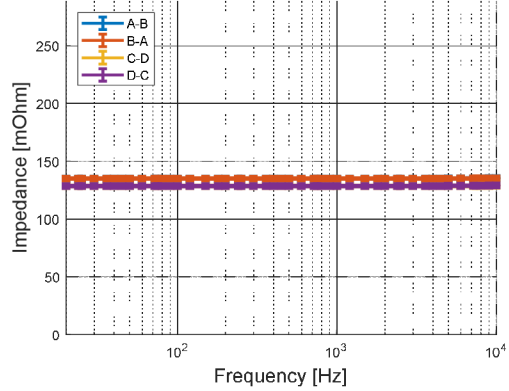
Resistance - Frequencies characteristic - long edge



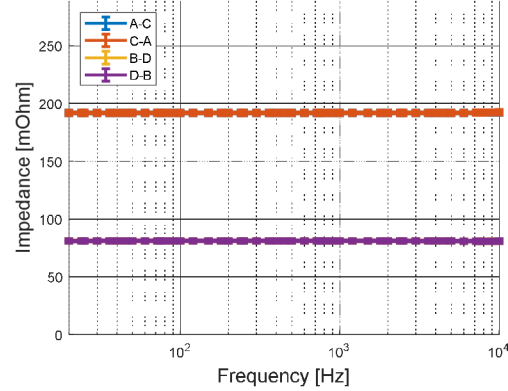
Resistance - Frequencies characteristic - diagonal



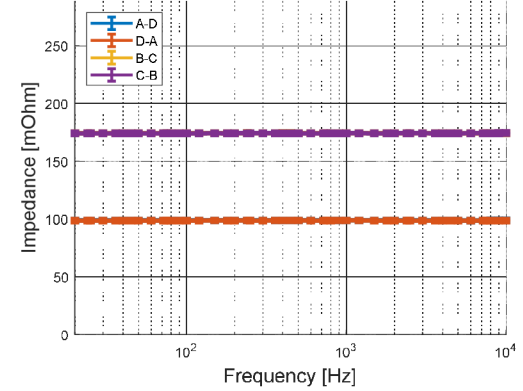
Impedance - Frequencies characteristic - short edge



Impedance - Frequencies characteristic - long edge

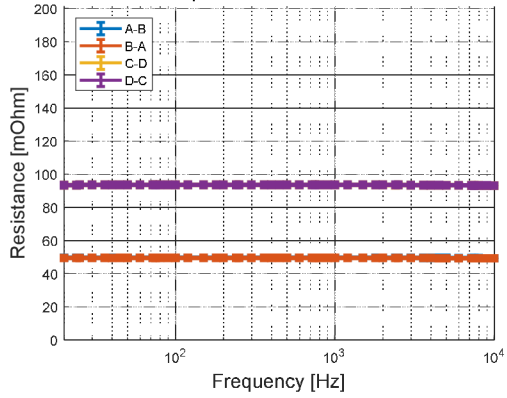


Impedance - Frequencies characteristic - diagonal

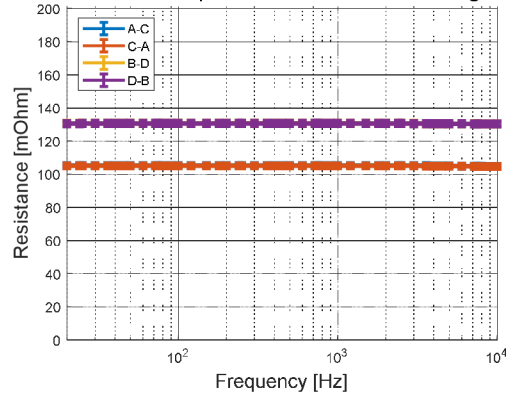


SampleSOP-056-2

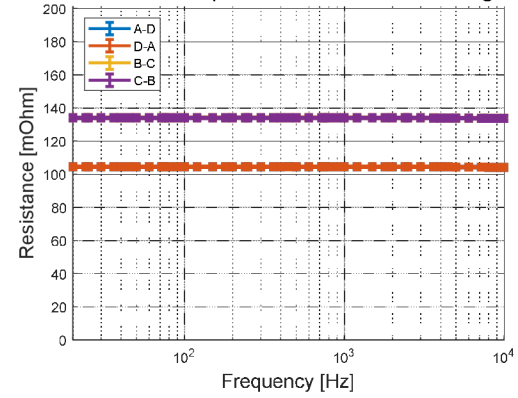
Resistance - Frequencies characteristic - short edge



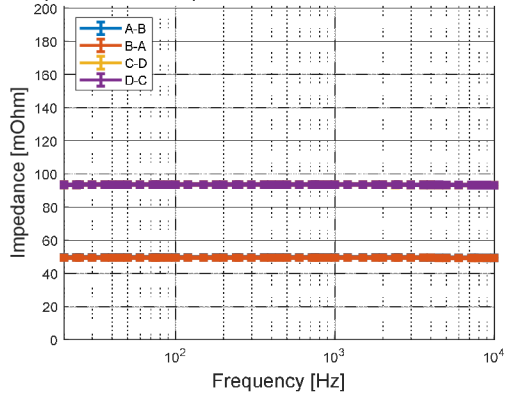
Resistance - Frequencies characteristic - long edge



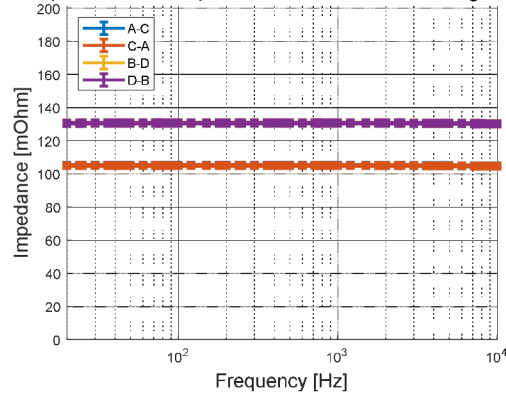
Resistance - Frequencies characteristic - diagonal



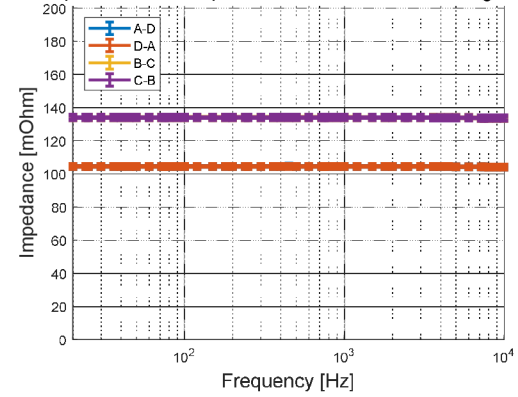
Impedance - Frequencies characteristic - short edge



Impedance - Frequencies characteristic - long edge

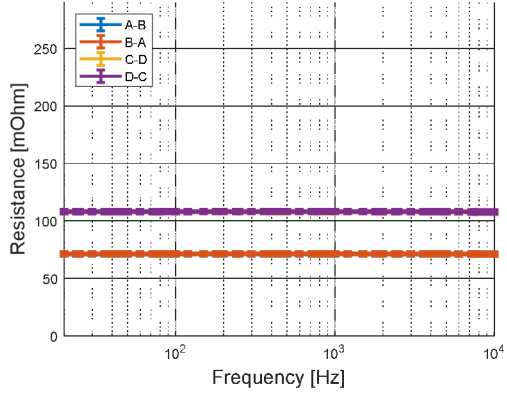


Impedance - Frequencies characteristic - diagonal

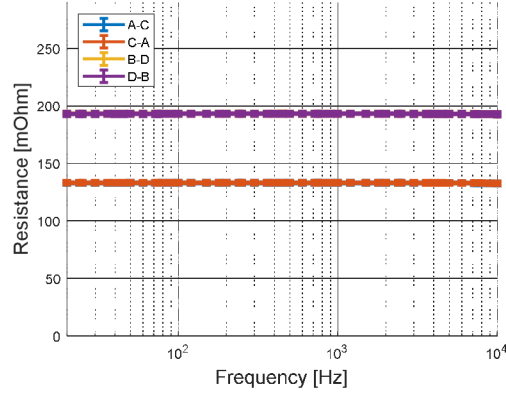


SampleSOP-056-4

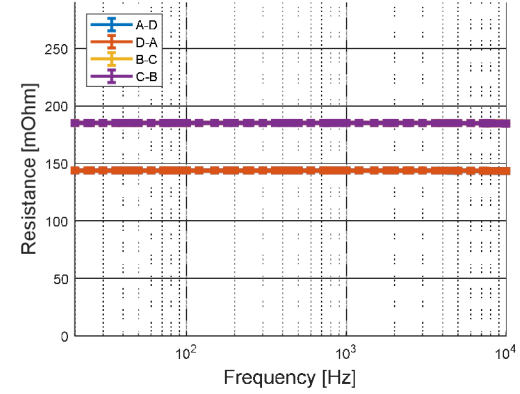
Resistance - Frequencies characteristic - short edge



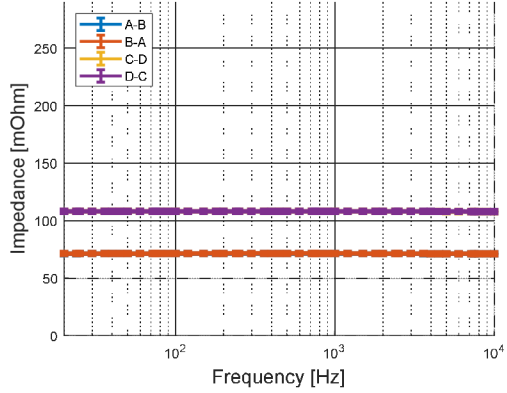
Resistance - Frequencies characteristic - long edge



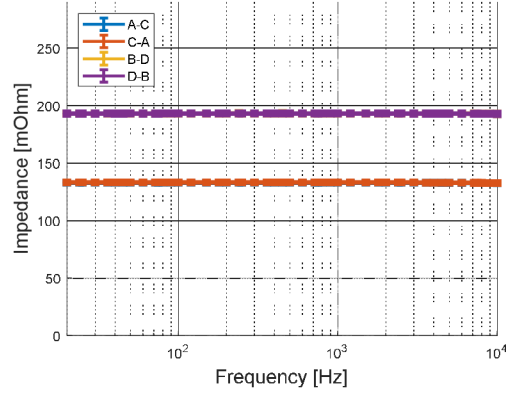
Resistance - Frequencies characteristic - diagonal



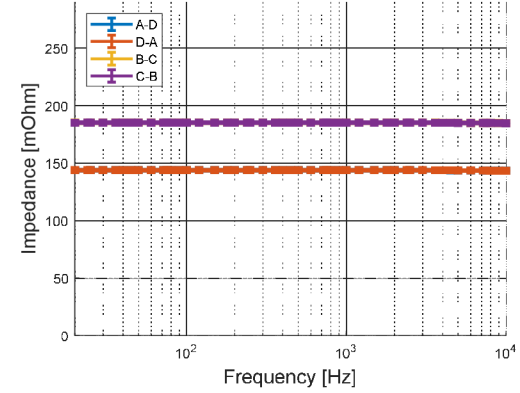
Impedance - Frequencies characteristic - short edge



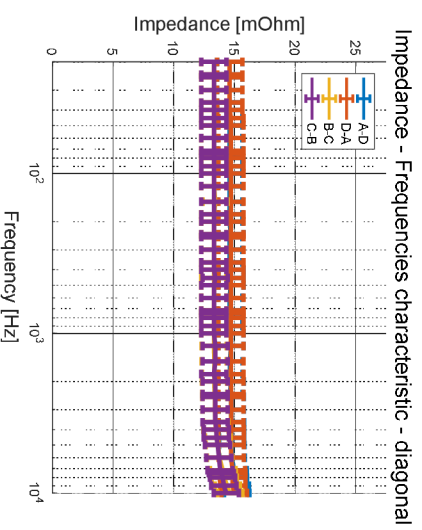
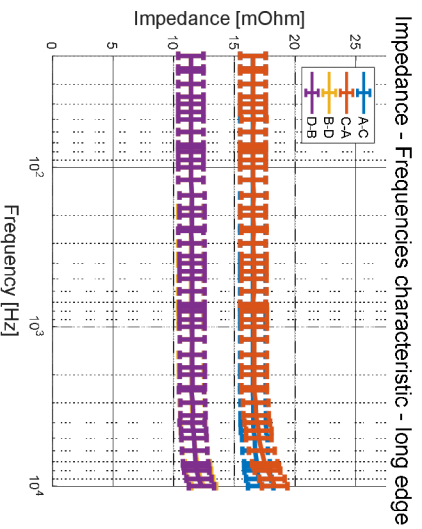
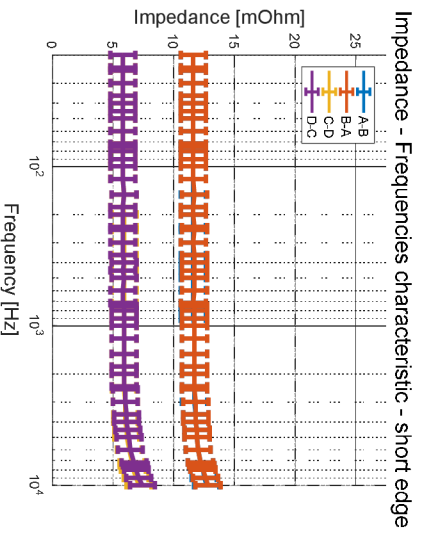
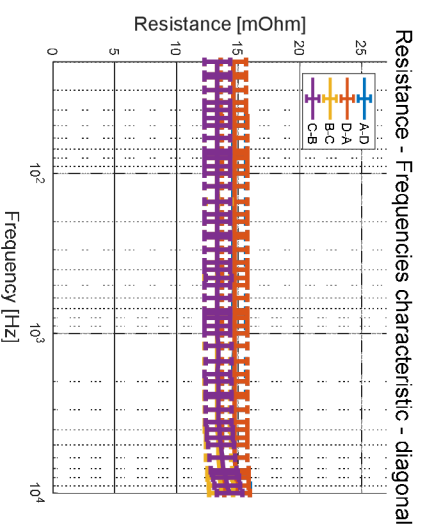
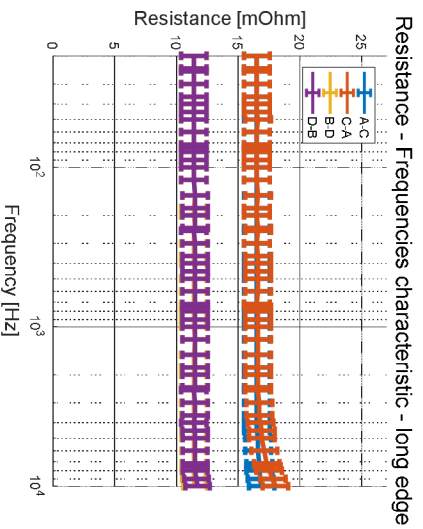
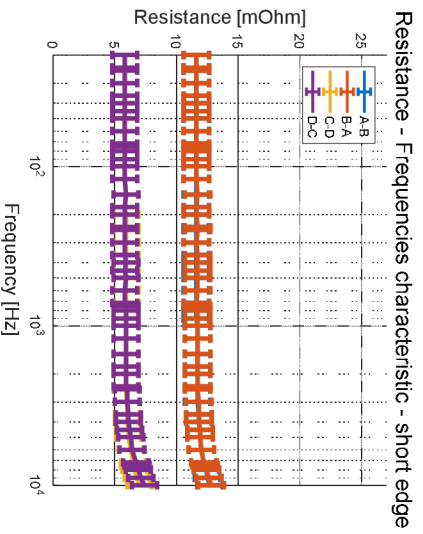
Impedance - Frequencies characteristic - long edge



Impedance - Frequencies characteristic - diagonal

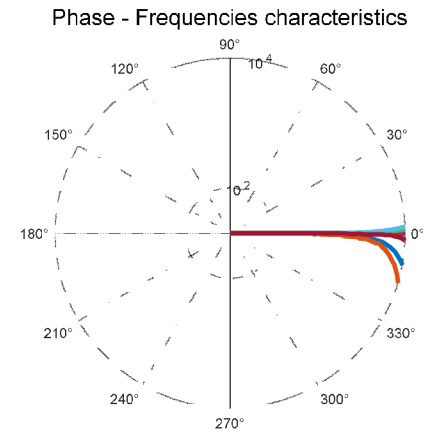
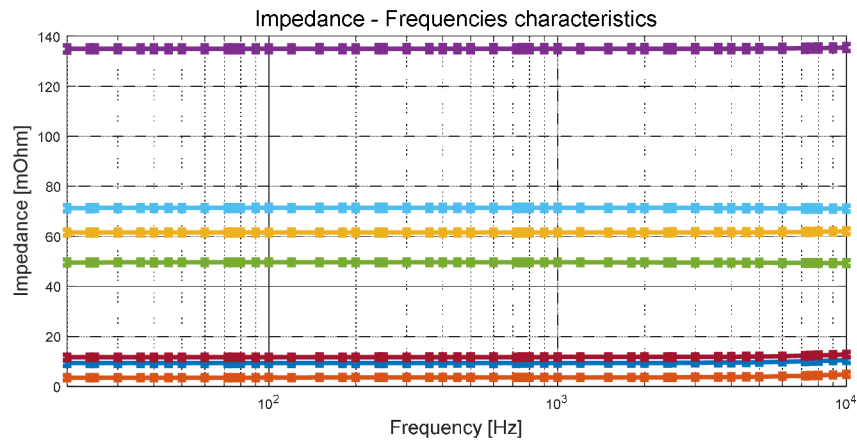
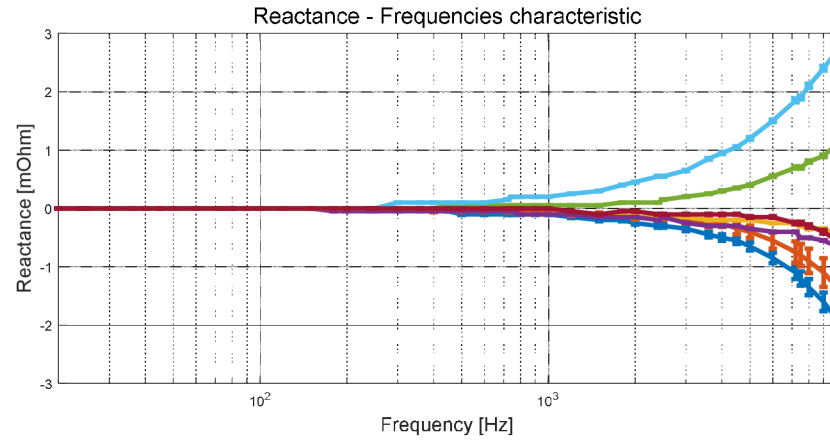
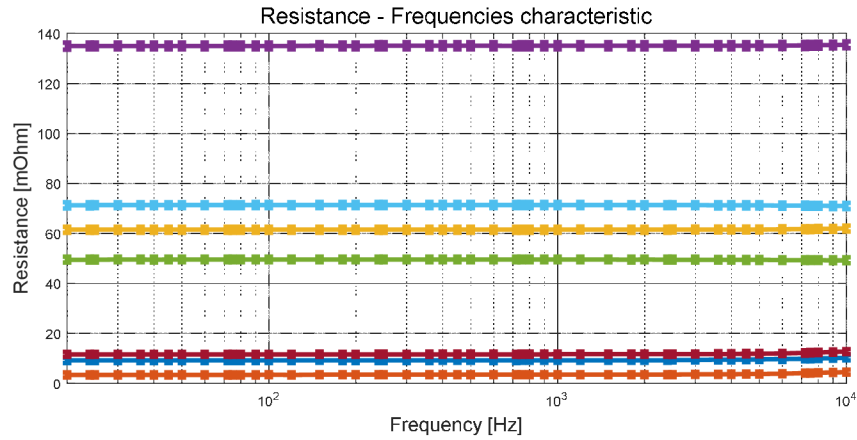


SampleSOP-057-3



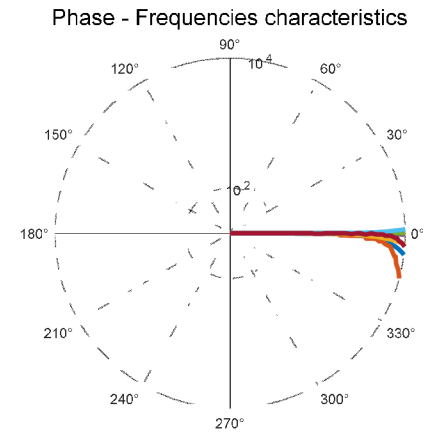
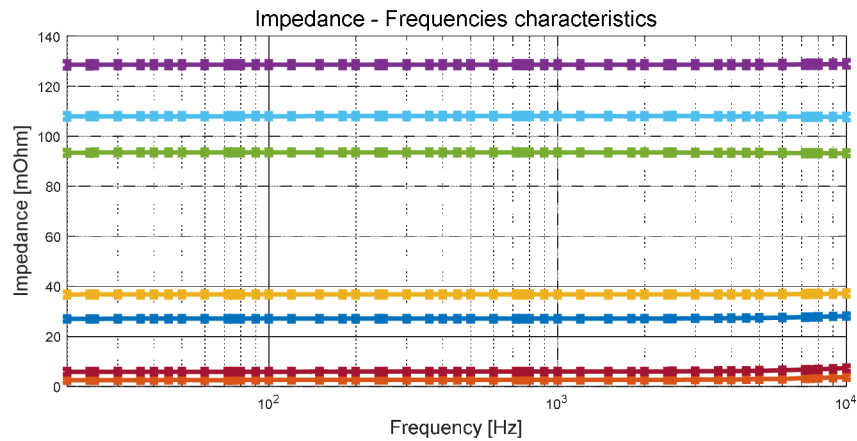
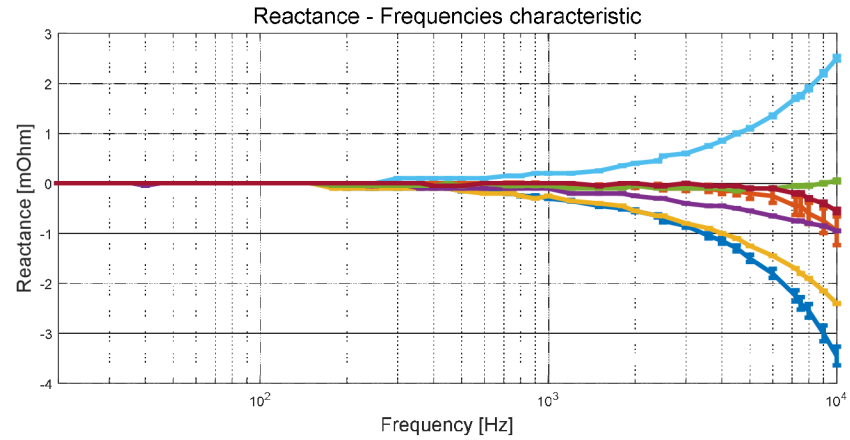
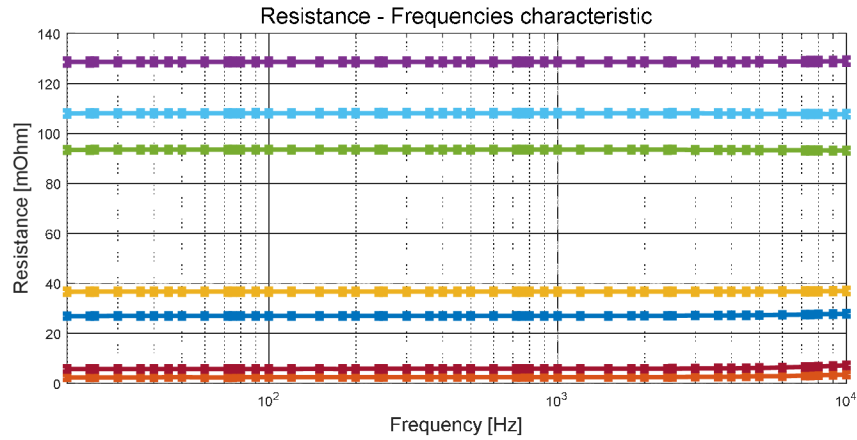
Appendix B - Sample Impedance Comparison

Comparison impedance between A and B - frequency to 10kHz



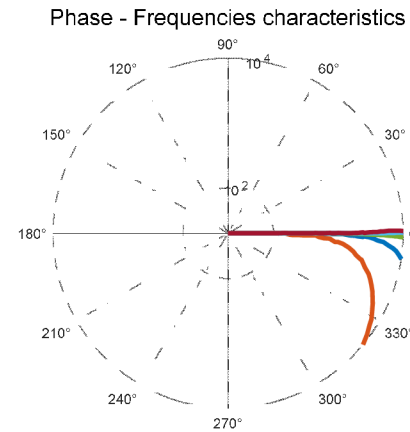
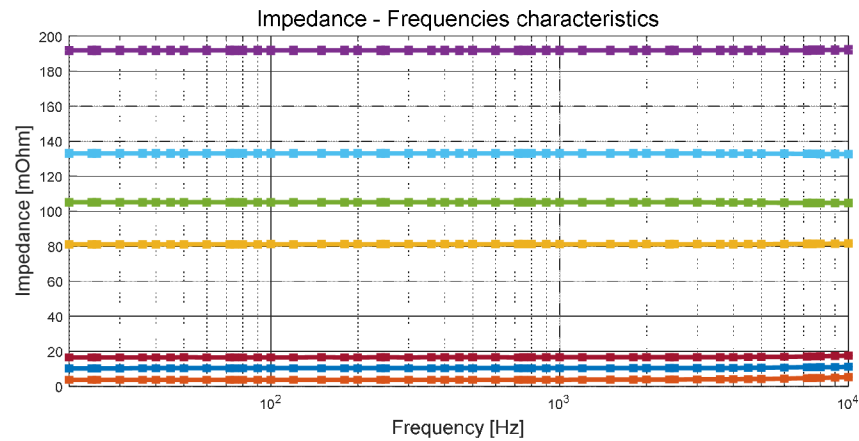
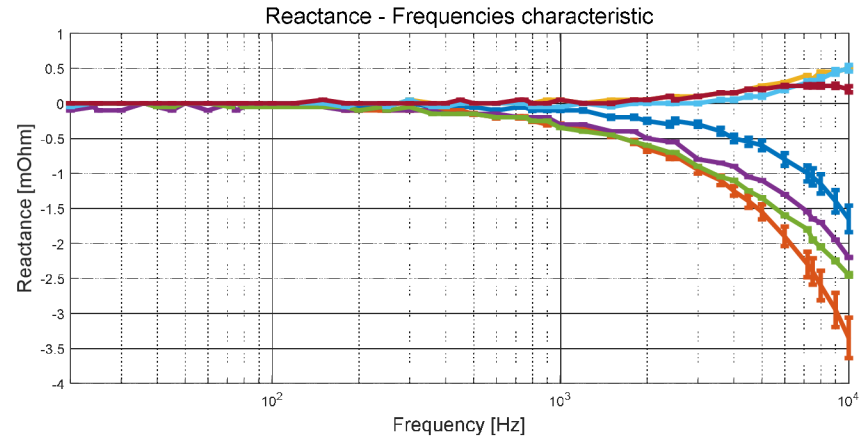
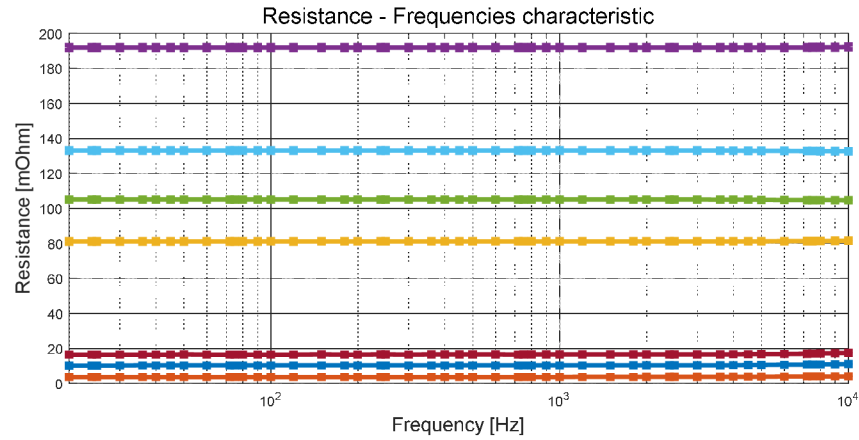
Legend	
Blue line	M1556860-1
Orange line	M1556860-2
Yellow line	M1712603-1
Purple line	M1712603-2
Green line	SOP-056-2
Light blue line	SOP-056-4
Dark red line	SOP-057-3

Comparison impedance between C and D - frequency to 10kHz



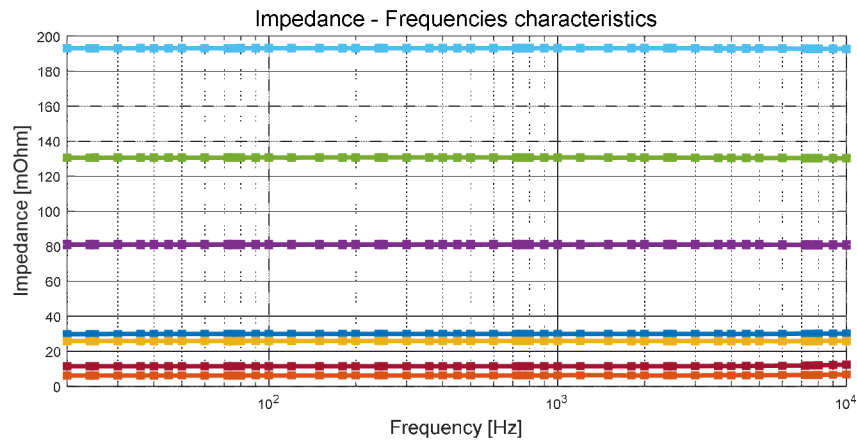
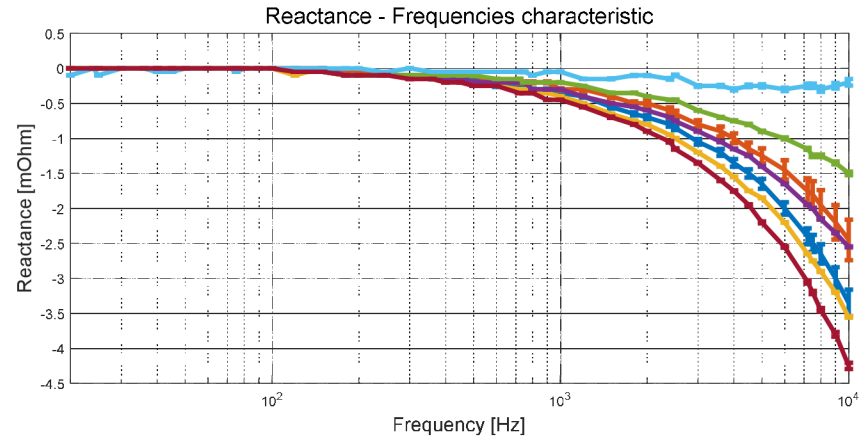
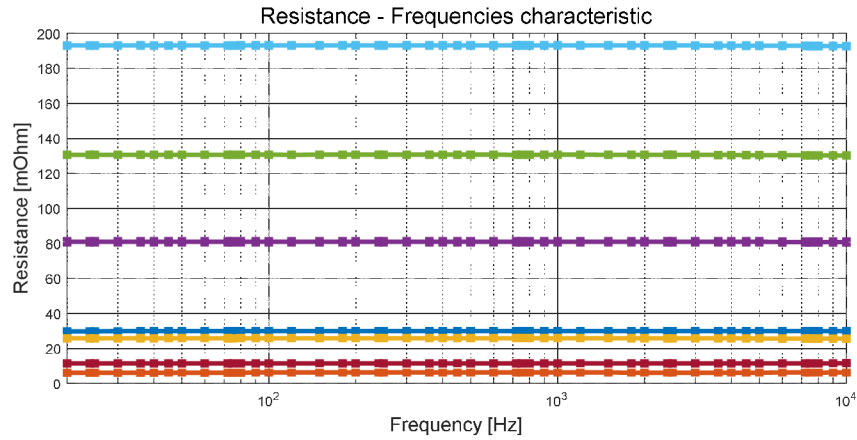
Legend	
—	M1556860-1
—	M1556860-2
—	M1712603-1
—	M1712603-2
—	SOP-056-2
—	SOP-056-4
—	SOP-057-3

Comparison impedance between A and C - frequency to 10kHz

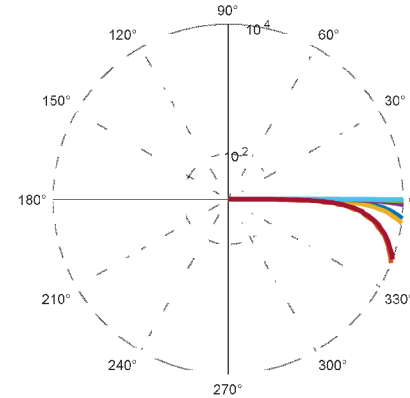


Legend	
—■—	M1556860-1
—■—	M1556860-2
—■—	M1712603-1
—■—	M1712603-2
—■—	SOP-056-2
—■—	SOP-056-4
—■—	SOP-057-3

Comparison impedance between B and D - frequency to 10kHz

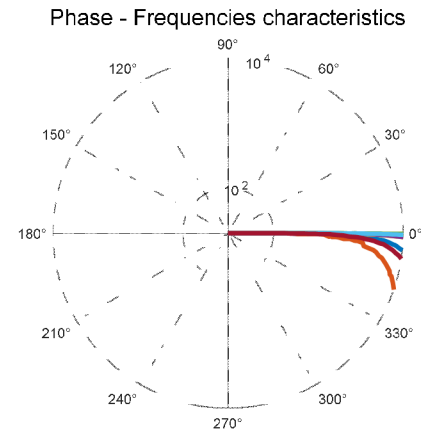
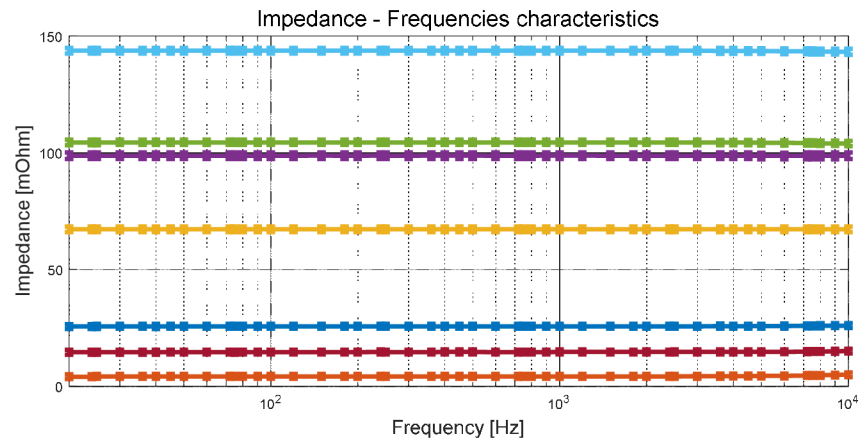
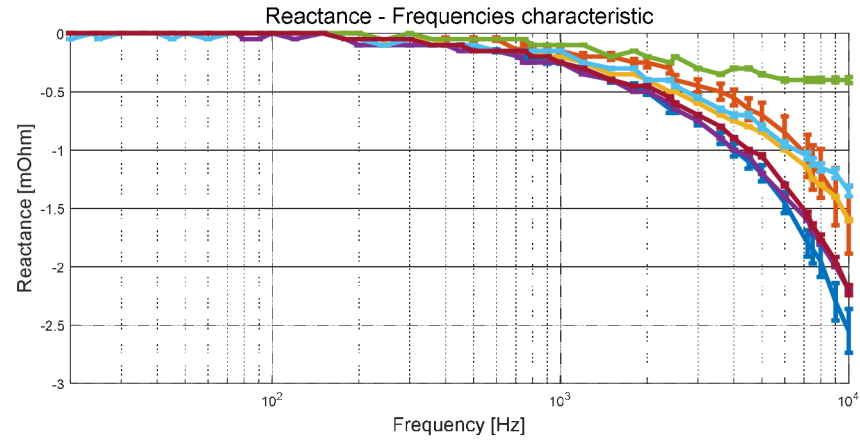
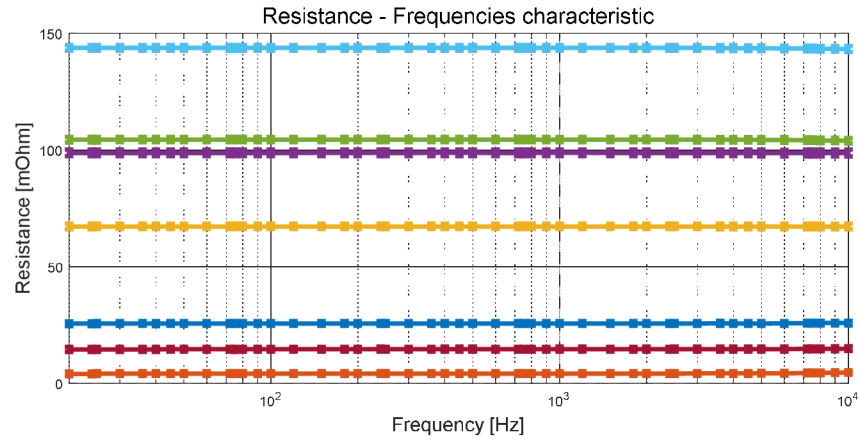


Phase - Frequencies characteristics



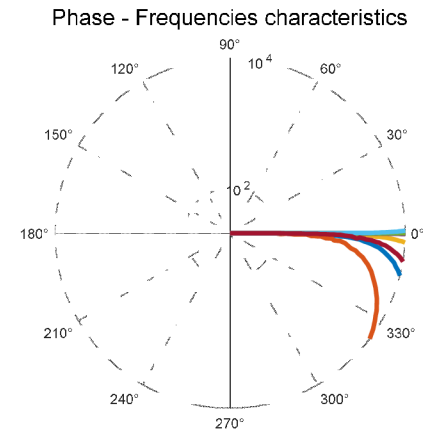
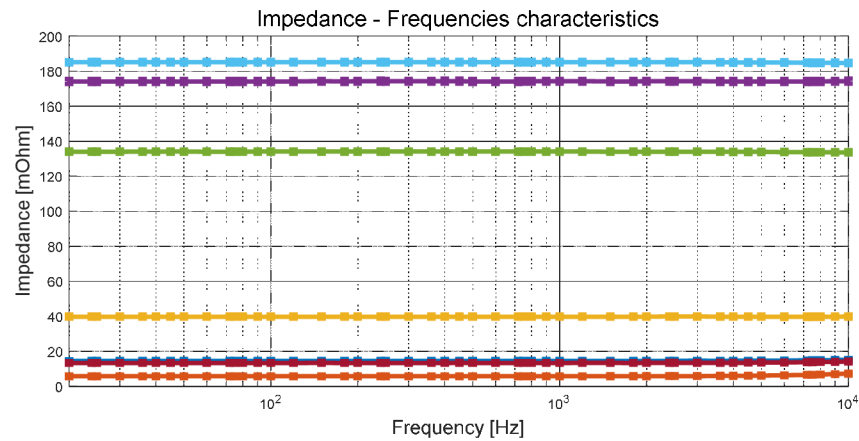
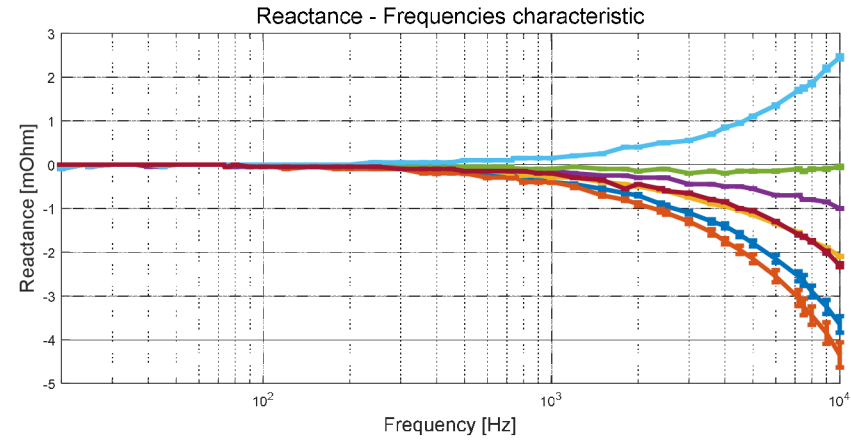
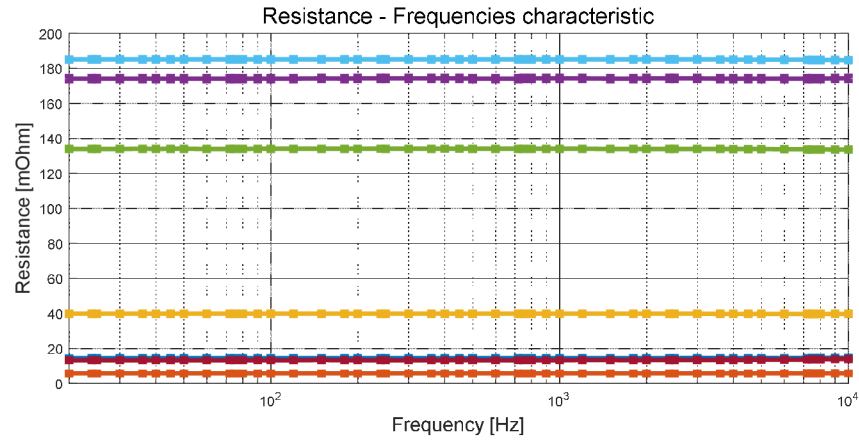
Legend	
—	M1556860-1
—	M1556860-2
—	M1712603-1
—	M1712603-2
—	SOP-056-2
—	SOP-056-4
—	SOP-057-3

Comparison impedance between A and D - frequency to 10kHz



Legend	
—■—	M1556860-1
—■—	M1556860-2
—■—	M1712603-1
—■—	M1712603-2
—■—	SOP-056-2
—■—	SOP-056-4
—■—	SOP-057-3

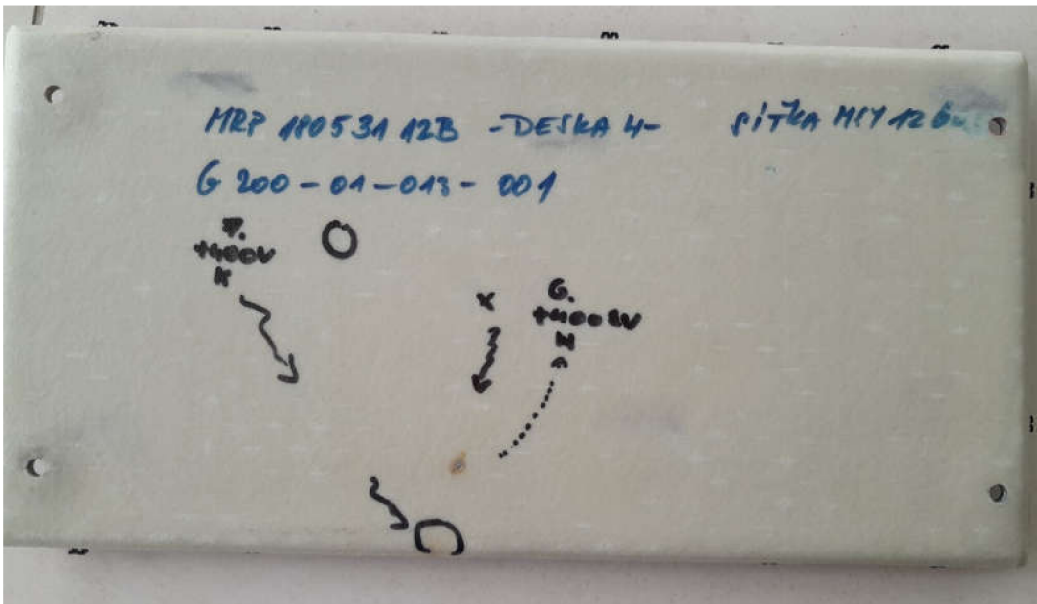
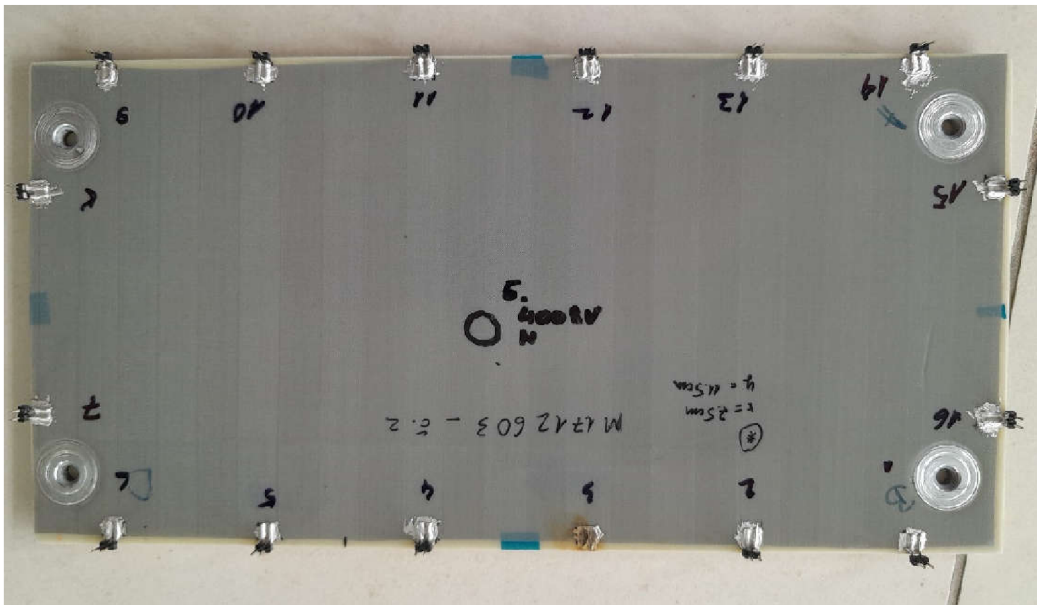
Comparison impedance between B and C - frequency to 10kHz



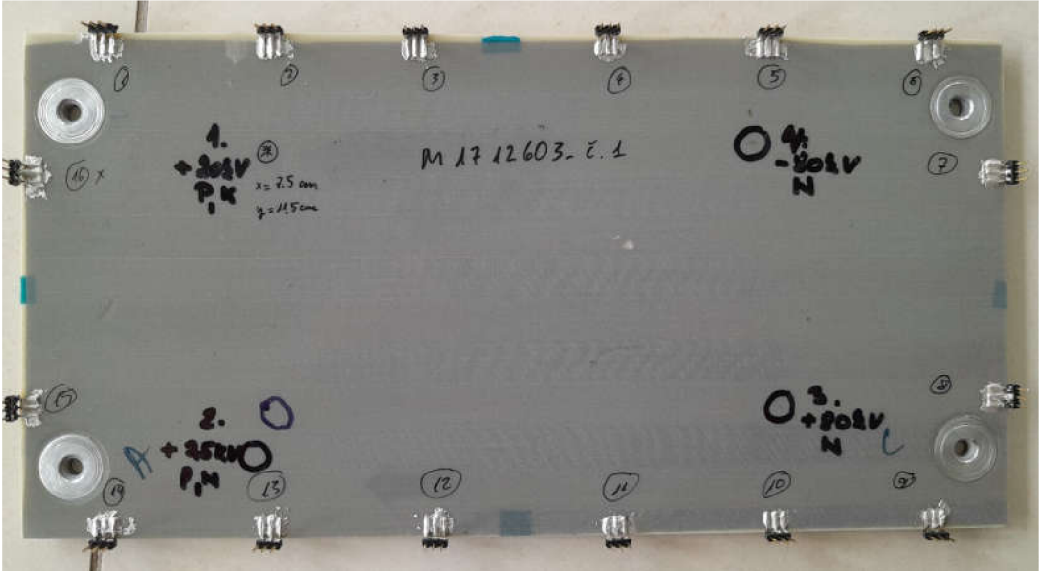
Legend	
—●—	M1556860-1
—●—	M1556860-2
—●—	M1712603-1
—●—	M1712603-2
—●—	SOP-056-2
—●—	SOP-056-4
—●—	SOP-057-3

Appendix C - Lightning strike tests

Specimens under test 1

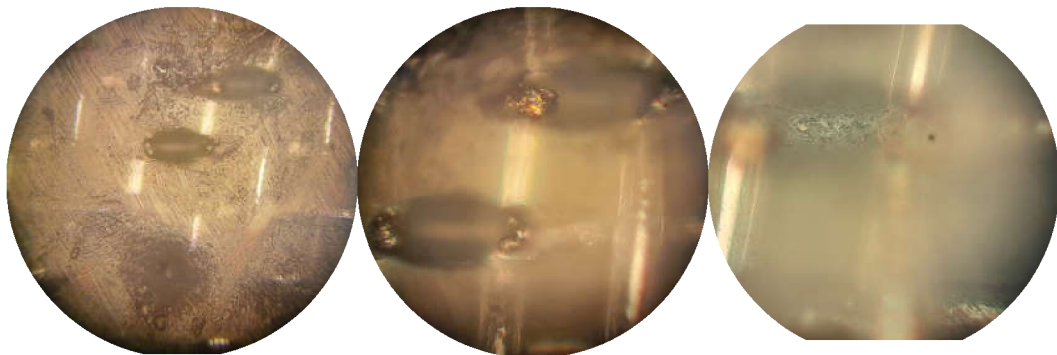
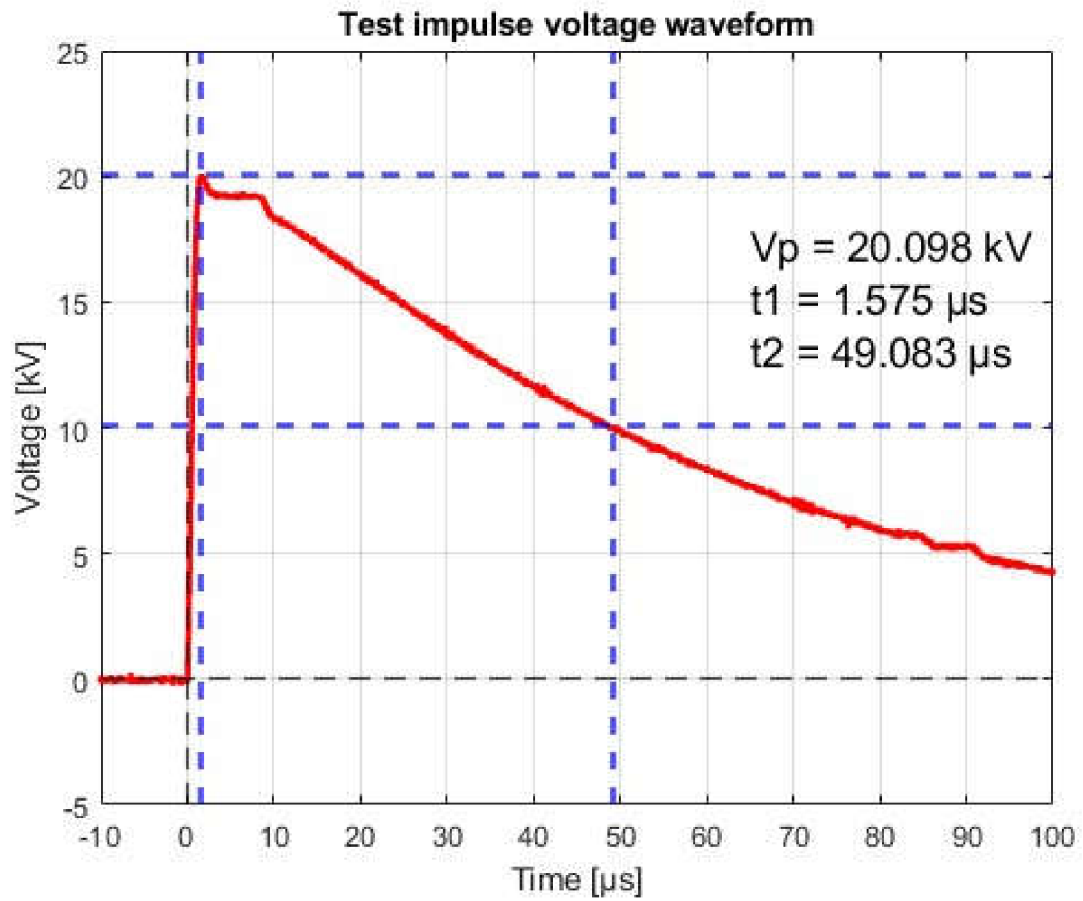


Specimens under test 2



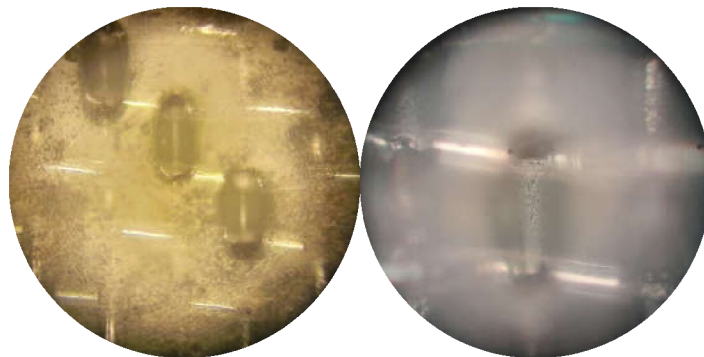
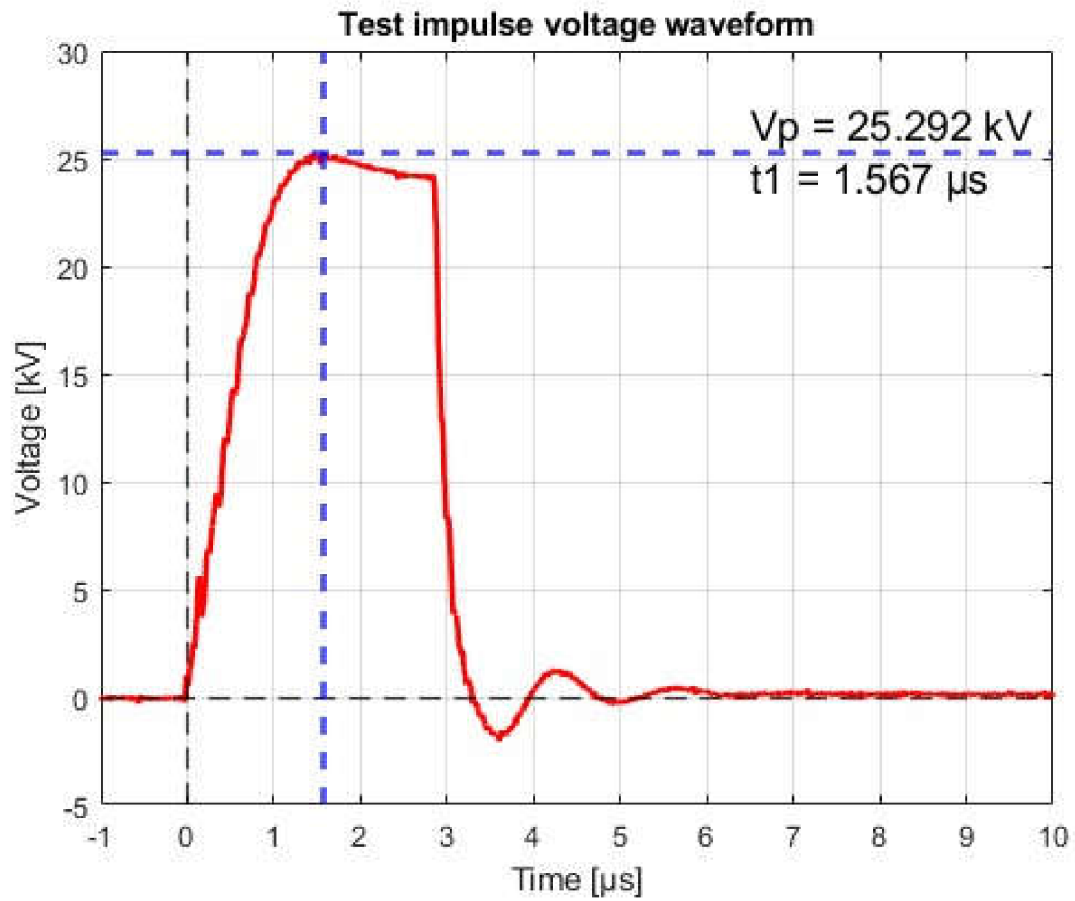
Test 1:

- Contact discharge, protected surface
- Setup voltage +20 kV
- Specimen 2



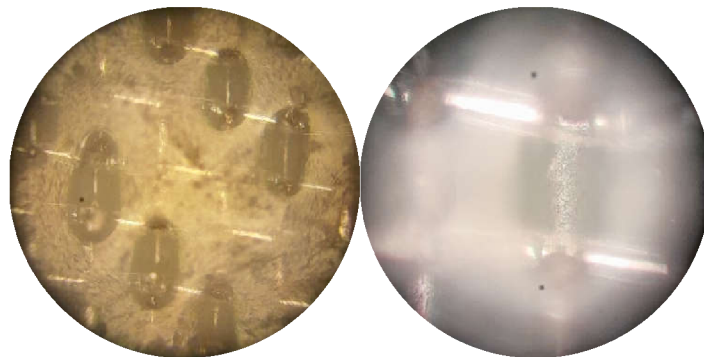
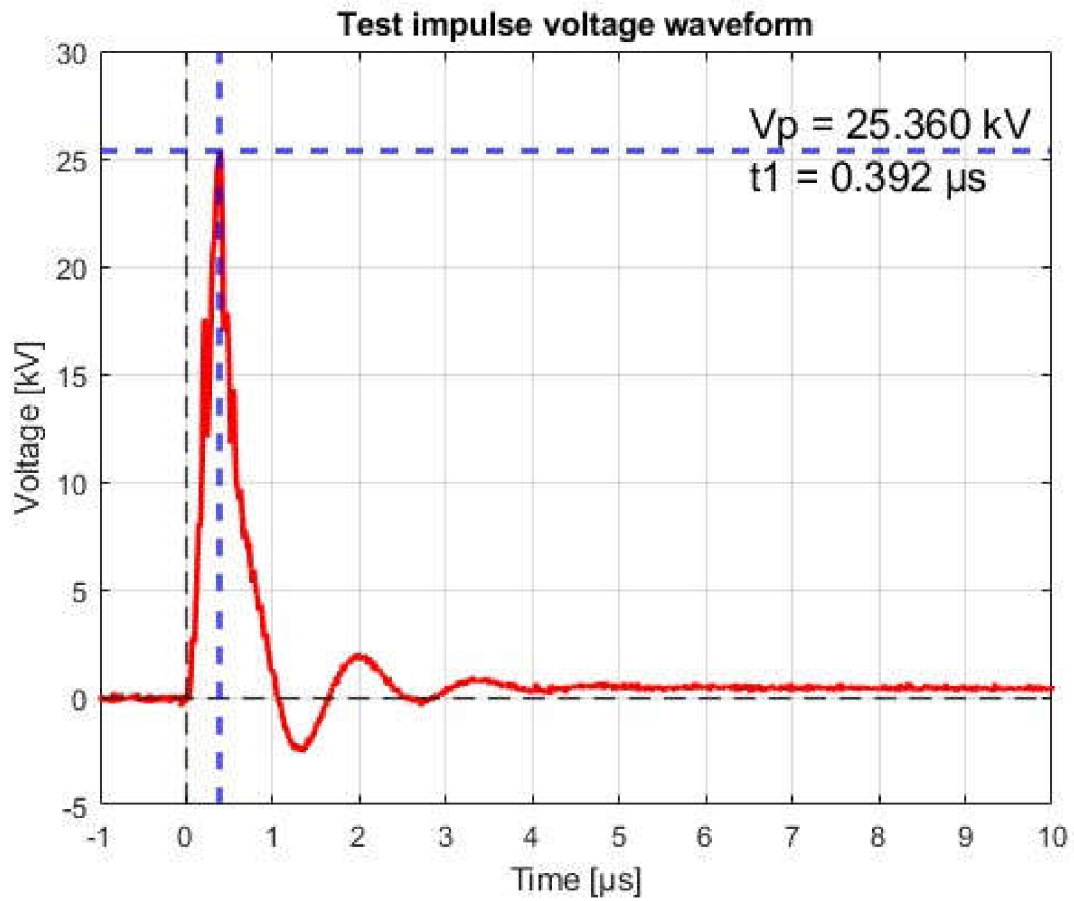
Test 2:

- Air discharge, protected surface
- Setup voltage +25 kV
- Specimen 2



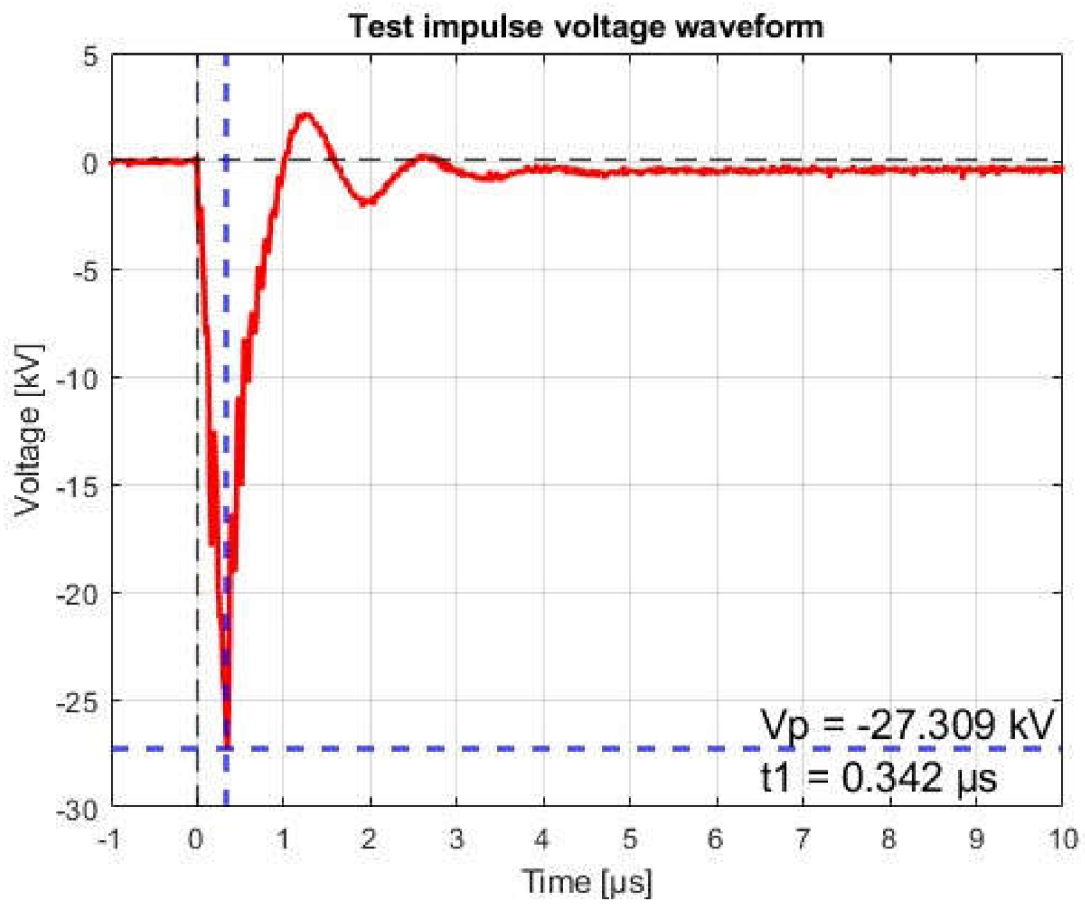
Test 3:

- Air discharge, protected surface
- Setup voltage +80 kV
- Specimen 2



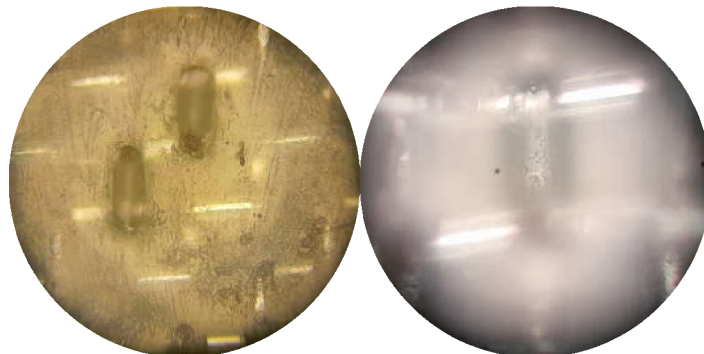
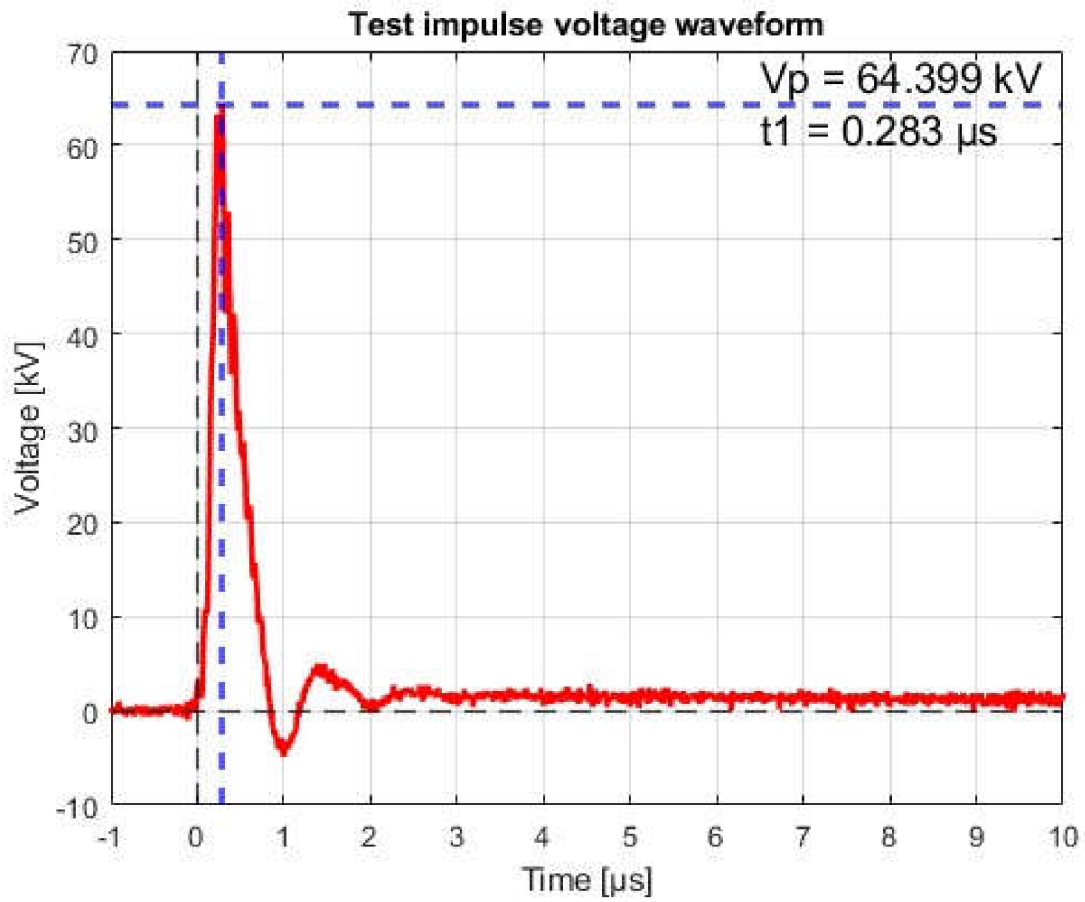
Test 4:

- Air discharge, protected surface
- Setup voltage -80 kV
- Specimen 2



Test 5:

- Air discharge, protected surface
- Setup voltage +400 kV
- Specimen 1



Test 6:

- Air discharge, unprotected surface
- Setup voltage +400 kV
- Specimen 1

